BMC Genomics

RESEARCH Open Access

Time-course human urine proteomics in space-flight simulation experiments

Hans Binder[1*], Henry Wirth[1], Arsen Arakelyan[2], Kathrin Lembcke[1], Evgeny S Tiys[3], Vladimir A Ivanisenko[3], Nikolay A Kolchanov[3], Alexey Kononikhin[4,6], Igor Popov[5,6], Evgeny N Nikolaev[4,5,6,7*], Lyudmila Kh Pastushkova[8], Irina M Larina[8]

From IX International Conference on the Bioinformatics of Genome Regulation and Structure\Systems Biology (BGRS\SB-2014)
Novosibirsk, Russia. 23-28 June 2014

Abstract

Background: Long-term space travel simulation experiments enabled to discover different aspects of human metabolism such as the complexity of NaCl salt balance. Detailed proteomics data were collected during the Mars105 isolation experiment enabling a deeper insight into the molecular processes involved.

Results: We studied the abundance of about two thousand proteins extracted from urine samples of six volunteers collected weekly during a 105-day isolation experiment under controlled dietary conditions including progressive reduction of salt consumption. Machine learning using Self Organizing maps (SOM) in combination with different analysis tools was applied to describe the time trajectories of protein abundance in urine. The method enables a personalized and intuitive view on the physiological state of the volunteers. The abundance of more than one half of the proteins measured clearly changes in the course of the experiment. The trajectory splits roughly into three time ranges, an early (week 1-6), an intermediate (week 7-11) and a late one (week 12-15). Regulatory modes associated with distinct biological processes were identified using previous knowledge by applying enrichment and pathway flow analysis. Early protein activation modes can be related to immune response and inflammatory processes, activation at intermediate times to developmental and proliferative processes and late activations to stress and responses to chemicals.

Conclusions: The protein abundance profiles support previous results about alternative mechanisms of salt storage in an osmotically inactive form. We hypothesize that reduced NaCl consumption of about 6 g/day presumably will reduce or even prevent the activation of inflammatory processes observed in the early time range of isolation. SOM machine learning in combination with analysis methods of class discovery and functional annotation enable the straightforward analysis of complex proteomics data sets generated by means of mass spectrometry.

Introduction

The physiological impact of human space flights missions exceeding several weeks poses problems such as radiation exposure, immunological depression and stress. Part of the concerns occur during the course of a mission, while others - such as cardiovascular deconditioning, bone and muscle losses and orthostatic intolerance - manifest themselves mainly upon return to earth only. These in-flight and post-flight physiological issues are vital to develop a sustainable program of human space exploration. Long-term space travel simulation experiments on earth are performed to discover the particular factors causing physiological and psychological problems and to develop methods helping to prevent or, at least to counteract them.

* Correspondence: binder@izbi.uni-leipzig.de; ennikolaev@rambler.ru
[1]Interdisciplinary Centre for Bioinformatics, Universität Leipzig, Leipzig, Germany
[4]Talrose Institute for Energy Problems of Chemical Physics, RAS, Moscow, Russia
Full list of author information is available at the end of the article

An interesting line of investigation was pursued as 'Mars isolation study' conducted at the Institute of Biomedical Problems in Moscow to simulate a journey to our neighbor planet. The purpose was to find out more about the effects of a long period of isolation on the human physiological and mental conditions in terms of data gathered over several weeks. Volunteers were confined to an enclosed, restricted environment where they obtained diets with defined amounts of salt (NaCl) and micro elements content and performed different activity programs. These studies were remarkable for their sustained duration and tight control of environmental variables. This ground-based space station model experiment enabled a novel, profound and extended trip to our 'inner space' to discover new aspects of human metabolism [1].

Particularly, the study provided a unique and detailed profile of physiological responses to decreasing salt intake. Besides playing a part in the development of hypertension (an actual study estimates that more than 1.5 million annual deaths from cardiovascular causes worldwide were attributed to increased sodium consumption [2]) and the weakening of the immune system, too much salt also seems to have a negative effect on the musculo-skeletal system due to acidification caused by the binding of salt to sugar-protein compounds. In consequence a high salt intake increases bone and muscle loss in humans on earth which is even exacerbated in the absence of gravity. One expects that a salt-reduced diet possibly diminishes negative effects such as bone degradation in space flights.

Although the physiology of salt balance is well understood (see the short review in [1] and the references cited therein) the space flight simulation experiment highlighted a new complexity in physiological responses that cannot be easily explained by previous knowledge [3-5]. For example, the studies raised doubts about the strict link between salt and water balance which are presumably caused by the storage of NaCl in a molecularly-bound, osmotically-inactive form paralleled by immune system driven micro-vascularization in skin which tends to reduce blood pressure [6-8].

One needs further exploration of these findings to improve our understanding of the effect of diet and of isolation on human physiology especially to understand the regulatory modes on the molecular level. So far measures estimating the kinetics of salt balance and of hormone production were analyzed and related to global parameters such as the blood pressure, extracellular water and body weight [3-5]. In addition to these measures, detailed urine proteomics data were collected during the Mars105 isolation experiment lasting 105 days potentially enabling a deeper insight into the molecular processes involved. First analyses report a high variability of protein abundance identified in the urine samples [9]. Another analysis established associations between clusters of proteins and a functional protein networks related to sodium intake which has been extracted from literature using bioinformatics methods [10]. A third study analyzed the possible tissue origin of the proteins detected. It founds an increased number of renal and urinary tract proteins after a real space mission compared with the ground-based flight simulation presumably reflecting the accumulation of sodium in cosmonauts body during space missions [11].

A comprehensive analysis of the time-dependent urine proteomics data set collected during the ground based flight simulation is still pending. In this publication we analyze the abundance of the about two thousand proteins measured during the experiment and discover its functional impact. We pursue a personalized view to disentangle the specifics of protein abundance in each of the six participating individuals. We demonstrate that machine learning using self organizing maps (SOM) in combination with different analysis tools enable a personalized and intuitive view on the data. Application and adaptation of SOM machine learning to time-resolved protein abundance data is novel and challenging due to the special data type, unknown error structure and possible methodical biases of the data.

In the first part of this publication we therefore address methodical issues related to the proteomics data set. In the second part we focus on the functional interpretational to answer question such as how urine protein abundance is affected by decreased salt consumption and isolation in the space flight simulation chamber and what biological processes were involved at different stages of the experiment.

Results

SOM abundance portraits and sample trajectories

Figure 1a shows the gallery of protein abundance landscapes as seen by the SOM-portraits. They visualize the mean protein abundances averaged over the individual volunteer data at each time point of sample collection. Hence, each landscape 'portrays' the proteomics phenotype of the about 2,000 protein species identified by mass spectrometry in the urine samples (IPI items). Proteins with high topmost over and under-expression levels are localized in the red and blue spot-like regions, respectively. The spot patterns clearly change in the course of the experiment reflecting alterations in the proteomics phenotypes potentially caused by isolation, modifications of salt (NaCl) consumption and presumably other factors.

Panel b of Figure 1 shows the so-called 2nd-level SOM which visualizes the mutual similarities between the samples in a two-dimensional plot. The samples pass virtually four time windows where the first and second ones were indicated by dotted ellipses: The first window includes the samples taken before starting the isolation

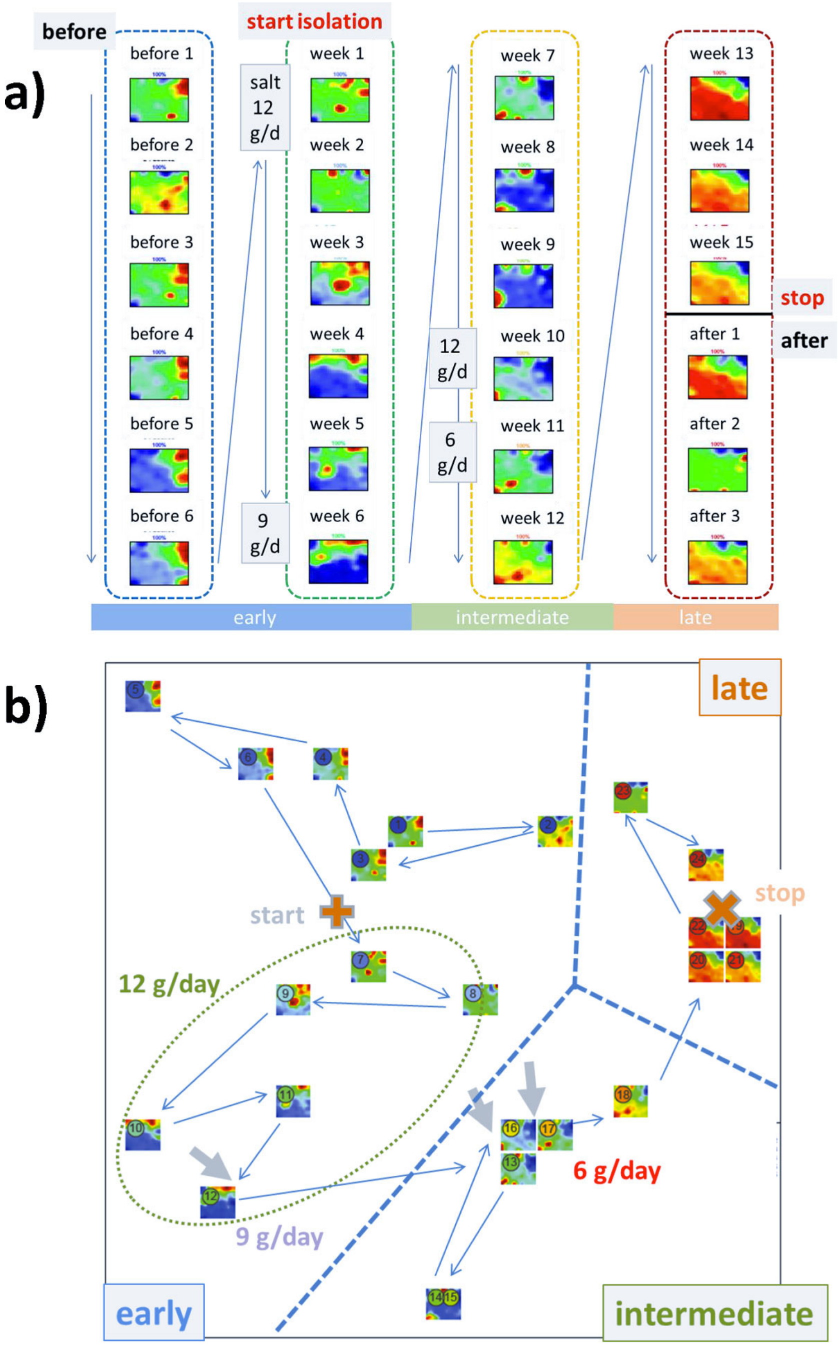

Figure 1 Time dependent SOM proteomics portraits of urine samples taken before, during and after the isolation experiment (panel a) and time trajectory as obtained using 2nd level SOM mapping (panel b). The results refer to the 'mean-volunteer analysis' by averaging the proteomics data over the six volunteers at each time point. Each column of images in panel a refers to one cluster as determined using 2nd level SOM similarity analysis shown in panel b. Thin arrows indicate the temporal order of the specimen and thus the trajectory of the urine proteomics samples. The amount a salt consumption per volunteer and day during the isolation experiment is indicated in the figures: the arrows indicate the times of changing salt consumption. The dashed lines divide the trajectory into early, intermediate and late time ranges. The 'early' time-regime further subdivides into two clusters of samples collected before and after start of the isolation experiment (ellipses). Alternative independent component analysis of the sample trajectory is given in the supplementary text (Additional file 1).

experiment. The second time window lasts roughly until the end of the sixth week of isolation in which salt consumption is reduced from 12 g/day to 9 g/day. The third period ends after week no. 11, i.e. two weeks after salt consumption is further reduced to 6 g/day. The last time window finally includes the samples taken in the last three weeks of the isolation experiment and the three sample points taken afterwards. Note that the transition between time window two and three forms a sort of turning point of the trajectory after that the proteomic landscapes in the phase space of the 2nd level SOM 'move' back in direction towards the starting point. According to the amount of salt consumption the samples taken before/after this turning point refer to higher and lower salt consumption, respectively. In a more rough view we divide the data into an 'early', 'intermediate' and a 'late' time regime as indicated in Figure 1: It considers the similarity of the abundance landscapes in the first two time windows and aggregates them into one early phase.

In the supplementary text we analyzed similarity relations using independent component analysis (ICA) projecting the samples in linear scale. ICA virtually confirms the results obtained using 2nd level SOM.

Spot trajectories and module selection

The SOM-algorithm distributes the proteins over the map such that co-expressed proteins become located nearby. In consequence, proteins specifically up-regulated in one of the time regimes aggregate into red spot-like textures at a certain position of the map. With evolving time of the experiment the spot patterns change and, in particular, existing spots disappear and new ones appear at new positions (see Figure 1a). Figure 2 (upper part) illustrates these spot trajectories for red over- (left panel) and blue under- (right panel) expression spots. The so-called summary maps aggregate all red or blue spots observed in the individual profiles into one master map, respectively. The arrows illustrate the temporal order of appearance of the respective spots: Due to the self-organizing properties of the map red and blue spots 'rotate' in counterclockwise direction along the edges of the map in a central-symmetrical fashion. I.e., as a rule of thumb red and blue spots often appear as antagonistic twins indicating that each state is characterized by a set of up-, and a set of down-regulated proteins as well.

This property of self-organization is reflected in the spot-spot correlation and anti-correlation maps which were calculated using a weighted-topology overlap network approach as described in the Methods section and in ref. [12]: The bottom left panel in Figure 2 shows that spots up-regulated in the early time range are mutually highly correlated forming a sort of continuum of states located in right-upper part of the map. The two time windows in the early range are consequently associated with spots along the right and upper border of the map, respectively. The intermediate and late time ranges are accompanied by a marked shift of the spot position towards the lower left corner of the map thus allowing to associate the proteins within the respective spots with the discontinuous changes in samples trajectory described above (see also Figure 1). The anti-correlation map (bottom right panel in Figure 2) supports the view that spots up-regulated in the early and intermediate/late time ranges are down regulated at intermediate/late and early time ranges, respectively. Hence, the characteristic breakpoints along the spot trajectories observed can be associated with discontinuous changes of protein abundance detected in the spot trajectories.

In the next step we address the question how to select the spots appropriately or, in other words, how to segment the map properly into regions of co-regulated proteins. Besides the over- and under-expression spot selection algorithm we also applied alternative methods based on correlation and K-means clustering. Details and results of this analysis were provided in the supplementary text.

We found that the spot selection method is not crucial for extracting the basal dynamic properties of the system. In dependence on partial needs, e.g. to extract strongly differentially expressed proteins or larger groups of mutually co-expressed or even largely invariant features we recommend the overexpression, correlation or K-means clustering method, respectively. Here we will focus on the overexpression spot selection method because it is a good choice for marker selection which includes up- and down-regulated features as well. Selected results for the correlation and K-means clustering methods are presented in the supplementary text (Additional file 1).

Spot profiles and functional analysis

Figure 3 assigns the spot profiles to selected overexpression spots. These profiles are mean time-dependent protein abundance data averaged over all meta-features included in the respective spot. The meta-features, in turn, are mean protein abundance data averaged over all single protein data contained in each meta-feature. Hence, the spot profiles are mean profiles characterizing the average abundance of the single proteins included in the respective spot. Most of the profiles show a wave-like shape with a maximum and minimum in different time windows reflecting the dynamic up- and down-regulation of proteins during the experiment. In direction of the spot trajectories discussed above, the abundance maximum seen in the individual spot profiles shifts to later times. The spot trajectory thus reflects first of all the phase-shift ϕ of the wave-like profiles which roughly increases from $\phi \sim$ 0-T*/2

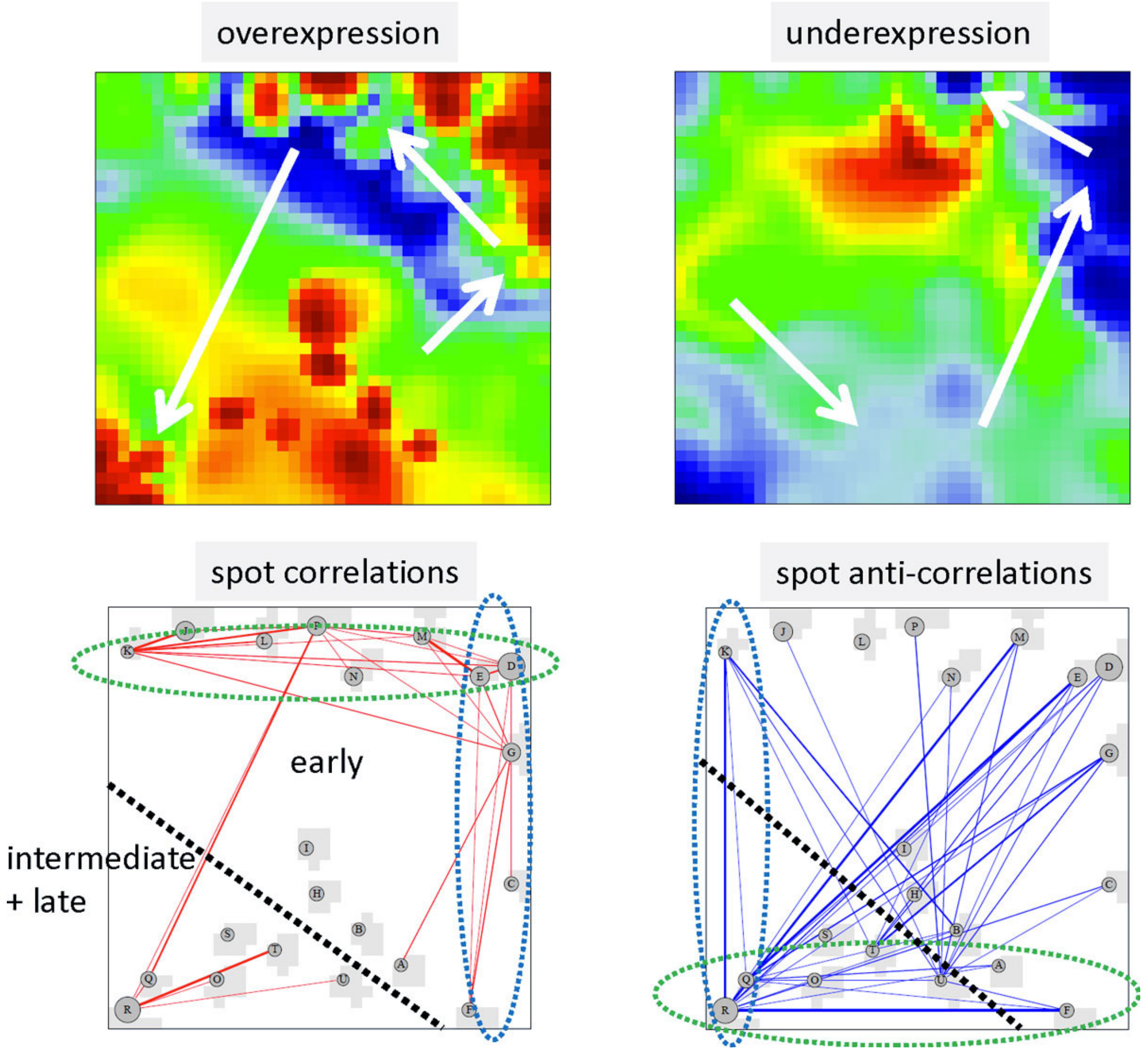

Figure 2 Spot trajectories (part above) and mutual spot correlations: The over- and under-expression spot summary maps collect the red and blue spots observed in the individual portraits into one master map, respectively. The arrows roughly illustrate the time-trajectories of over- and under-expression spots before, during and after the isolation experiment (see also the individual SOM portraits shown in Figure 1a). The correlation and ant-correlation maps visualize mutual correlations between the spots in terms of the weighted topological overlap (wto) measures for positive and negative correlations, respectively. Spots are connected by lines for strong correlations/anti-correlations.

for early activation (e.g. spot D) to $\phi \sim T^*/2$ - T^* for activation at intermediate and late times (e.g. spot R). Here T^* denotes the period of the changes, e.g. given as total time of the experiment. The spot profiles differ however not only in the position of their abundance maximum but also in the time delay between maximum and minimum abundance and also in their shape which can resemble more a harmonic cosine (e.g. spots G and R) or more a single peaked function (e.g. spots M and Q). The period can cover the whole duration of the experiment, i.e. T^*~105 days (e.g. spots D and J) or a considerably longer or shorter time, $T \sim 2\ T^*$ (e.g. spots E and R) or $T<T^*$ (e.g. spots L and P), respectively. Note that periodic changes of protein abundance can be induced by different extrinsic factors such as the activity, nutrition and working regime (e.g. night shift work during the experiment) of the volunteers, salt consumption but also intrinsic ones such as hormone activities (e.g. of andosterone, see discussion) and thus the period, or in other words, the degree of recovery of protein abundance after its perturbation, can deviate from the time span of the experiment.

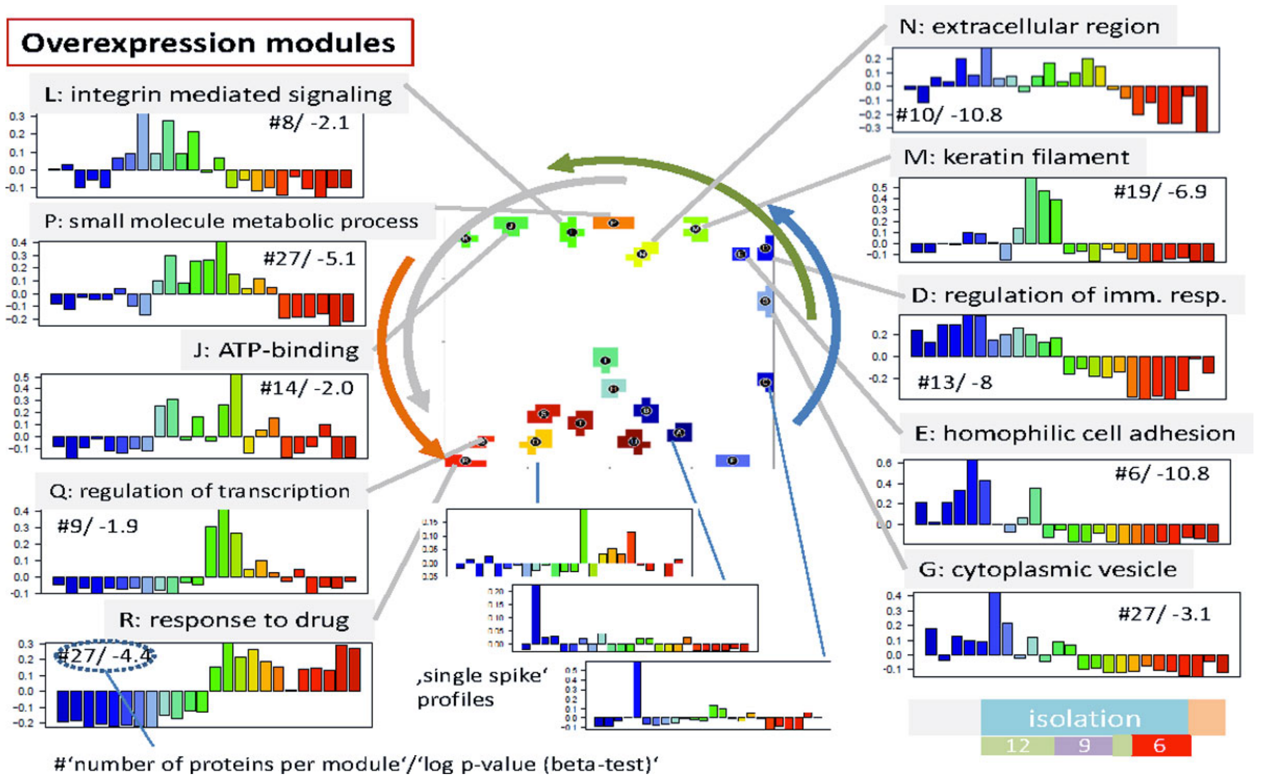

Figure 3 Protein abundance profiles are assigned to the overexpression spot modules together with the leading functional context as obtained using gene set enrichment analysis. Spots are assigned by capital letters. So-called single spiked profiles accumulate in rare spots in the lower-right part of the map. Lists of leading proteins are given for each spot in the supplementary text (Additional file 2). The vertical axis of the profiles is scaled in units of differential abundance, ΔE, representing the mean binary detection level centralized with respect to the mean abundance in all samples at all times.

Hence, the spots along the spot trajectory represent clusters of proteins concertedly activated and deactivated in sequential order during the experiment and differing also in the time of activation and the degree of recovery of the initial state at the end of the experiment. The overexpression spots contain from 6 to 27 proteins (as given in Figure 3) whereas the correlation and K-means spot clusters are markedly larger with 23-76 and 39-93 proteins per cluster, respectively (see respectively (see supplementary text; Additional file 2 and 3). Despite their differing size, the respective spot profiles taken from comparable regions of the map look very similar (compare Figure 3 with the respective figures shown in the supplementary text for correlation and K-means clustering).

The different time profiles of the spots allow us to relate them to different properties of the sample trajectory depicted in Figure 1. Particularly, spots showing different levels of protein abundance at the start and the end of the experiment (i.e. with periods T ≠ T*) are responsible for the shift between the start and end points of the sample trajectories whereas spots with cosine-like profiles and T~T* and also spots with peak-shaped profiles are mainly responsible for the turning point of the trajectories because the respective proteins mostly recover their abundance state during the experiment (see Figure 1).

Enrichment analysis using more than 2000 predefined groups of proteins referring to different GO-terms from the categories ‘biological process’, ‘cellular component’ and ‘molecular function’ allowed us to assign the functional context to each of the spot clusters selected. In Figure 3 the leading gene set is given for each overexpression spot cluster. The results of a more detailed analysis are given in the heat map shown in Figure 4 (see refs. [13,14] for the description of the method) and in the supplementary text where we map and profile selected protein sets in detail. According to these analyses the early time range is characterized by the activation of inflammatory processes and angiogenesis (gene sets inflammation, extracellular region, cell adhesion, complement activation, proteolysis, angiogenesis and Calcium ion binding) whereas intermediate and late responses are related to developmental and regenerative processes (development, mitosis, regulation of transcription, chromatin remodeling) and stress and drug response (small

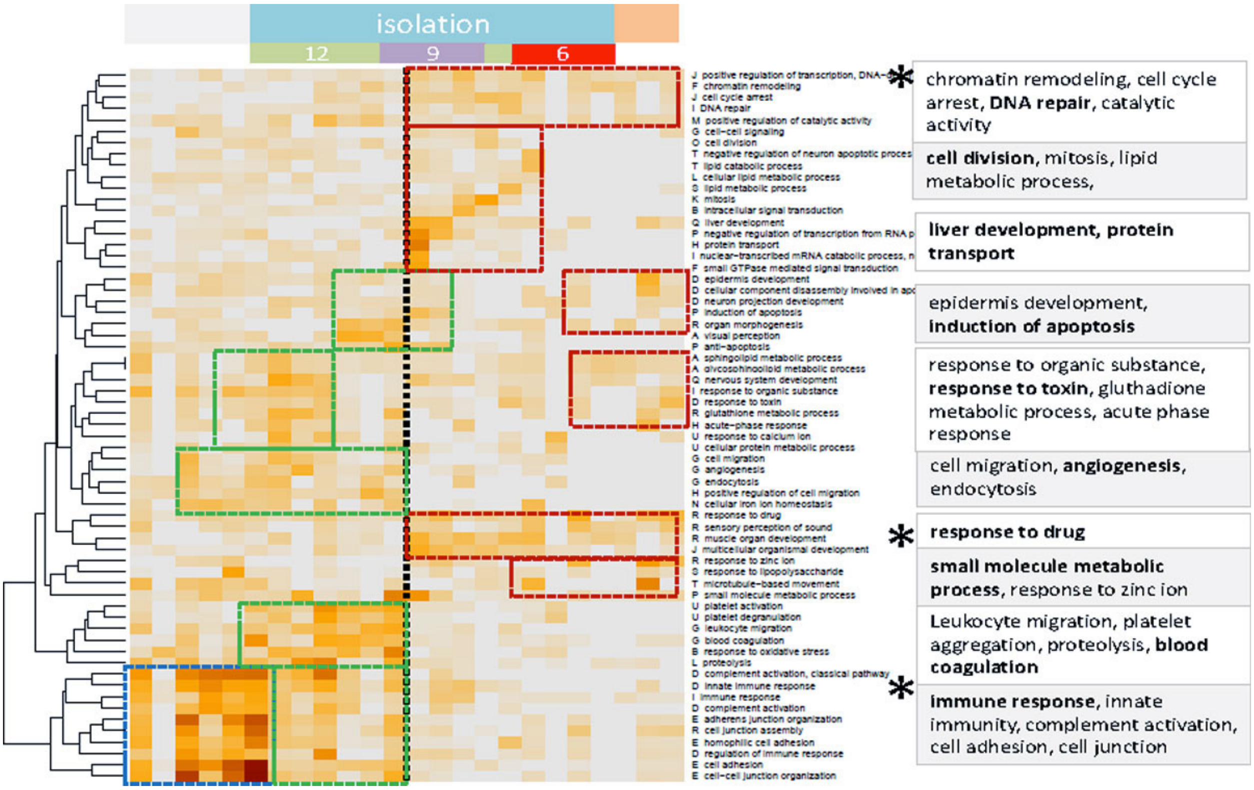

Figure 4 Global enrichment analysis heat map: The map clusters top GO-sets of the category 'biological process' enriched in overexpression spots of the time series. The dashed rectangles indicate time regions of marked enrichment of the processes listed in the right part of the figure (orange to brown colors refer to increasing enrichment). The vertical dotted line divides early from late time regimes. Processes marked with an asterisk do not fully recover during the experiment. They are related to the shift between the start and end points of the sample trajectories (see Figure 1)

molecule regulative process, response to oxidative stress, hypoxia, apoptosis, response to Zinc, Magnesium ion binding, G-protein coupled activity), respectively. Note that part of the processes related to inflammation, drug response and also to genome and transcriptome activity (chromatin remodeling, DNA repair) can be attributed to the lack of recovery of the sample trajectories (these processes are marked by the asterisks in Figure 4).

Clusters of proteins associated to the response of the organism to 'NaCl' deficiency are identified previously using a comprehensive interactome network analysis [10]. We mapped proteins from these clusters into SOM space and found that they mostly refer to the early, and to a less degree, to the intermediate-time response (see supplementary text).

Pathway signal flow analysis (PSF) represents an independent option to discover the functional context of the spot profiles. In contrast to gene set enrichment analysis it takes into account the network topology of selected pathways taken from the KEGG database to obtain PSF-profiles which are compared with the abundance profiles of the spots. It turned out that early and intermediate protein abundance changes are associated with inflammatory responses and metabolic processes (fatty acids, nucleic acids and amino acids) indicating alterations of nutrition and partly starvation followed by activation of regenerative processes (Wnt-pathway, N-glycan biosynthesis) in the intermediate time range and of stress response signaling (p53 and mTOR-signaling pathways) and digestion at late times of the experiment (see Figure 5 and supplementary text for details). Many pathways lead to the activation of protein kinase C and inositol-triphosphate signaling cascades in agreement with the enriched protein sets related to signal transduction such as Ca^{2+} binding and G-protein coupled receptor activity.

Individual volunteer analysis

So far we presented results based on the averaging of the abundance of each protein at each time point over all six volunteers. This 'mean volunteer' analysis allowed extracting mean effects induced by isolation and varying salt consumption but it neglects individual differences between the volunteers. We therefore performed a second independent SOM analysis of the individual data of

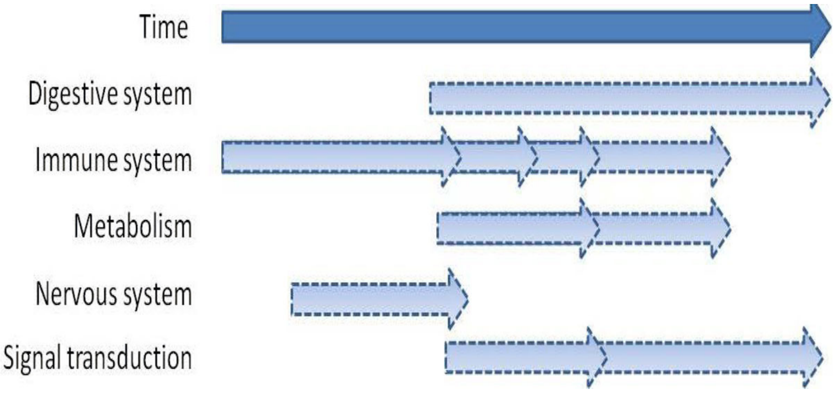

Figure 5 Summary of results obtained from pathway flow analysis: The light blue arrows indicate characteristic processes activated with progressing time of the experiment. The processes are identified by comparing the PSF of KEGG-pathways with the spot profiles of protein abundance (see supplementary text for details).

each volunteer. Figure 6 shows the gallery of time-dependent 'personalized' portraits of all six probands (P1 - P6). As for the 'mean volunteer analysis', the protein abundance landscapes can be divided into typical color textures assigned to the early-, intermediate- and late-response types, respectively. Simple visual inspection of the portraits shows that the abundance patterns of most of the volunteers alter in parallel (see the colored frames in Figure 6). Partly, one observes however small variations in the time-dependent changes: For example, the portraits of P4-P5 switch into the time regime of the 'late' type almost one-two weeks earlier than that of P1-P3. Late-type protein abundance patterns were observed for P5 in three samples taken before starting isolation.

Figure 7 shows the individual sample trajectories of each of the volunteers using 2nd level SOM analysis. One sees that virtually each trajectory can be clearly divided

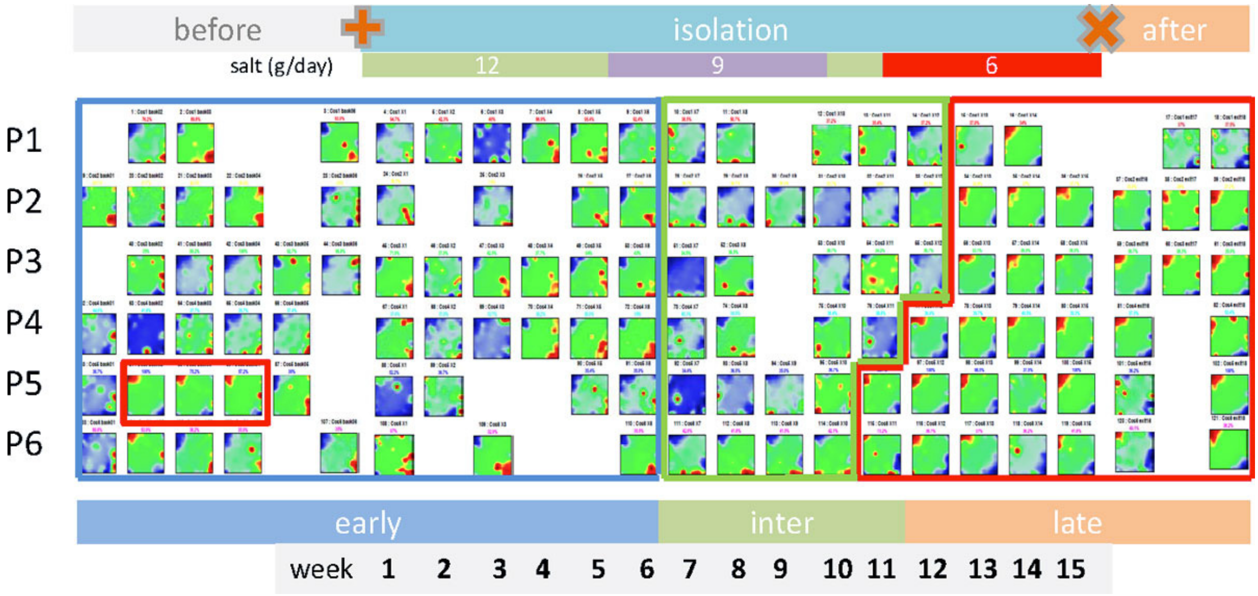

Figure 6 Gallery of SOM portraits of the individual volunteers: Each row refers to one proband (P1 to P6) and each column to one time point of sample collection. Empty positions in the matrix refer to missing data because no samples were collected. The blue, green and red frames include samples showing the characteristics of early, intermediate and late responses, respectively. Note that the SOM textures cannot be directly compared to the textures of the mean volunteer analysis (shown in Figure 1) because both sets of maps are trained independently. Note that three out of five urine samples taken from proband no. 5 (P5) and possibly one taken from P6 before starting isolation express proteomics characteristics observed apart from that in the samples of all volunteers in the late time range only (see the red frames for P5).

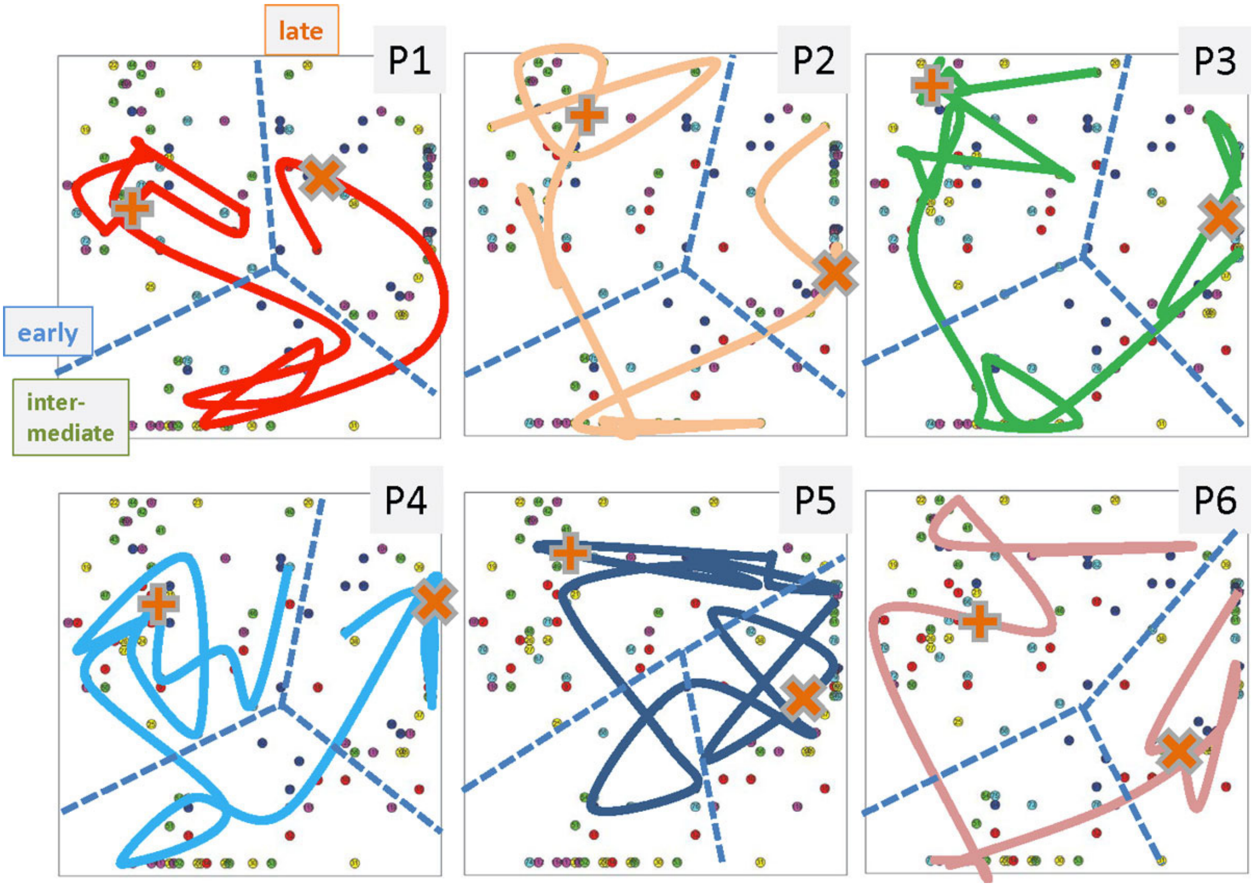

Figure 7 Individual sample trajectories of each of the six probands (P1 - P6) in 2nd level SOM coordinates. Each of the trajectories can be divided into early, intermediate and late time regimes despite small individual differences (dashed lines). The 2nd level SOM was trained with the data of all volunteers. The trajectories shown connect the time-dependent samples of the respective proband. The symbols '+' and 'x' indicate the start and the end of isolation. Note that the trajectory of proband no. 5 (P5) enters the 'late time range' still before starting isolation in correspondence with the respective proteomics portraits shown in Figure 6.

into the early, intermediate and late time ranges. The borderlines separating the different time regimes however slightly shift between the individuals. One also sees that volunteer P5 is characterized by a certainly more intricate trajectory reflecting his individual specifics.

Next, we performed functional analysis by applying gene set enrichment clustering to the single volunteer data (see supplementary text for details). In general, the functional context of the different time ranges agrees with that of the mean volunteer analysis. However, the larger set of individual sample data provides a more detailed view on the specifics of each volunteer. For example, features related to 'immune response' were either up-regulated in the early phase of the experiment only (P1, P4, P6) or, in addition, again in the late phase (P2, P3, P5).

Organ related protein abundance

Proteins not of renal origin fall in urine from blood and in blood from the respective tissues and cells. We used Tissue specific Gene Expression and Regulation data base (TiGER, [15]) to assign protein species to different tissues and assess their abundance in the urine samples studied (see Figure 8 and supplementary text). First we map the tissue-related protein sets to SOM space: It turned out that the respective species of a series of tissue sets accumulate in different regions of the map which were assigned to different time ranges. For example, pancreas and liver proteins show an increased local density in the area of early_up proteins, muscle proteins in the region of intermediate_up region and testis proteins in the late_up region. The respective time profiles confirm the expected activation patterns. We found that proteins from liver, pancreas and kidney show increased abundance before and at the beginning of the isolation experiment. Proteins from muscle are overexpressed at intermediate times of isolation and proteins related to testis and stomach at the end and after isolation. Protein sets related to skin, lymph nodes, blood, prostate, brain

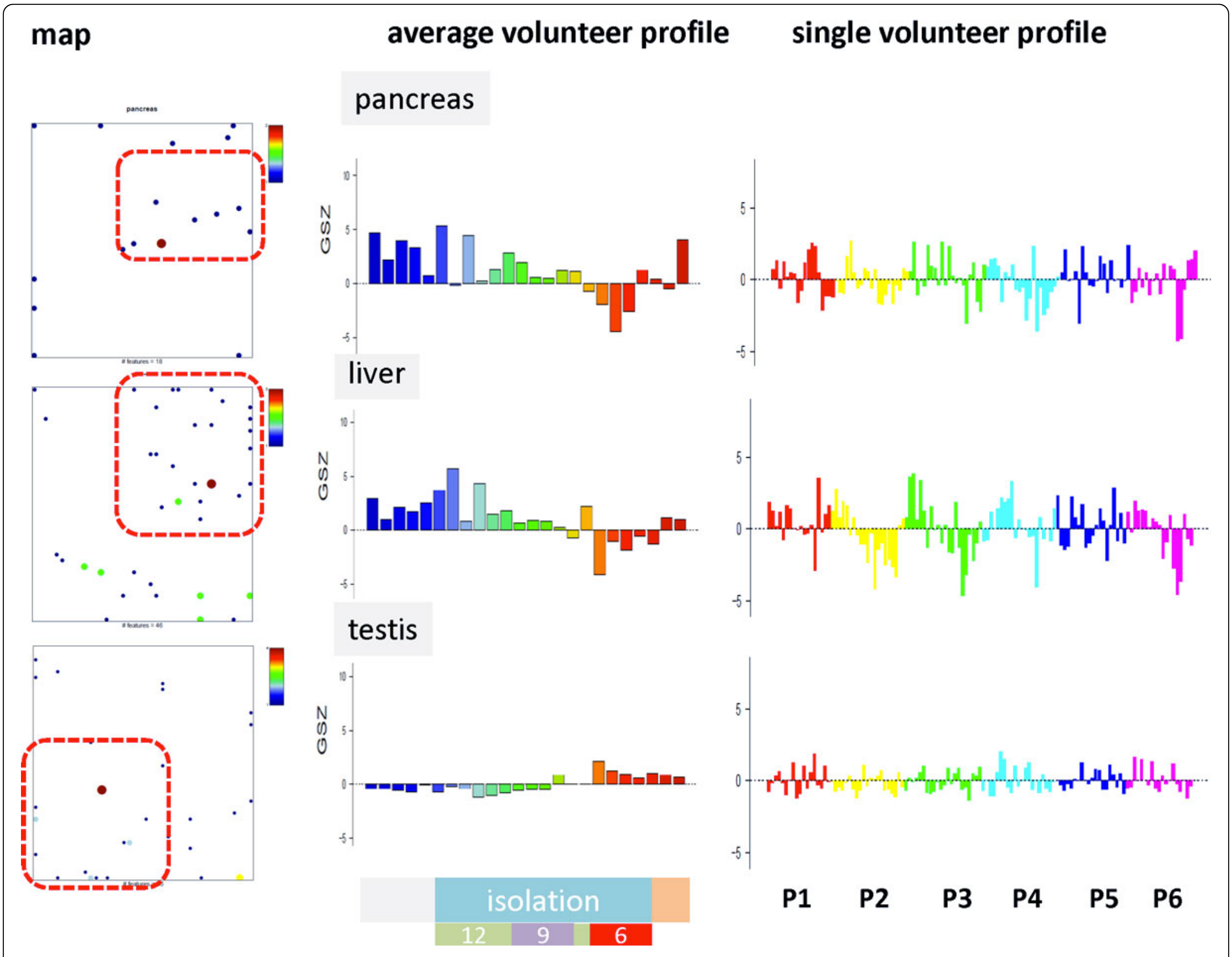

Figure 8 Tissue specific protein abundance: Tissue specific protein sets are taken from TiGR [15]**and mapped into the single volunteer map (left part)**. The red rectangles illustrate regions of increased local density of the respective proteins. These regions refer to the early_up, and late_up time ranges. The set-profiles shown in the middle part clearly reveal the different time profiles in the average volunteer analysis. The respective single volunteer analysis reflects proband-specific differences between their tissue abundances. The respective data of additional tissues (kidney, muscle, stomach, skin, lymph node, blood, prostate, brain, colon) is given in the supplementary text.

and colon show virtually no or only a very weak time dependence in the single volunteer analysis.

The single volunteer tissue profiles again reveal individual differences between the probands: For example, liver proteins of P1 and P5 respond much weaker than liver proteins of the other volunteers. The individual profiles of prostate proteins clearly show time dependencies which however are averaged out in the average volunteer profile due to their asynchronous character (see supplementary text provided in Additional file 1).

Total protein abundance analysis

In addition to single-, meta-feature and spot related abundance levels using centralized values (i.e. normalized ones with respect to the mean value averaged over all volunteers and time points) we analyzed the time profile of the total protein (i.e. integral) abundance level in terms of the variance of the respective meta-feature abundance landscapes (Figure 9). The abundance landscapes refer to a separate SOM training described below and in the supplementary text. It turned out that, on average, the total abundance level slightly increases before isolation in the early time range but then, after a plateau, it steeply decreases in the intermediate and late time ranges until the end of isolation of the volunteers. Hence, isolation causes the overall decrease of protein abundance in the urine samples. In other words, processes down-regulated in the intermediate and late time regimes obviously involve a larger number of proteins and/or their stronger abundance changes than processes up-regulated in the late time regime. Analysis of the population map supports this expectation (see supplementary text): About 27% of the

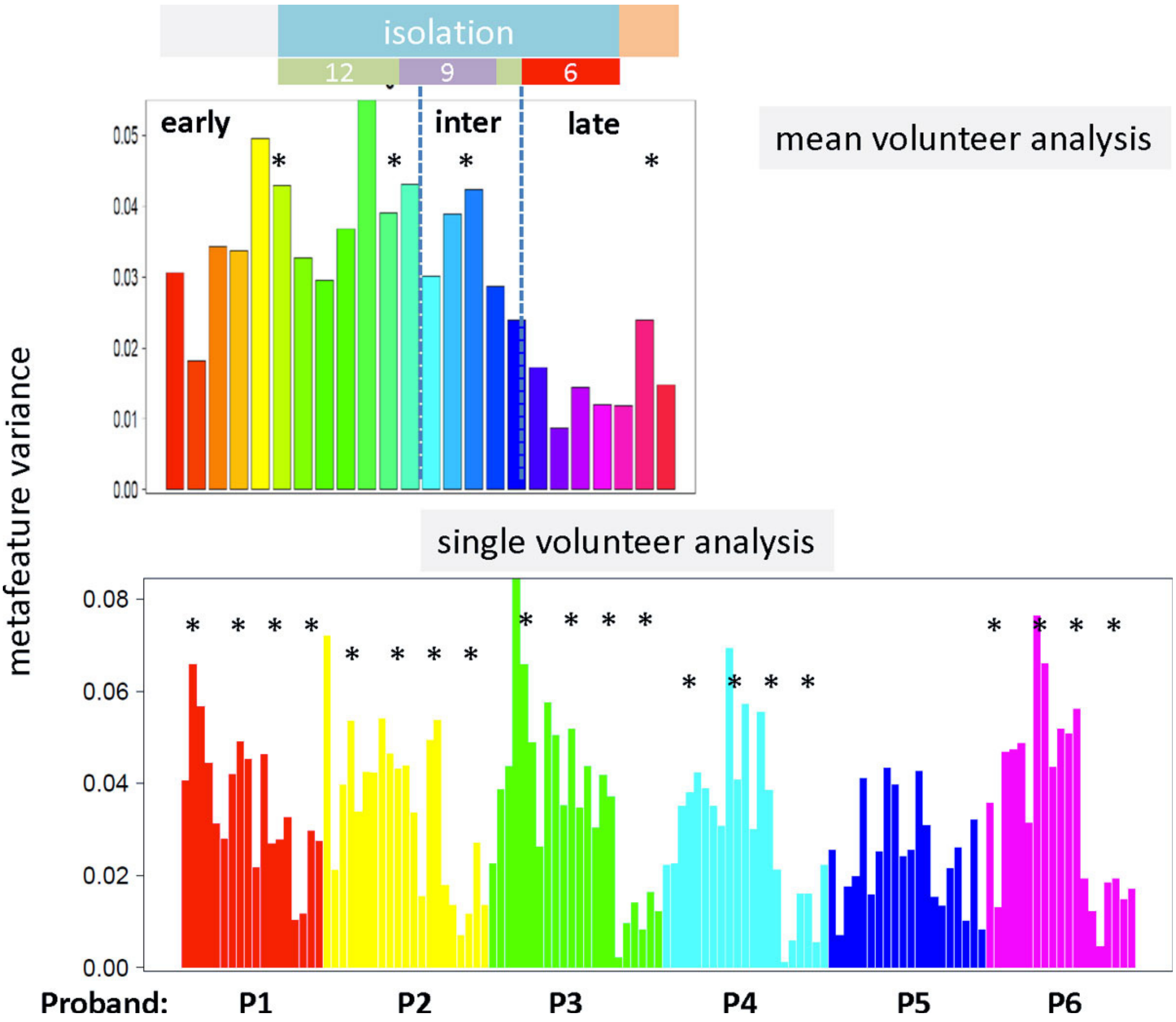

Figure 9 Total level of protein abundance averaged over all probands (part above) and separately for each proband (part below) as a function of time: We calculated the variance of the meta-feature abundance landscapes obtained after SOM training using not-centralized protein abundance profiles. The oordinate values thus estimate the mean squared amplitude of overall abundance as a function of time. The asterisks indicate the sequence of four peaks observed virtually in all data sets.

proteins and 33% of the meta-features are up-regulated in the early time range whereas only 20%/13% of the proteins/meta-features up-regulate in the late regime. The remaining 53%/54% refer to rare and single spiked features. Inspection of the individual volunteer data again reveals slight differences between the total abundance levels of the probands and between details of their respective time courses (Figure 9). For example, P5 shows a decreased total level of protein abundance.

The detailed inspection of all total profiles indicates a certain fine structure in terms of three to four local peaks which appear immediately before or at starting isolation, after reducing salt consumption from 12 to 9 g/day and further to 6 g/day and at the end of the experiment (see the asterisks in Figure 9). Interestingly, adjacent local peaks of total protein abundance are separated by about five weeks possibly reflecting an intrinsic infradian rhythm in protein abundance. The total abundance level slightly increases after finishing isolation indicating slow regeneration of the volunteers. Part of this fine structure is found also in the abundance profiles of selected spot modules, e.g. of the overexpression spots G, E, M, P, J and Q (see Figure 3) expressing one or two sharp peaks in the time regions identified in the total abundance analysis.

To get deeper insight into this phenomenon we performed a full and detailed SOM analysis of the absolute abundance profiles using a similar approach as developed for differential abundance data. Recall that analysis using centralized profiles applied so far focuses on abundance changes independent of the abundance level. For example, virtually invariant profiles of high and of low abundance levels were clustered together in this case. Absolute abundance values certainly distinguish between these two situations. Thus the analysis of absolute abundance profiles is expected to provide additional information about the abundance levels of the proteins in the course of the experiment. Detailed results were described in the supplementary text (Additional file 1). We found that a series of processes become activated in relatively narrow time windows of peaked abundance at the four fixed times identified in total abundance analysis, namely at or immediately before isolation (angiogenesis, complement activation and others), at or immediately after reducing salt consumption to 9 g/day (focal adhesion and cytoskeleton) and to 6 g/day (cell differentiation and organ development) and near the end of the experiment after isolation. The latter trend suggests recovery of the initial state before starting isolation. Double peaked profiles combine peaks at late and intermediate times (e.g. metabolic process and apoptosis). Importantly, immune response processes are permanently active during the experiment with a slight decay in the late time range. About 60% of the proteins are permanently expressed on low abundance levels during the experiment whereas about 7% - 10% are permanently expressed on high abundance levels. This result agrees with our estimation using centralized data.

Discussion

SOM portrays urine proteome abundance landscapes with high temporal and individual resolution

From a methodical point of view we aimed at analyzing a complex high-content data set of about 2000 protein species measured at 24 different time points for six individuals in terms of clustering and class discovery, feature selection an functional information mining using SOM machine learning. The data set is unique and exceedingly valuable with respect to its scope, duration, and level of environmental control. It has been shown that the analysis pipeline chosen is well suited to extract longitudinal (i.e. time dependent) as well as transversal (i.e. volunteer specific) information in detail. One special strength of the approach can be seen in its visualization capabilities allowing the intuitive perception of essential properties of the data such as the detection of spot-like clusters of differentially and co-expressed proteins, and especially, of their time-dependent changes and/or their volunteer-specific variations. The basal results of our SOM analysis are summarized in Figure 10 and Table 1.

We found that

- The dynamics of urine proteomics can be described in terms of sample trajectories reflecting similarity relations between the protein abundance landscapes of the samples as a function of time; or alternatively, in terms of spot trajectories reflecting similarity relations between the time profiles of different groups of co-expressed proteins. Both types of trajectories describe the dynamics of urine proteomics in a complementary fashion.

- The time course of urine proteomics splits roughly into three time ranges, an early, an intermediate and a late one using data averaged over all six volunteers studied. Each of the time ranges is characterized by relatively similar protein abundance landscapes and thus by similar biological processes activated (and deactivated).

- The abundance of about one half (47%) of the 2000 protein species clearly changes in the course of the experiment. The total protein abundance level is maximum in the early time region and then it progressively decreases until the end of the experiment.

- The remaining other half of all proteins (53%) is either expressed invariantly virtually not or weakly responding to the experiment or it shows so-called rare, noisy and single-spiked profiles. The respective protein species are expressed only at very few time points for a small part of the volunteers only. The further analysis and interpretation of these profiles is beyond the scope of this study.

- The volunteer averaged sample trajectory passes through a turning point at the end of the early time range and then it moves backwards in direction of the starting point revealing the partial recovery of the protein abundance state observed before starting isolation on one hand, but also certain differences between the start and end points of the experiment on the other hand.

- The three characteristic time ranges are consistently observed in the individual time course proteomics of all six volunteers. Small but clear individual differences are observed (e.g. relatively low abundance levels of proband no. 5 and slight variations of the start and end points of the time ranges between the individuals). Here we focus on the ubiquitous effects. We note however, that our method enables the personalized view on these individual differences.

- The similar time courses of urine proteomics of all volunteers let us conclude that the three time ranges reflect representative and essential physiological regimes associated with isolation, salt consumption and presumably also other factors. Note that the intermediate and late time ranges start one week after reducing the daily salt consumption from 12 to 9 g and further to 6 g, respectively.

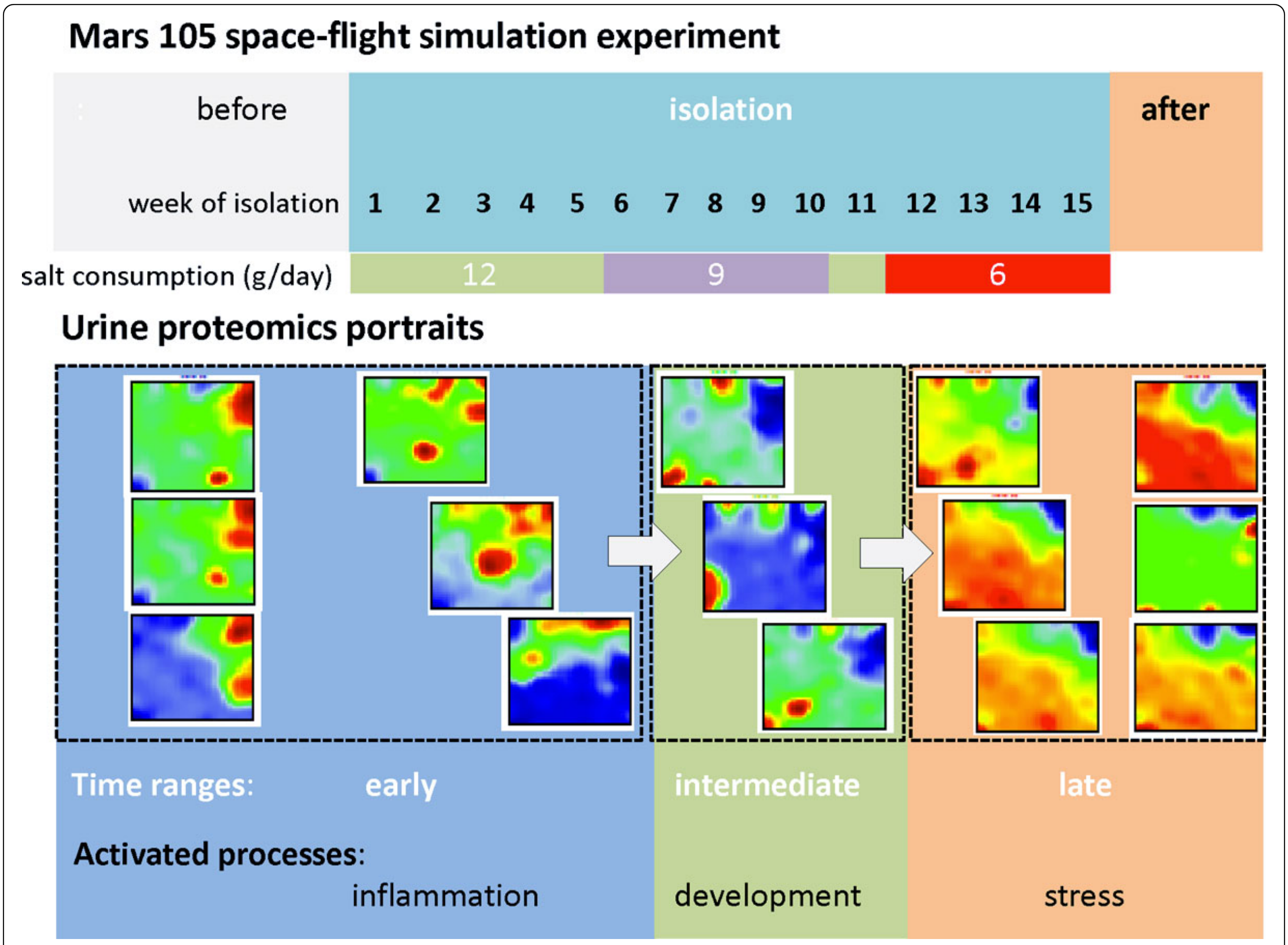

Figure 10 Summary graphics of the time course of urine proteomics during the Mars 105 space-flight simulation experiment.

Table 1 Overview over effects observed in space-flight isolation experiments after analysis of urine proteomics

Time range	early	intermediate	late
week of isolation	before isolation and week 1-6	week 7 - 11	week 12 - 15 and after isolation
NaCl consumption	12 g/day (week 1-6)	9 (week 7-9), 12 (week 10) and 6 g/day (week 11)	6 g/day (week 12-15)
Activated biological processes (enrichment analysis)	inflammation, cell adhesion, blood coagulation, proteolysis, angiogenesis, Ca^{2+} binding, extracellular region	cell division, lipid metabolism, skin development, keratinization, chromatin remodeling, response to oxidative stress and hypoxia, regulation of apoptosis	response to drug/toxin, small molecule metabolic process, intracellular, Mg^{2+} binding, response to Zinc, Cell death, G-protein coupled receptor, regulation of blood pressure (renin/angiotensin)
Activated pathways (PSF analysis)	immune response; nervous system; nucleotide, amino acid and lipid (butanoate) metabolism	digestive system; metabolism; regenerative processes (Wnt-signaling pathway and N-glycan biosynthesis)	signal transduction; response to stress (p53-, mTOR-signaling pathway), energy metabolism (ubiquinone biosynthesis)
Activated tissue responses	Liver, kidney, pancreas, (partly skin)	muscle	testis, stomach, (partly liver and kidney)
Relation to previous results	NaCl related interactome activated [10], NaCl storage in an osmotically inactive form and micro-vascularization [6,7], renal proteins activated [11]		blood pressure decrease and aldosterone level increase [4]
Total protein abundance	increasing and high	decreasing	low
Percentage of proteins up-regulated	27%	20%	

Table 1 Overview over effects observed in space-flight isolation experiments after analysis of urine proteomics *(Continued)*

Percentage of invariant, noisy and single spiked proteins		>50%	
Up-regulated modules	G, E, D, M, N, L	J, P, Q	R
Down-regulated modules	R, Q, J, P	D, E, G, Q, R	G, E, D, M, N, L, P
Module-related proteins (differential abundance)		see Additional file 2	
Module-related proteins (absolute abundance)		see Additional file 3	

- The so-called ‘spots’ collect co-expressed proteins representing regulatory modes associated with distinct biological processes which can be identified using previous knowledge by applying enrichment or pathway flow analysis. In total we identified about ten different modes of protein abundance. Application of different methods of spot selection (e.g. using overexpression, correlation or K-means clustering techniques) essentially provides a consistent picture however with different numbers of proteins associated with the different modules. Significance of co-expression of the proteins of each module was estimated using a beta test adapted to the spot clusters identified in the SOM analysis.

- The larger number of spot modules exceeding the number of time ranges specified reflects the fact that this rough classification into three ranges further splits into different dynamic modes characterized by their phase shift, period and particular shape.

- The separate SOM analysis of absolute abundance values provides additional and complementary results: It allows to identify permanently present and weakly expressed proteins, respectively and it allows to extract single and double peaked abundance profiles presumably indicating immediate responses of urine proteomics to changes of salt consumption and/or infradian rhythms due to other factors.

Urine proteome abundance reflects variations of sodium balance and of related molecular processes

The similar time courses of urine proteomics of all volunteers let us conclude that the three time ranges reflect representative and essential physiological regimes associated with the duration of isolation and salt consumption, the only dietary factor that systematically and markedly changed in the course of the experiment. The intermediate and late time ranges start not later than one week after reducing the daily salt consumption from 12 to 9 g and further to 6 g, respectively (recall that samples were collected only once a week which limits the time resolution of the experiment). Note that a salt consumption of 12 g/day to 6 g/day is considered as the normal range of human daily salt intake. Hence the observed effects are not related to excessive or deficient salt intake compared with this normal range but rather reflect subtle responses to slight but systematic alterations of salt consumption within the normal physiological limits.

For functional interpretation we applied enrichment and pathway signal flow analysis. In general, early protein activation can be related to pro-inflammatory processes as indicated by the GO sets immune response and inflammatory processes, activation at intermediate times to developmental and proliferative processes and late activations to stress and responses to chemicals. It has been reported previously that macrophages, a type of cells in the immune system, besides defending the body against infections appear also to be involved in the regulation of the salt balance and blood pressure [4,6,7]. In body regions with high salt concentrations, they cause the formation of new blood and lymph vessels especially in skin, thus helping to regulate the body’s microcirculation with consequences for the blood pressure. In support of this mechanism we find that processes like angiogenesis, cell adhesion, proteolysis and proteins in cellular components like extracellular region became activated in parallel to pro-inflammatory processes. Moreover, also a set of proteins involved into an interaction network related to organisms response to salt (NaCl) taken from [10] were activated in the early time region immediately following the adjustment of the daily NaCl-dosis to 12 g. Interestingly, the activity of the protein set ‘regulation of blood pressure’ increases slightly in the late phase of the experiment only (see supplementary results). This set collects a group of proteins involved in regulation of blood pressure via the ‘conventional’ renin/angiotensin mechanisms: Their expression stimulates the release of aldosterone which in turn reduces blood pressure. Indeed, the blood concentration of aldosterone is found to continuously increase during the isolation experiment paralleled by the continuous decrease of systolic blood pressure [4].

Part of protein abundance in the early time range can be related to kidney involved in excretion and water balance in agreement with [11]. According to the generally accepted view, sodium accumulation in the human body takes place in the extracellular space and is accompanied by an increase in the rate of fluid retention and body weight gain. In space-flight isolation experiments the relative rate of body weight gain was however lower than the relative rate of gain in the total body sodium, which suggested that sodium accumulated in an osmotically inactive form presumably in bone, skin (connective tissue) or cartilage (see [7] and references cited therein). Proteins usually expressed in skin were only weakly activated in the early time range. Note however that related processes such as keratinization were clearly up-regulated. Other organ specific abundance patterns characteristic for liver and pancreas become also activated in the early time regime. These alterations in protein abundance presumably reflect the effect of isolation, nutrition and salt consumption on digestion and homeostasis. Activation of muscle-specific proteins in the intermediate and of testis-specific proteins in the late time regime are presumably consequences of the physical activity and/or of hormone production of the volunteers during the experiment.

Activation of regenerative processes in the intermediate time range at least partly might be related to reorganization of tissues involved in salt balance and storage. With progressive time of isolation protein abundance strongly decreases. Stress related signatures became increasingly into play accompanied by signatures related to drug metabolism.

Analysis of absolute abundance values shows that part of proteins related to immune response and extracellular space are permanently expressed with a slight decay in the late time range. In contrast, proteins involved in stress response and signal transduction gain in activity in the late phase of isolation. Interestingly, the abundance of proteins related to organ morphogenesis, angiogenesis and cell differentiation seem to respond immediately to changes of salt consumption by abundance peaks of 1-3 weeks duration. The question whether these effects are affected by infradian rhythms due to other effects such as the night-shift of the working regime and/or periodic changes of hormone production and salt balance [3,4] requires further studies.

Summary and conclusions

Ground-based space station model experiments enabled a novel, profound and extended trip to our 'inner space' to discover different aspects of human metabolism. Analysis of urine proteomics data using SOM machine learning in combination with biological function mining provided detailed insights into the physiological status of healthy cosmonaut-volunteers on protein level. Protein abundance characteristics support previous results about alternative mechanisms of salt storage paralleled by the activation of immune response in the context of their influence on micro-vascularization. Based on our results we hypothesize that reduced NaCl consumption of about 6 g/day presumably will reduce or even prevent the activation of inflammatory processes observed in the early time range of isolation. Moreover, the physiological status of the volunteers systematically and consistently changed during the 105 day experiment. Extended studies such as the 500 day isolation study (Mars 500) are required to discover long term effects. Our data also show that the turning point of the time trajectories suggest a first phase of adaptation to the conditions of isolation about two months after starting the experiment. Recovery to the 'normal' physiological status before the experiment is not observed during and directly after isolation.

Methods and data

Experimental setup

Six healthy men aged from 26 to 41 year participated in the ground based isolation experiment. They spent 105 days in an airtight chamber with autonomous systems of life support which is installed in the Institute of Biomedical Problems of the Russian Academy of Sciences. The isolation study was approved by several ethical boards of the Russian Federation and European Space Association authorities. Written informed consent was obtained and all studies were done as outlined in the Declaration of Helsinki.

The regime of salt consumption was reduced from 12 g/day and volunteer in week 1 - 5, to 9 g/day (week 6 - 9) and finally to 6 g/day (week 11 - 15) (see Results section for details). In week 10 volunteers consumed 12 g/day. Urine was sampled (15 ml) once a week in the morning after breakfast (middle jet collection) as described previously [10,16]. In addition, four to six samples were collected from each subject before the isolation experiment and one to three after the experiment. Urine proteomics data were obtained by High Performance Liquid Chromatography and Tandem Mass Spectrometry (HPLC-MS/MS).

Sample Preparation for Mass Spectrometry

Urine samples (15 mL) were concentrated using Amicon UltraUltracel-15 5 k tube (Millipore, USA) at 1,000 g for 1 h at 4°C. The resultant concentrate (300 ml) was then evaporated to dryness in a centrifuge evaporator. Samples were normalized up to total protein concentration of 10 mg/mL using reduction buffer containing 0.2 M Tris-HCl, pH 8.5, 2.5 mM EDTA, 8 M urea. Urinary protein level was measured by standard method with Bradford Protein Kit (Bio-Rad) according to manufacturer recommendations. To reduce cysteine residues the solution of urinary proteins was mixed with dithiothreitol (0.1 M final concentration) and incubated at 37°C. For alkylation of reduced SH-groups, the reaction mixture was cooled and mixed with small amount of concentrated aqueous solution of iodoacetamide up to its final concentration of 0.05 M. After incubation of the reaction mixture at room temperature for 15 min in darkness, the reaction was stopped by adding molar excess of 2-mercaptoethanol (10 ml per mg of added dithiothreitol). Proteins were precipitated by addition of 10 volumes of acetone containing 0.1% (v/v) trifluoro acetic acid and overnight incubation at -20°C. After centrifugation at 12,000 g for 10 min at 4°C the sediment was re-suspended in 96% ethanol (v/v), centrifuged again at 12,000 rpm for 10 min at 4°C, and dried in the centrifuge evaporator for 1 h at 45°C. Trypsinolysis of the urinary protein fraction was performed in 200 mM NH_4HCO_3 buffer (protein concentration about 1 mg/mL) with modified porcine trypsin (Promega, USA) added at the ratio enzyme/protein of 1:100 (w/w). After 6 h incubation at 37°C hydrolysis was stopped with formic acid (final concentration of 3.5%). The solution was centrifuged at 12,000 g for 10 min at 4°C, and the supernatant was analyzed by HPLC-MS/MS [16].

High Performance Liquid Chromatography and Tandem Mass Spectrometry (HPLC-MS/MS)

HPLC-MS/MS experiments were performed in triplicate on a nano-HPLC Agilent 1100 system (Agilent Tech-nologies, Santa Clara, CA, USA) in combination with a 7-Tesla LTQ-FT Ultra mass spectrometer (Thermo Electron, Bremen, Germany) equipped with a nanospray ion source (in-house system) as described in [10,11,16]. A sample volume of 1 µl was loaded by autosampler onto a homemade capillary column (75 µl id, length 12 cm, Reprosil-Pur Basic C18, 3 µm, 100 A; Dr. Maisch HPLC GmbH, Ammerbuch-Entringen, Germany) which was prepared as described in [17]. Separation was performed at a flow rate of 0.3 ml/min using 0.1% formic acid (v/v, solvent A) and acetonitrile 0.1% formic acid (v/v, solvent B). The column was pre-equilibrated with 3% (v/v) solvent B. Linear gradient from 3% to 50% (v/v) of solvent B in 90 min followed by isocratic elution (95% v/v, of solvent B) for 15 min was used for peptide separation. MS/MS data were acquired in data-dependent mode using Xcalibur (Thermo Finnigan, San Jose, CA, USA) software. The precursor ion scan MS spectra (m/z 300-1600) were acquired in FT mode with a resolution of 50000 at m/z 400. The three most intense ions were isolated and fragmented by collision-induced dissociation (CID), MS/MS spectra were measured in the linear ion trap (LTQ). In data-dependent experiments, dynamic exclusion was used with 20 s exclusion duration. In data-dependent experiments, dynamic exclusion was used with 20 s exclusion duration.

Urine proteomics data preprocessing

Raw MS/MS data from the LTQ-FT were processed to msm-files using the software RAW2MSM (version 1.10_2007.06.14) [17]. Mascot database searching was performed using Mascot Server 2.2 software (Matrix Science, London, UK; version 2.2.06); all tandem mass spectra were searched against the human IPI protein sequence database from the European Bioinformatics Institute (version 3.82; released 06.04.2011; 92104 entries) assuming the digestion enzyme trypsin. Search criteria included two missed cleavage, carbamidomethyl of cysteine as a fixed modification, oxidation of methionine as a variable modification, fragment ion mass tolerance of 0.50 Da (10 ppm). Protein identifications were accepted if they contained at least 2 identified peptides with ion scores >24. The results were verified against reverse database to a false discovery rate of less than 1% using Scaffold 4.0 software (version Scaffold-01_07_00, Proteome Software Inc., Portland, OR). All Mascot search results and parameters are submitted to the PeptideAtlas (submission PASS00592) repository and are freely available for download with the URL: http://www.peptideatlas.org/PASS/PASS00592. The data file with peptides and proteins are also provided as Additional file 4.

This preprocessing provides 2,038 species indexed by the international protein indices (IPI) in the Mascot data base. All protein species indexed by IPI were included into our analysis. 1660 (71%) of them were explicitly assigned to genes using the biomaRt program package available in the bioconductor repository with query to Ensemble gene annotations http://www.bioconductor.org/packages/release/bioc/html/biomaRt.html. The presence/absence of each protein species in each sample was defined by binary 1/0 values providing an abundance matrix for each volunteer where each row corresponds to one protein and each column to one time point of sample selection (Additional file 5). For downstream analysis we used either these individual, volunteer-specific data (single volunteer analysis) or we calculated the mean abundance for each protein and time point by averaging protein data over the individual volunteers (mean volunteer analysis). Single volunteer abundance data are provided as Additional file 5.

The time course of abundance of each protein is called abundance or expression time profile whereas the abundance of all proteins considered at one time point is called abundance or expression state. We will use the terms 'abundance' and 'expression' (of proteins in urine) as synonyms throughout the paper. Effectively a protein species is present if its MS-signal exceeds the mean detection threshold in a constant volume of urine (15 ml). Note that the amount of proteins detected refers to a constant volume collected and thus 'protein abundance' estimates protein concentration in urine. Decreased amounts of proteins detected thus can be explained by decreased protein penetration into urine at stable water reabsorption/dilution and/or by decreased water reabsorption by kidney at a constant amount of penetrated proteins. This latter 'dilution' effect seems however to play a minor role (i) because total water balance and/or urine excretion varies to a much less extent compared with the decrease in total protein abundance detected [4]; and (ii) because the protein composition alters very strongly reflecting marked changes of the underlying physiology. Upon simple dilution one would expect only weak alterations of the protein composition.

For further analysis we used centralized abundance profiles as standard by subtracting the mean abundance value of each profile from the raw profile data. Positive and negative values consequently define the range of over- and under-presence of each protein species relatively to its mean value, respectively. Such centralized data accent alterations of protein expression independent of its absolute expression level. The SOM algorithm (see below) clusters profiles of proteins showing similar changes together. Hence, also invariantly high and invariantly low expressed proteins are clustered together. To analyze the absolute abundance level of the data we also used data without centralization. Detailed results of this analysis are presented in the supplementary text.

SOM machine learning

We used an analysis pipeline based on the R-program opoSOM developed previously for high-throughput gene expression analysis [13,14]. It transforms the abundance values of all proteins measured into an abundance landscape per state. It serves as fingerprint portrait of the respective proteomic phenotype. The program also performs a series of useful downstream analysis tasks such as sample similarity-, differential feature selection- and gene set enrichment-analyses.

After appropriate initialization (see [14]) the SOM-algorithm distributes the proteins over a 40x 40 two-dimensional quadratic grid such that each protein profile is associated with the most similar grid point using the Euclidian distance as criterion. The grid points are called 'meta features'. Then the method iteratively adjusts the meta-feature profiles in small increments to agree better with the observed protein profiles. In consequence, the resulting two-dimensional map of meta-profiles optimally covers all protein profiles observed experimentally. Moreover, the map becomes self-organized, which means that proteins of similar profiles are clustered together, whereas proteins with distinct abundance profiles localize in different regions of the map.

The training thus translates the abundance data given as N × M matrix (N = 2037: number of proteins, M= 24 number of time points in mean volunteer) into a K × M matrix (K = 1600: number of meta-features). Each proteomic phenotype is visualized by color-coding the grid points in the two-dimensional grid of meta-features according to their abundance values from red to blue for high to low abundance values, respectively. Neighbored meta-features tend to be colored similarly owing to their similar profiles. In consequence the obtained mosaic images show a smooth texture with red and blue spot-like regions referring to clusters of over- and under-expressed proteins, respectively.

The SOM portraying methods has been applied before to different omics data including also proteomics data for MALDI-typing [18] (see also [19] and references cited therein). In extensive benchmark tests we showed that SOM outperforms alternative methods for dimension reduction of high-dimensional data [13]. Finally, parameter settings for optimal performance of the methods have been systematically studied before [13,14,19].

Spot module selection, enrichment analysis and Beta correlation testing

To identify groups of co-expressed proteins we applied an over- and under-expression spot module selection method: It first averages each meta-feature value over all individual expression states considered and then selects the maximum and minimum 2-percentile of them, respectively. Then the spot-modules were defined as closed areas of adjacent, i.e. mutually connected meta-features in the map. Alternatively we tested two different module selection methods based on correlation and K-means clustering, respectively (see supplementary text).

Proteins from the same module are co-abundant in the experimental series and define a functional module according to the 'guilt-by-association' principle [20]. We applied *gene set enrichment analysis* to discover the functional context of the module using a data base of a few thousand predefined gene sets according to gene ontology (GO) classification as described in [14]. Enrichment scores are calculated using either Fishers exact test or the 'gene set enrichment Z-score' (GSZ) as proposed in [21]. The former score estimates the probability that the number of proteins from the set is found in the list of proteins in a module given the total number of proteins studied. The GSZ-score in addition considers the degree of overexpression of the proteins in the spot (see also [14] for details).

Interrelations between the spot modules are characterized in terms of the *weighted topological overlap network* (wTO) based on correlations between the meta-features as described in [12]. It considers not only direct correlations between all pairwise combinations of meta-features in the spots but also 'mediated' ones acting via all possible third meta-features in the map [22].

We adapted a multi-test-adjusted *correlation test* based on beta-test statistics as proposed previously [23] to estimate the significance of concerted expression of the proteins in each of the modules identified. This test calculates the significance that the group of proteins collected in a given module shows concerted abundance profiles. Significance is estimated using the beta value of each spot. It is defined as the squared ratio of two sum correlations, namely of the sum correlation between the mean module profile and the single feature profiles of the module and the sum correlation between all single features of the module. Our method substitutes the single feature profiles by the profiles of the respective meta-features to reduce the computational efforts. The beta test statistics is transformed into a p-value which estimates the multi-test-adjusted probability of the null hypothesis, namely that the single protein expression values of the module do not correlate each with another. Details of the method are given in the Supplementary Text section provided as Additional file 1.

Pathway signal flow analysis of selected KEGG pathways

The Pathway Signal Flow (PSF) algorithm evaluates the changes in signal flows for a given pathway depending on the pathway topology and relative protein expression measured [24]. Particularly, it evaluates how a signal from network inputs spreads downstream from source nodes to sink nodes depending on the relative expression of the proteins forming the nodes and the types of interactions between them [25]. The more changes in the pathway flow are observed, the more it is likely that the given pathway will be involved into biological processes underlying the phenotypic differences between the conditions studied. The relative expression of a node is calculated as the mean of the relative abundance (fold change) of all items in the given node. The PSF method uses Kyoto Encyclopedia of Genes and Genomes (KEGG) Pathway database as the source of molecular pathway information [26]. We compared PSF time profiles with the time profiles of selected modules to assign the respective biological functions as described in Additional file 1.

Time trajectories

Time trajectories aim at visualizing the time-dependent changes of the proteomics phenotypes studied. We applied standard sample similarity analysis using 2nd level SOM and independent component analysis (ICA). Both methods project the samples into 'similarity space' which allows establishing the trajectory as the sequence of subsequent time points. Similarity analysis compares the protein expression states as seen by the SOM portraits. It uses the abundance of meta-features as the input data, which has the advantage of improving the representativeness and resolution of the results [13]. We applied 2nd level SOM analysis as proposed in [27] to visualize the similarity relations between the samples. This method has the advantage that it projects also high-dimensional multivariate data into two dimensions which allows their straightforward evaluation. Its disadvantage is that the obtained phase space is scaled non-linearly and non-orthogonally with respect to different, mutually independent variables. We therefore also applied ICA [28] to the SOM meta-feature data using the R-package 'fastICA'. It distributes the samples in the phase space spanned by the components of minimal mutual statistical dependence. These components point along the directions of maximum information content in the data which is estimated by their deviation from a (non-informative) normal distribution [29].

Additional material

Additional file 1: Supplementary text includes supplementary methods, results, figures and tables.

Additional file 2: Lists of differentially expressed proteins in the overexpression spot modules.

Additional file 3: List of proteins in the K-means clusters segmented in the SOM of absolute protein abundance data.

Additional file 4: Single volunteer proteomics data.

Additional file 5: Protein abundance matrix used for SOM analysis.

Competing interests

The authors declare that they have no competing interests.

Authors' contributions

Conceived and designed the experiments: IML, ENN; performed the experiments and performed primary LC/MS-proteomics analysis: AK, IP, ENN, IML, LKP, conceived and designed downstream proteomics analysis (SOM and pathway analysis): HB, HW, AA, VI; NAK; performed downstream analysis: HB, HW, AA, KL, EST; wrote the paper: HB, IL, AK.

Acknowledgements

AA thanks DAAD (German Academic Exchange Service) for financial support during his stay in Leipzig at IZBI in summer 2013.

Declarations

Publication of this article has been funded in part by the BMBF within the frame of the German-Russian network of Bioinformatics and Biotechnology (the SOM analysis); Russian Science Foundation grant No 14-24-00114 (AK, IP and EN acknowledge the support in performing of all mass spectrometry measurements); Russian Science Foundation grant No 14-24-00123 (EST, VAI and NAK acknowledge the support in performing of the computer analysis of biological pathways and processes).
This article has been published as part of *BMC Genomics* Volume 15 Supplement 12, 2014: Selected articles from the IX International Conference on the Bioinformatics of Genome Regulation and Structure\Systems Biology (BGRS\SB-2014): Genomics. The full contents of the supplement are available online at http://www.biomedcentral.com/bmcgenomics/supplements/15/S12.

Authors' details

[1]Interdisciplinary Centre for Bioinformatics, Universität Leipzig, Leipzig, Germany. [2]Institute of Molecular Biology NAS RA; Yerevan, Armenia. [3]Institute of Cytology and Genetics SB RAS, Novosibirsk, Russia. [4]Talrose Institute for Energy Problems of Chemical Physics, RAS, Moscow, Russia. [5]Emanuel Institute for Biochemical Physics, RAS, Moscow, Russia. [6]Moscow Institute of Physics and Technology, Dolgoprudnyi, Russia. [7]Skolkovo Institute of Science and Technology, Skolkovo, Russian Federation. [8]Institute of Biomedical Problems - Russian Federation State Scientific Research Center RAS, Moscow, Russia.

Published: 19 December 2014

References

1. Ortiz-Melo D, Coffman Thomas M: **A Trip to Inner Space: Insights into Salt Balance from Cosmonauts.** *Cell metabolism* 2013, **17(1)**:1-2.
2. Mozaffarian D, Fahimi S, Singh GM, Micha R, Khatibzadeh S, Engell RE, Lim S, Danaei G, Ezzati M, Powles J: **Global Sodium Consumption and Death from Cardiovascular Causes.** *New England Journal of Medicine* 2014, **371(7)**:624-634.
3. Rakova N, Jüttner K, Rauh M, Dahlmann A, Goller U, Beck L, Agureev A, Vassilieva G, Lenkova L, Johannes B, Wabel P, Moissl U, Vienken J, Gerzer R, Eckardt KU, Müller DN, Kirsch K, Morukov B, Luft FC, Titze J: **Ultra long-term sodium balance studies during the Mars500 campaign.** *Aktuel Ernahrungsmed* 2012, **37(03)**:P9_5.
4. Rakova N, Jüttner K, Dahlmann A, Schröder A, Linz P, Kopp C, Rauh M, Goller U, Beck L, Agureev A, Vassilieva G, Lenkova L, Johannes B, Wabel P, Moissl U, Vienken J, Gerzer R, Eckardt KU, Müller Dominik N, Kirsch K, Morukov B, Luft Friedrich C, Titze J: **Long-Term Space Flight Simulation Reveals Infradian Rhythmicity in Human Na+ Balance.** *Cell metabolism* 2013, **17(1)**:125-131.
5. Titze J, Larina IM, Garib K, Kirsch KO, Maye A, Lang R, Gunga HK, Johanes B, Gochlen-Koch H, Kim E: **Monitoring of Sodium Balance during Long-Term Isolation of Humans in a Ground-Based Space Station Model.** *Hum Physiol* 2003, **29(5)**:595-605.
6. Kleinewietfeld M, Manzel A, Titze J, Kvakan H, Yosef N, Linker RA, Muller DN, Hafler DA: **Sodium chloride drives autoimmune disease by the induction of pathogenic TH17 cells.** *Nature* 2013, **496(7446)**:518-522.
7. Machnik A, Neuhofer W, Jantsch J, Dahlmann A, Tammela T, Machura K, Park JK, Beck FX, Muller DN, Derer W, Goss J, Ziomber A, Dietsch P, Wagner H, van Rooijen N, Kurtz A, Hilgers KF, Alitalo K, Eckardt KU, Luft FC, Kerjaschki D, Titze J: **Macrophages regulate salt-dependent volume and blood pressure by a vascular endothelial growth factor-C-dependent buffering mechanism.** *Nat Med* 2009, **15(5)**:545-552.
8. Marvar PJ, Gordon FJ, Harrison DG: **Blood pressure control: salt gets under your skin.** *Nat Med* 2009, **15(5)**:487-488.
9. Valeeva OA, Pastushkova LK, Pakharukova NA, Dobrokhotov IV, Larina IM: **Variability of urine proteome in healthy humans during a 105-day isolation in a pressurized compartment.** *Hum Physiol* 2011, **37(3)**:351-354.
10. Larina IM, Kolchanov NA, Dobrokhotov IV, Ivanisenko VA, Demenkov PS, Tiys ES, Valeeva OA, Pastushkova LK, Nikolaev EN: **Reconstruction of associative protein networks connected with processes of sodium exchange regulation and sodium deposition in healthy volunteers based on urine proteome analysis.** *Hum Physiol* 2012, **38(3)**:316-323.
11. Pastushkova LK, Kireev KS, Kononikhin AS, Tiys ES, Popov IA, Starodubtseva NL, Dobrokhotov IV, Ivanisenko VA, Larina IM, Kolchanov NA, Nikolaev EN: **Detection of Renal Tissue and Urinary Tract Proteins in the Human Urine after Space Flight.** *PLOS one* 2013, **8(8)**:e71652.
12. Hopp L, Wirth H, Fasold M, Binder H: **Portraying the expression landscapes of cancer subtypes: A glioblastoma multiforme and prostate cancer case study.** *Systems Biomedicine* 2013, **1(2)**.
13. Wirth H, Loeffler M, von Bergen M, Binder H: **Expression cartography of human tissues using self organizing maps.** *BMC Bioinformatics* 2011, **12**:306.
14. Wirth H, von Bergen M, Binder H: **Mining SOM expression portraits: Feature selection and integrating concepts of molecular function.** *BioData Mining* 2012, **5**:18.
15. Liu X, Yu X, Zack D, Zhu H, Qian J: **TiGER: A database for tissue-specific gene expression and regulation.** *BMC Bioinformatics* 2008, **9(1)**:271.
16. Agron IA, Avtonomov DM, Kononikhin AS, Popov IA, Moshkovskii SA, EN N: **Accurate mass tag retention time database for urine proteome analysis by chromatography-mass spectrometry.** *Biochemistry (Mosc)* 2010, **75(5)**:636-641.
17. Ishihama Y, Rappsilber J, Andersen JS, M M: **Microcolumns with selfassembled particle frits for proteomics.** *J Chromotography A* 2002, **979(1-2)**:233-239.
18. Wirth H, von Bergen M, Murugaiyan J, Rösler U, Stokowy T, Binder H: **MALDI-typing of infectious algae of the genus Prototheca using SOM portraits.** *Journal of Microbiological Methods* 2012, **88(1)**:83-97.
19. Binder H, Wirth H: **Analysis of large-scale OMIC data using Self Organizing Maps.** In *Encyclopedia of Information Science and Technology.* Third Edition edition. IGI global;Khosrow-Pour M 2014:1642-1654, in press.
20. Quackenbush J: **Microarrays–Guilt by Association.** *Science* 2003, **302(5643)**:240-241.
21. Toronen P, Ojala P, Marttinen P, Holm L: **Robust extraction of functional signals from gene set analysis using a generalized threshold free scoring function.** *BMC Bioinformatics* 2009, **10(1)**:307.
22. Zhang B, Horvath S: **A general framework for weighted gene co-expression network analysis.** *Statist Appl Genet Mol Biol* 2005, **5(1)**:17.
23. Läuter J, Horn F, Rosolowski M, Glimm E: **High-dimensional data analysis: Selection of variables, data compression and graphics - Application to gene expression.** *Biometrical Journal* 2009, **51(2)**:235-251.
24. Arakelyan A, Nersisyan L: **KEGGParser: parsing and editing KEGG pathway maps in Matlab.** *Bioinformatics* 2013, **29(4)**:518-519.
25. Arakelyan A: **High-throughput Gene Expression Analysis Concepts and Applications.** *Sequence and Genome Analysis II - Bacteria, Viruses and Metabolic Pathways* Hong Kong: iConcept Press; 2013.
26. Kanehisa M, Goto S: **KEGG: kyoto encyclopedia of genes and genomes.** *Nucleic Acids Res* 2000, **28(1)**:27-30.
27. Guo Y, Eichler GS, Feng Y, Ingber DE, Huang S: **Towards a Holistic, Yet Gene-Centered Analysis of Gene Expression Profiles: A Case Study of Human Lung Cancers.** *Journal of Biomedicine and Biotechnology* 2006, **2006, Article ID 69141.**
28. Hyvärinen A, Oja E: **Independent component analysis: algorithms and applications.** *Neural Networks* 2000, **13(4-5)**:411-430.
29. Liebermeister W: **Linear modes of gene expression determined by independent component analysis.** *Bioinformatics* 2002, **18(1)**:51-60.

doi:10.1186/1471-2164-15-S12-S2
Cite this article as: Binder *et al.*: Time-course human urine proteomics in space-flight simulation experiments. *BMC Genomics* 2014 **15**(Suppl 12): S2.

Supplementary Text

Time-course human urine proteomics in space-flight simulation experiments

Hans Binder[1]*, Henry Wirth[1], Arsen Arakelyan[2], Kathrin Lembcke[1], Evgeny S. Tiys[3], Vladimir A. Ivanisenko[3], Nicolay A. Kolchanov[3], Alexey Kononikhin[4,6], Igor Popov[5,6], Evgeny N. Nikolaev[4,5,6,7]*, Lyudmila Kh. Pastushkova[8], Irina M. Larina[8]

[1] Interdisciplinary Centre for Bioinformatics, Universität Leipzig, Leipzig, Germany
[2] Institute of Molecular Biology NAS RA; Yerevan, Armenia
[3] Institute of Cytology and Genetics SB RAS, Novosibirsk, Russia
[4] Talrose Institute for Energy Problems of Chemical Physics, RAS, Moscow, Russia
[5] Emanuel Institute for Biochemical Physics, RAS, Moscow, Russia
[6] Moscow Institute of Physics and Technology, Dolgoprudnyi, Russia
[7] Skolkovo Institute of Science and Technology, Skolkovo, Russian Federation
[8] Institute of Biomedical Problems – Russian Federation State Scientific Research Center RAS, Moscow, Russia

*Corresponding authors:
Hans Binder. University of Leipzig, Interdisciplinary Centre for Bioinformatics (IZBI), 04107 Leipzig, Haertelstr. 16-18, Germany; e-mail: binder@izbi.uni-leipzig.de; Tel.: +49-341-9716671; Fax: +49-341-9716679

E.N. Nikolaev. Institute for Energy Problems of Chemical Physics Russian Academy of Sciences, Leninskij pr.38 k.2, 119334 Moscow, Russia, e-mail: ennikolaev@rambler.ru

Content

1 Supplementary methods

1.1 Beta correlation test of spot modules

We consider a spot-module taken from the SOM map representing a cluster of s=1,…,S meta-features which, in turn, are ‘micro-clusters’ of n_s single features. In total, the spot thus contains $P = \sum_{s=1}^{S} n_s$ single features. Meta features and single features are given as time profiles of protein expression values (E_{pt}, E_{st}^{meta}, respectively) centralized with respect to their mean value, averaged over all time points t=1,…, T of the measurement:

$$\begin{aligned} \Delta E_{st}^{meta} &= E_{st}^{meta} - \tfrac{1}{T}\sum_{t=1}^{T} E_{st}^{meta} \quad and \\ \Delta E_{pt} &= E_{pt} - \tfrac{1}{T}\sum_{t=1}^{T} E_{pt} \quad , \quad p = 1...P \end{aligned} \quad , \qquad (1)$$

respectively. The ΔE thus define differential expression values given in units of the mean binary detection level (E=0 for absent and E=1 for present). Each spot cluster is characterized by the spot-averaged expression profile

$$\Delta E_t^{spot} = \frac{1}{S \cdot P}\sum_{s=1}^{S} n_S \cdot \Delta E_{st}^{meta} \approx \frac{1}{P}\sum_{p=1}^{P} \Delta E_{pt} \; . \qquad (2)$$

The latter equation considers the fact, that each meta feature profile is given to a good approximation by the average over all single features of the microcluster. The meta-feature profiles in Eq. (2)are weighted with the respective numbers of single features per meta-feature.

We now aim at testing whether ΔE_t^{spot} is significantly co-expressed with the set of single expression values contained in the meta-features of the spot Δe_{pt} or not. For this purpose we make use of the correlation test introduced previously [1, 2]: It states that the correlation of a set of variables x_{tp}(p=1,…,P; t=1,…,T) with a selected variable y_t is significant at level α if it meets the condition

$$\begin{aligned} beta &\geq BETA_{1-\alpha}(\tfrac{1}{2}, \frac{T-2}{2}) \quad with \\ beta &\equiv \frac{\left((Y-\overline{Y})'(Z-\overline{Z})\right)^2}{(Y-\overline{Y})'(Y-\overline{Y}) \cdot (Z-\overline{Z})'(Z-\overline{Z})} \end{aligned} \qquad (3)$$

and

$$X = \begin{pmatrix} x_{11} & \cdots & x_{1P} \\ \vdots & \ddots & \vdots \\ x_{T1} & \cdots & x_{TP} \end{pmatrix} \quad , \quad Z = XD \quad and \quad Y = \begin{pmatrix} y_1 \\ \vdots \\ y_T \end{pmatrix}. \qquad (4)$$

The diagonal matrix D with the elements $d_{pp} = \mathrm{var}(X_p)^{-1/2} \equiv \left(\left(X_p - \overline{X_p}\right)'\left(X_p - \overline{X_p}\right)\right)^{-1/2}$ z-normalizes X_p, the column vectors of X. $\overline{X_p} \equiv \tfrac{1}{T}\sum_{t=1}^{T} x_{tp}$ denotes the respective column-average (in Eq. (3), analogously for Y and Z). Eq. (3)states that the beta test statistics is distributed according to the beta-distribution,

$$f(beta) = beta^{-1/2} \cdot (1 - beta)^{T/2-2} \,/\, BETA_1(\tfrac{1}{2}, \frac{T-2}{2}) \,.$$

Eqs. (3) - (4) apply to Eqs. (1) - (2) if one simply sets

$$y_t = \Delta E_t^{spot} \quad and \quad x_{tp} = \Delta E_{pt} \ . \tag{5}$$

The test statistics can be expressed as

$$beta = q^2 \quad with \quad q = \frac{\sum_{p=1}^{P} r_{yp}}{\left(\sum_{p=1}^{P} \sum_{p'=1}^{P} r_{pp'} \right)^{1/2}} \qquad , \tag{6}$$

where q is the ratio of two sum correlations, namely the correlation between Y and Z and the correlation between the columns of Z, i.e.

$$r_{yp} = \frac{(Y - \overline{Y})'(Z_p - \overline{Z_p})}{\mathrm{var}(Y)^{1/2}} \quad and \quad r_{pp'} = (Z_p - \overline{Z_p})'(Z_{p'} - \overline{Z_{p'}}) \quad , \tag{7}$$

respectively. Then the p-value estimates the probability that the single features in the spot cluster are not significantly correlated and thus not co-expressed,

$$beta \sim BETA_{1-p}(\tfrac{1}{2}, \frac{T-2}{2}) \qquad . \tag{8}$$

Let us assume

$$\sum_{p=1}^{P} r_{yp} \approx \tfrac{1}{P} \sum_{s=1}^{S} n_s r_{ys} \quad and \quad \sum_{p=1}^{P} \sum_{p'=1}^{P} r_{ij} \approx \tfrac{1}{P^2} \sum_{s=1}^{S} \sum_{s'=1}^{S} n_s n_{s'} \cdot r_{ss'} \qquad , \tag{9}$$

to a good approximation, i.e. we replace the sum correlations of the single features with that of the meta features and weight them with their populations. Accordingly, the elements of the X-matrix in Eq. (5) should be replaced with

$$x_{sp} = \Delta E_{ps}^{meta} \qquad . \tag{10}$$

The beta test was also applied to the meta-features of the map. In this case Eq. (3) applies with

$$y_t = \Delta E_{st}^{meta} \quad , \quad x_{tp} = \Delta E_{pt} \quad and \quad P = n_{meta} \,. \tag{11}$$

It relates the sum correlation of the single features with the meta feature to the mutual sum correlation of the single features.

1.2 Pathway signal flow analysis

Biological pathways are directed and spatially defined sets of bio-molecular physical and regulatory interactions that represent information propagations (or signal flow) leading to functional realizations of biological processes. Thus, molecular pathways can be represented as directed graphs with nodes corresponding to genes, proteins, and compounds and edges depicting directed relationships between nodes (Figure S 1).

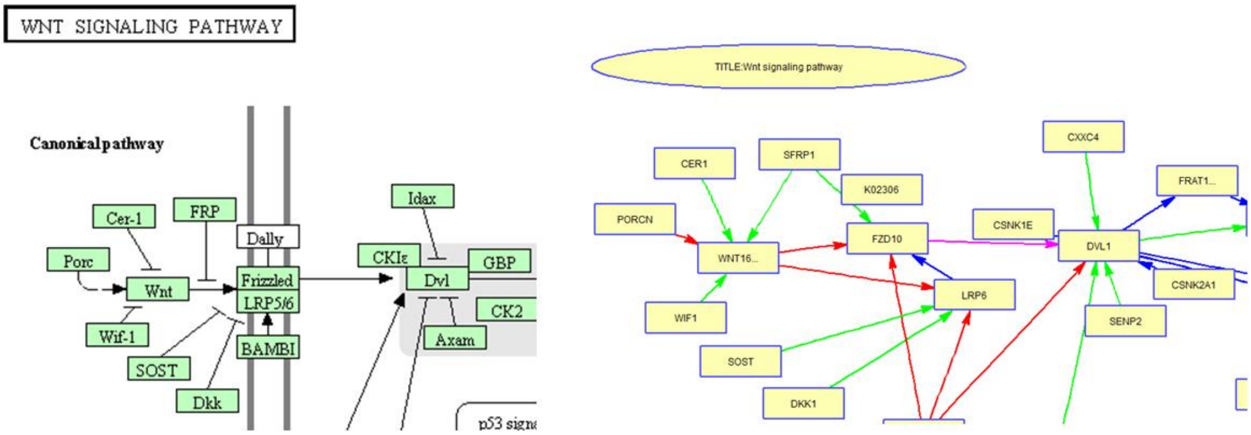

Figure S 1: Fragment of the KEGG Pathway Wnt-signaling pathway map image and corresponding graph object parsed from the KGML file.

Graph structure representation is often used to store pathway information in machine-readable format, usually, as xml files. For KEGG pathway images graph structures are stored in KGML (KEGG pathway xml format) files that can be used for automated analysis of pathways. Using KEGG parser - a Matlab tool for parsing and editing pathways maps we obtained graphs object for 258 pathways containing in KEGG pathway database[3]. Different interaction types present in KEGG pathways (i.e. phosphorylation, de-phosphorylation, ubiquitination, methylation, glycolysation, indirect effect, binding, etc.) were generalized in terms of their functional effect into two types: activation and inhibition.

Pathway topology is an important characteristic of a pathway and is pivotal for its functioning. The terminal (source and sink) genes seem to be more important from the viewpoint of signal transduction, than genes located in the middle of the pathway. On the other hand, pathway branching and mean number of interactions per gene may also highly influence gene-expression dependent signal transduction. Next parameter influencing pathway activation is the expression level of individual genes/gene products ingiven pathway. Expression, being the marker of gene/protein activity in the cell, is estimated based on the amount of mRNA/protein that has been synthesized from the given gene. Thus based on these two parameters it is possible to identify how pathway activity can be changed compared to reference state.

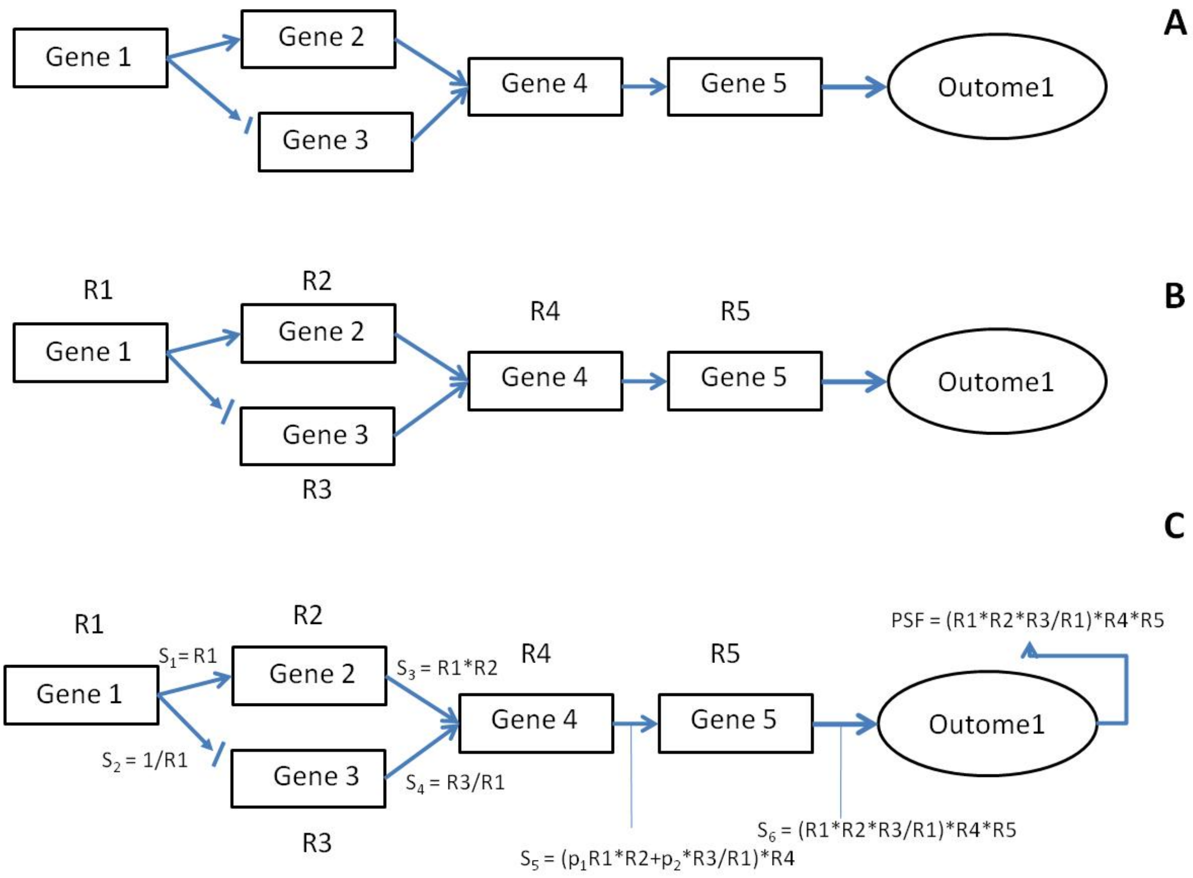

Figure S 2: Schematic representation of PSF algorithm workflow on hypothetic pathway graph.

Figure S 2 schematically shows main steps of pathway signal flow (PSF) calculation. It starts with topological sorting of pathway graphs to identify source (input/ gene1) and sink (output/outcome) nodes. Feedback loop containing pathways is sorted partially. After this step an initial unity signal is applied to the pathway source node(s). The signal flow at the outgoing edge is set equal to the product of input signal and relative expression of source node:

$$S_i= S_{i-1}^{k}R_i,$$

where R_i is the relative expression of node i; S_{i-1}^{k} is signal flow at the node incoming edges. k defines the activation exponent with k = 1, if node (i-1) activates node i and k = -1, if node (i-1) inhibits node i. If a node has two or more inputs, its relative expression is partitioned based on the value of input signals and then it is summarized. Signal flow at the sink nodes of a pathway is considered as pathway signal flow (PSF). Significance of pathway flow perturbation is calculated by reshuffling node relative expressions 1000 times and constructing the empirical distribution.

We compared temporal profiles of spot expressions with profiles of pathway flow perturbations in order to identify pathways associated with each spot cluster derived from SOM analysis. Temporal association of pathway signal perturbations with spot expression were performed using regression. R^2>0.8 cutoff for association was chosen.

It should be noted that many pathways have more than one functional outcome. For example activation of WNT signaling pathway (Figure S 3) may cause activation of Cell Cycle, Adherens junction pathways, proteolysis, gene expression trough activation of NFAT, etc. Thus differential activation of genes belonging to different pathway branches may lead to perturbations of different outcomes. In such multi-branch pathways PSF and its significance is calculated for each functional outcome separately.

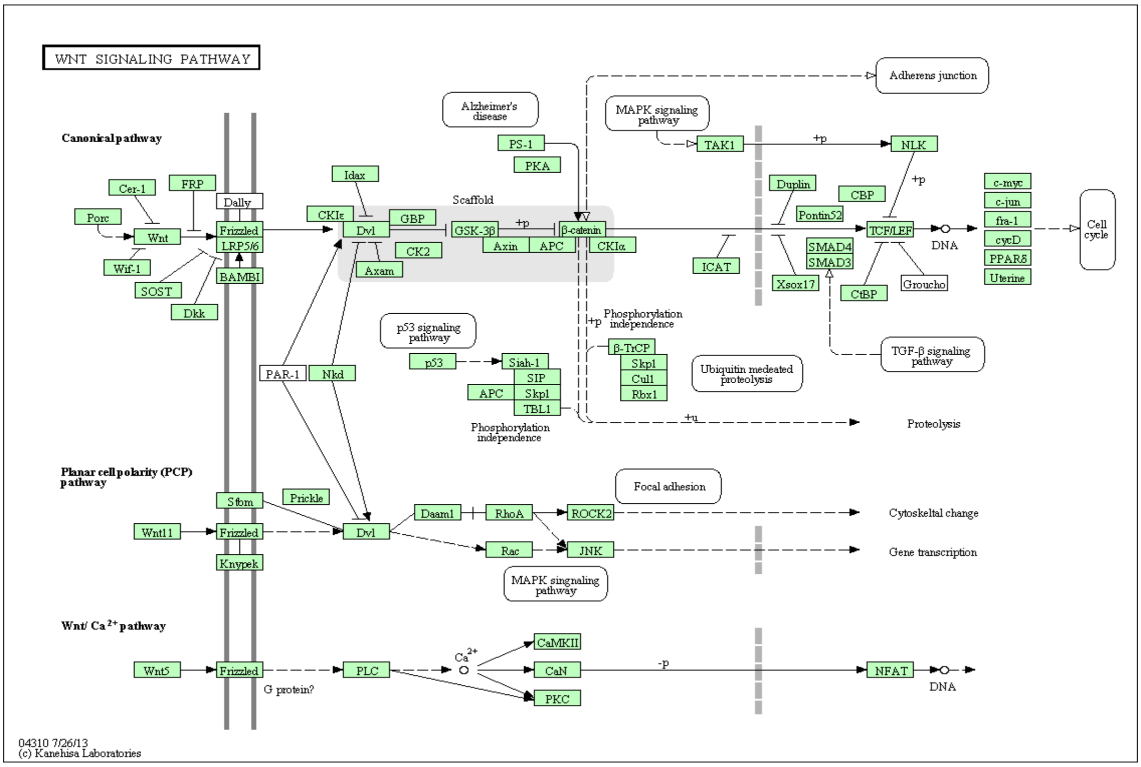

Figure S 3: Example of multi-branch pathway map.

2 Supplementary results

2.1 Independent component analysis

The 2nd-level SOM presentation as used in the main paper is advantageous because it visualizes multivariate relations within a relatively simple two-dimensional image using however distorted non-linear distance metrics. We analyzed similarity relations using independent component analysis (ICA) projecting the samples in linear scale. Figure S 4 shows the sample trajectory in the three-dimensional space spanned by the first three independent components (IC1 – IC3) obtained after independent component analysis (ICA).

ICA virtually confirms the results obtained using 2nd level SOM presented in the main paper: During the experiment the samples move along the first independent component (IC1), until week 6 in one direction and afterwards backwards (‘early time range’). Both oppositely directed parts of the trajectory refer to the ranges of high and low salt consumption, respectively. They are shifted each to another along IC3 so that the system doesn’t reach its starting point after the experiment.

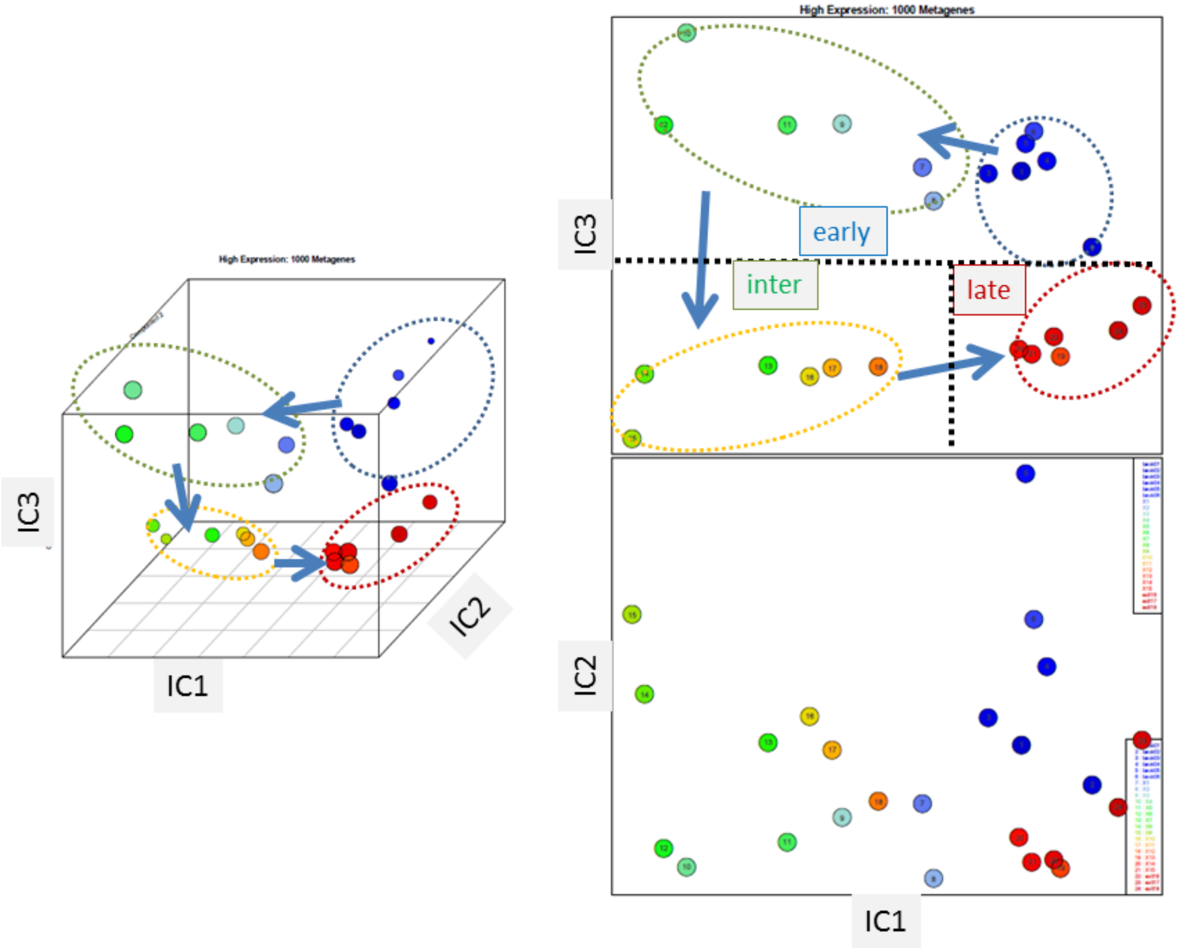

Figure S 4: Independent component analysis (ICA): The left part shows the three dimensional distribution of samples in the space spanned by the first three independent components IC1, IC2 and IC3. The right part shows two-dimensional projections into IC1/IC2 and IC1/IC3 planes.

2.2 Supporting maps: population, variance and entropy maps

The population map color codes the number of single features per meta-features in the map (Figure S 5). Empty meta-features not containing single features are colored in white. The single features mainly cluster into three regions which can be assigned to features up-regulated in the early and in the late (and the intermediate) time ranges and to single spiked and rare features as indicated. Most of the proteins refer to the former cluster (see the table in Figure S 5). The variance map visualizes the variance of each meta-feature profile, $\mathrm{var}_m = \sum_t \Delta E_{mt}^{meta\,2} / (T-1)$ (m=1…M denotes the number of meta features), using an appropriate color code (red to blue means high to low). It reveals that the highly variant profiles in the early_up and late_up clusters are separated by the region of relatively invariant single-spiked profiles.

The entropy map plots the standard entropy of each meta feature profile, $h_m = -\sum_{i=1}^{3} p_{mi} \log_2 p_{mi}$ where p_{mi} is the relative frequency of three levels of protein expression, overerexpression (i=1), underexpression (i=2) and non-differential expression (i=3), in the profile of meta feature m. To estimate p_{mi} we divided the expression values of the meta feature profiles in to three levels by application of a defined threshold (here the 25- and 75-percentile of all meta feature expression values was used). h_m is restricted to values in the interval [0, $\log_2 3$]. An entropy value of 0 represents a perfectly ‘ordered’ profile, where all meta-feature values are assigned to only one of the expression levels. Contrary, the maximum value of $\log_2 3 \approx 1.58$ is reached if the meta-feature values of the profile uniformly distribute over the three levels. The entropy is an information content measure by definition. A virtually invariant profile with a low entropy consequently reflects the fact that it is almost uninformative with respect to the time course of protein expression. Contrarily, a high entropy value means that the information content of the respective profiles is high. Note that variance and entropy reveal similar but partly also complementary properties of the meta-features: A low variant profile is typically less informative with low entropy too. A highly variant profile however can possess only medium entropy because it lacks maximum diversity (e.g. if it shows a high but constant differential expression). Finally, profiles of maximum diversity and thus maximum entropy usually of medium variance only. Comparison of the variance and entropy maps in Figure S 5 reveal an interesting substructure of the high variant areas: Particularly, one identifies a region of less diverse but highly differently expressed profiles in the to-right corner of the map.

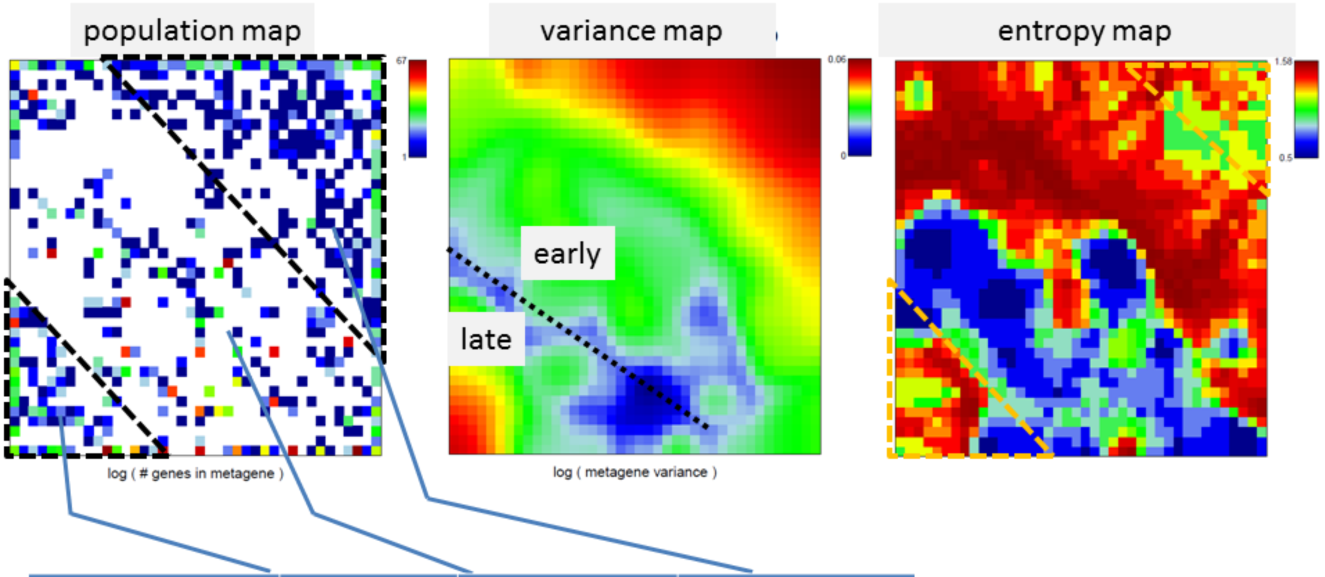

	Late_up	Single-spiked	Early_up
# proteins	404 (20%)	1072 (53%)	562 (27%)
# meta features	210 (13%)	863 (54%)	527 (33%)

Figure S 5: Supporting maps characterizing the meta-feature landscapes. The population map visualizes the occupation of meta features with single features (blue to red refers to 1 to 67 single feature/meta features, white are empty meta features). The variance map color codes the variance of the meta feature profiles red (high variance) to blue (small). The entropy map color codes the entropy of the meta-feature profiles from red (high entropy) to blue (low). The ranges referring to early and late time ranges are separated by areas of low populated, low variant and low entropy meta-features. Note that the entropy in the area of highest variance near the top right corner of the map is only medium because the respective profiles are less diverse than that in the ranges of intermediate variant meta-features.

2.3 Spot module selection

We compared three different methods to identify groups of co-expressed proteins that we call modules: (i) *Over- and under-expression spot-modules* are calculated by averaging each meta-feature value over all individual expression states considered and then selecting the maximum and minimum 2-percentile of them, respectively. Then the spot-modules were defined as closed areas of adjacent, i.e. mutually connected meta-features in the map. (ii) *Correlation spot modules* are calculated using a ‘seed algorithm’ starting with the pair of meta-features showing the largest Pearsons correlation coefficient between their profiles. Then adjacent meta-features are added to this module if the mutual correlation coefficient with the seed features exceeds a certain threshold (here 0.5). Otherwise a new seed-pair is selected among the still ‘free’ meta-features (i.e. that which are not assigned to another correlation module so far) defining a new module which grows by adding adjacent free meta-features using the same correlation threshold. This algorithm is repeated until no seed-pair satisfies the correlation criterion. (iii) *K-means cluster modules* are calculated by applying K-means clustering to the profiles of the meta-features using the *Euclidian* distance between them as similarity metrics. The desired number of cluster is set to the number of overexpression spots determined before. Note that K-means clustering assigns all meta-features to a certain cluster whereas overexpression and correlation clustering leaves a certain number of meta-features unassigned with respect to the clusters determined.

Figure S 6 (upper part) illustrates that the degree of area occupancy of the map increases in this order. In the supplementary material we present a series of so-called supporting maps which have been designed to analyze intrinsic properties of the SOM [4]. The population map shows that the proteins distribute heterogeneously over the map and preferentially accumulate in the regions of overexpression in the early (27 %) and late/intermediate (20 %) time ranges. About 53 % of the proteins are classified into invariant and ‘single spiked’ ones as will be discussed below. They are of limited interest here.

The overexpression spot criterion selects 388 (19% of all) proteins where about 178 (46% of selected) can be assigned to the interesting fraction of variable profiles, not referring to the invariant or single spiked proteins. The correlation and K-means cluster methods select 1,288 (63%) and 2,038 (100%) proteins, respectively, where however the fraction of interesting proteins increases only slightly to 63% (correlation spots) and 47% (K-means spots). The heat maps shown in Figure S 6 document that either of the methods well reproduces the time course of the system in terms of spot profiles. We applied beta-testing to estimate the significance of the protein clusters selected by the different methods (see next subsection). It turned out that spots selected in the upper right and lower left regions of the map, independently of the clustering method, collect clusters of proteins concertedly changing with time whereas proteins in the remaining regions in the map do virtually not.

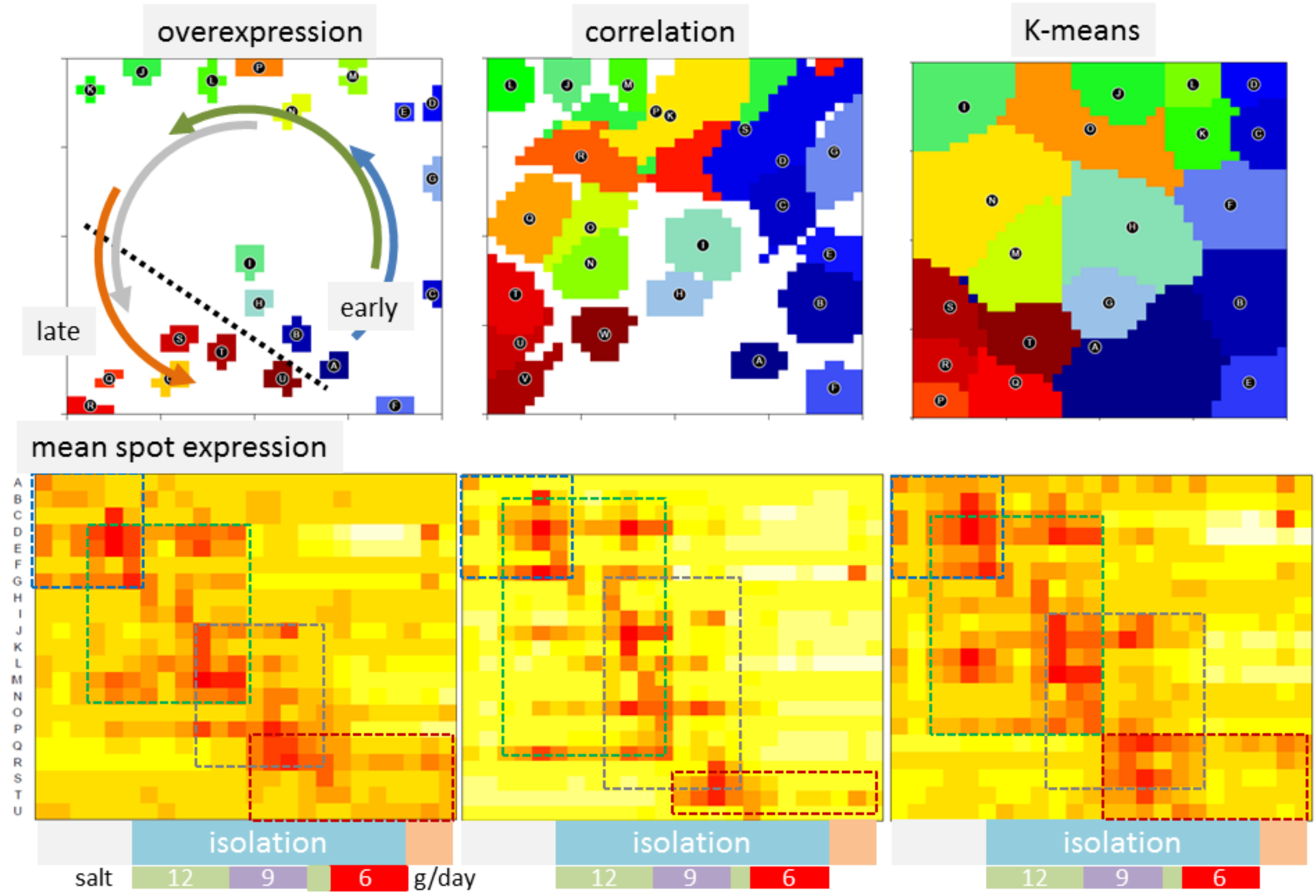

Figure S 6: Comparison of overexpression, correlation and K-means spot selection methods: Note that each method selects cluster-areas of different size and shape in the SOM map (see the colored areas in the respective maps). Temporal sequence of protein up-regulation follows roughly the spot trajectory as indicated by the arrows in the overexpression map. The heat maps show the mean abundance of each spot (red…high, white…low) sorted in temporal order in vertical direction. Essentially one finds analogous abundance patterns for all methods. All clusters are assigned by letters: Enlarged plots and lists of proteins in each of the overexpression spots are provided in additional file 2..

2.4 Estimating beta significance of meta-features and spot modules

The beta map in Figure S 7 color codes the beta value of each meta feature ($\log_{10}$-scale), thus estimating the degree of mutual correlation between the meta feature profile and the profiles of the associated single features (see Eq. (3)). It again identifies the late_up and early_up regions by large beta values. The spot significance maps shown in the lower panes in Figure S 6 color code the spot clusters obtained by means of three independent methods according to their $\log_{10}p$ values obtained by means of the beta test described above. The clusters are largely insignificant in the region of rare and single-spike profiles meaning that their meta-features are not co-expressed in terms of correlated profiles. Note that the p-value is governed by q^2 (see Eq. (6)) which scales with the variance of the meta-features (Eq. (7)). Hence, highly variant regions of the map (see Figure S 5) well match to regions of significant spot clusters.

Figure S 7 compares the beta-test significance maps of the mean-volunteer and the single volunteer analyses. The exact localization of the spots differs between both maps because they were obtained in independent training runs. The number of significant spots and their split into an early_up and a late_up cluster agree between both maps. On the other hand, the number of insignificant single spike spots largely increases in the single volunteer map owing to the fact that these profiles mostly refer to proband-specific spikes.

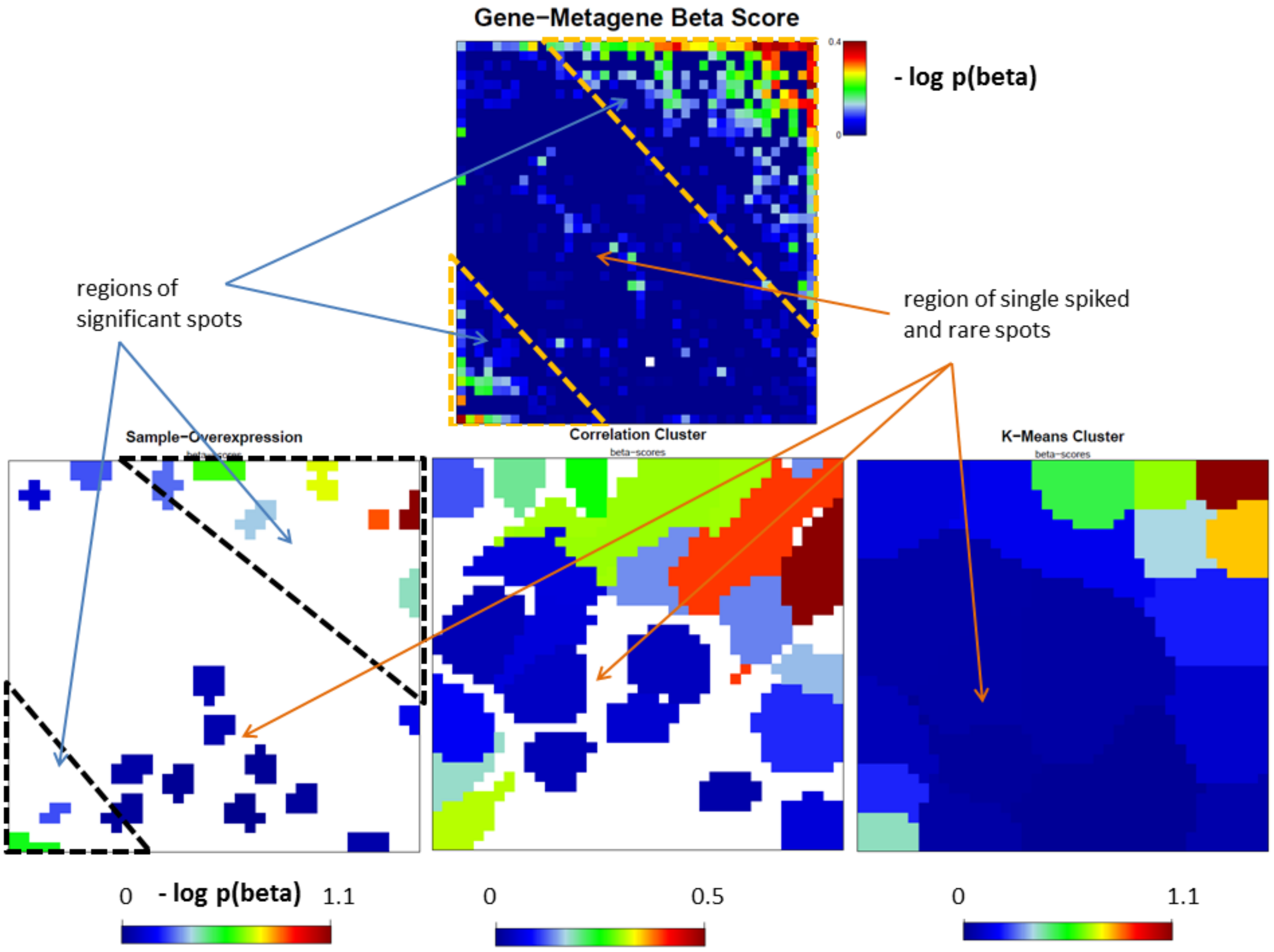

Figure S 7: Beta test significance maps of spots obtained using the overexpression, correlation and K-means clustering methods. Significance for each spot was estimated using the correlation beta test. Green to brown refers to $\log_{10}p<-0.5$ (overexpression and K-means clustering spots) and $\log_{10}p<-0.25$ (correlation cluster). Single spiked and rare spots are found in the central area of the map. They are insignificant in terms of correlated set of genes included in each of the spots. The beta map visualizes the log beta value of each meta-features (see Eq. (3), blue refers to small values, red to large ones).

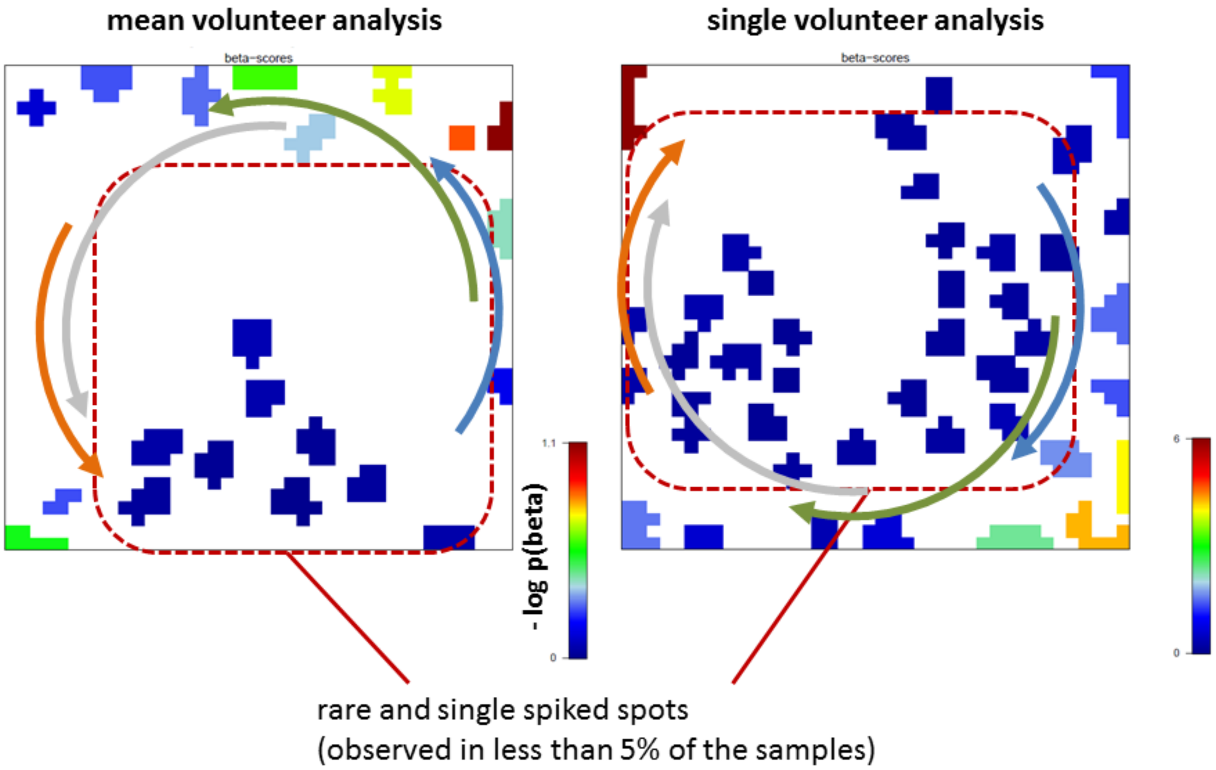
mean volunteer analysis

single volunteer analysis

rare and single spiked spots
(observed in less than 5% of the samples)

Figure S 8: Beta test significance maps of the overexpression spots obtained in the ‘mean volunteer analysis’ (left, see also Figure S 7, left panel) and ‘single volunteer analysis’ (right). In both maps insignificant spots accumulate in the central area of the map. Their number is much larger in the ‘single volunteer’-map (~30) than in the ‘mean volunteer’-map (~10) whereas the number of significant spots roughly agrees (8-10). Note also that spot overexpression changes with time either in counter-clockwise or in clockwise direction in both maps due to the independent SOM training of the data.

2.5 Alternative spot selection: correlation and K-means clustering

Figure S 9 shows the spot profiles of the significant expression modules obtained by means of the correlation clustering and K-mean clustering methods together with the most enriched gene set per module. Profiles and leading gene sets mostly agree between the different methods. Note that the K-means cluster modules contain the largest numbers of single proteins whereas the overexpression modules contain the least number of proteins with correlation clusters in between.

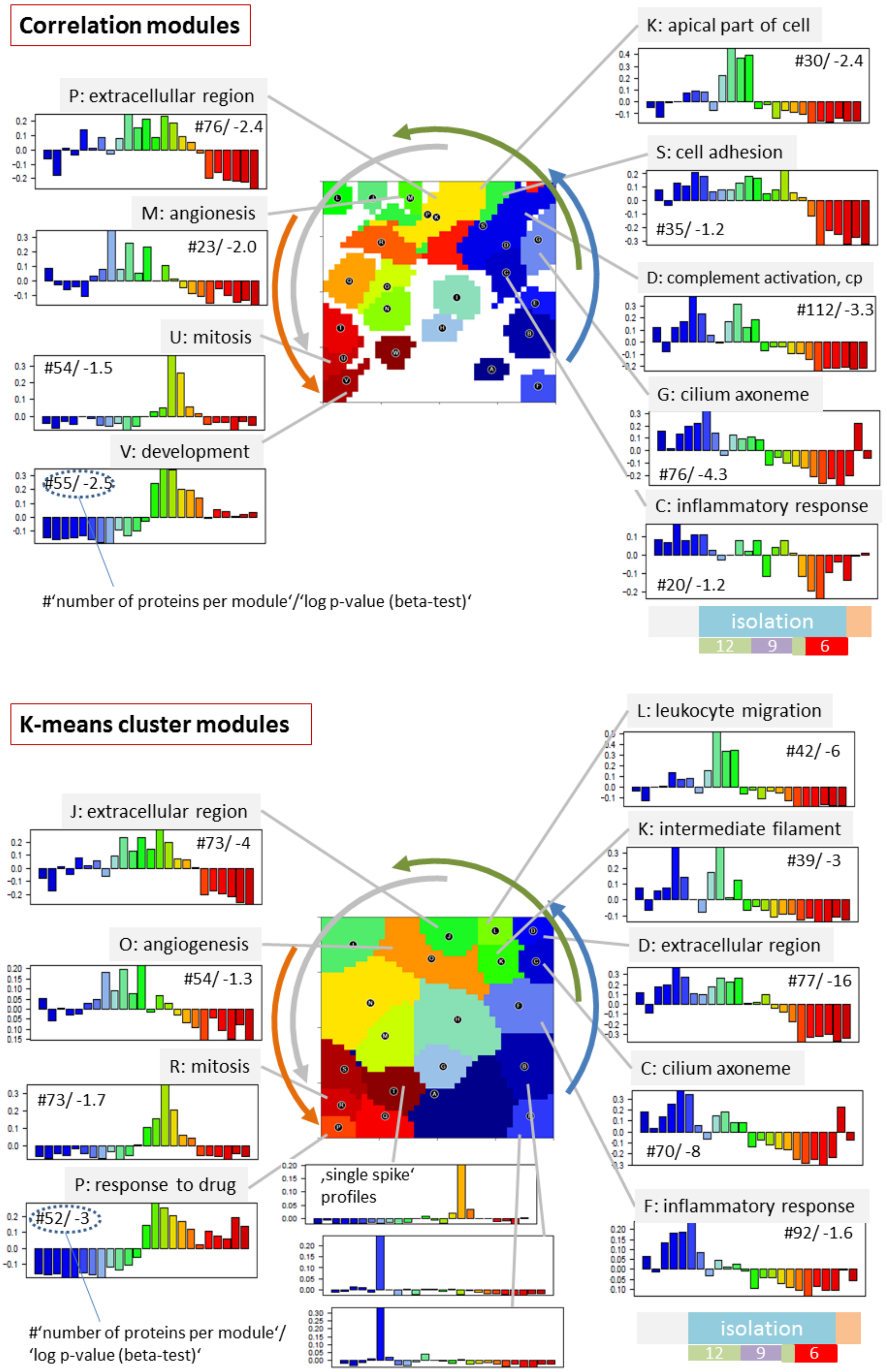

Figure S 9: Spot profiles and top enriched gene set per spot as seen by the correlation spot (part above) and K-mean clustering (part below) module selection methods. Selected single-spiked spots are shown in the K-means clustering map only.The vertical axis of the profiles is scaled in units of differential expression, ΔE, representing the mean binary detection level centralized with respect to the mean expression in all samples at all times (see supplementary text).

2.6 Overexpression spot analysis: protein lists

Figure S 10 lists the proteins in the overexpression spots ranked with decreasing significance as estimated using the correlation t-test.

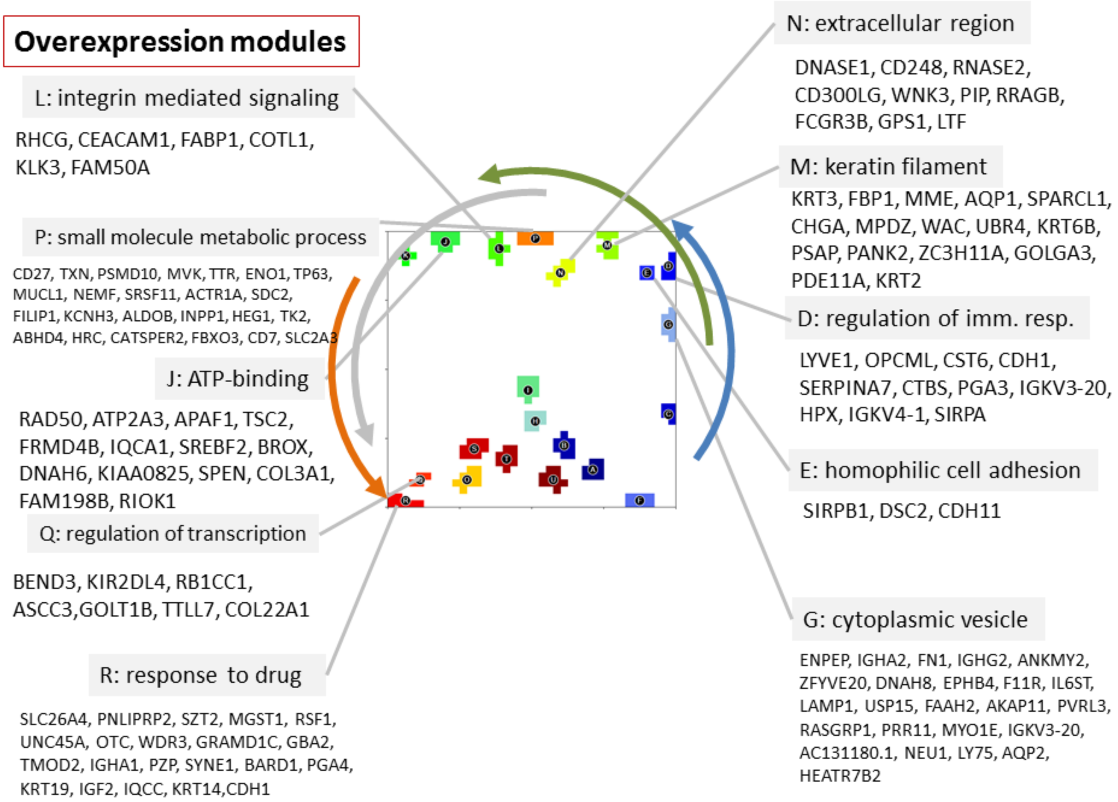
Overexpression modules
L: integrin mediated signaling
RHCG, CEACAM1, FABP1, COTL1, KLK3, FAM50A
P: small molecule metabolic process
CD27, TXN, PSMD10, MVK, TTR, ENO1, TP63, MUCL1, NEMF, SRSF11, ACTR1A, SDC2, FILIP1, KCNH3, ALDOB, INPP1, HEG1, TK2, ABHD4, HRC, CATSPER2, FBXO3, CD7, SLC2A3
J: ATP-binding
RAD50, ATP2A3, APAF1, TSC2, FRMD4B, IQCA1, SREBF2, BROX, DNAH6, KIAA0825, SPEN, COL3A1, FAM198B, RIOK1
Q: regulation of transcription
BEND3, KIR2DL4, RB1CC1, ASCC3,GOLT1B, TTLL7, COL22A1
R: response to drug
SLC26A4, PNLIPRP2, SZT2, MGST1, RSF1, UNC45A, OTC, WDR3, GRAMD1C, GBA2, TMOD2, IGHA1, PZP, SYNE1, BARD1, PGA4, KRT19, IGF2, IQCC, KRT14,CDH1
N: extracellular region
DNASE1, CD248, RNASE2, CD300LG, WNK3, PIP, RRAGB, FCGR3B, GPS1, LTF
M: keratin filament
KRT3, FBP1, MME, AQP1, SPARCL1, CHGA, MPDZ, WAC, UBR4, KRT6B, PSAP, PANK2, ZC3H11A, GOLGA3, PDE11A, KRT2
D: regulation of imm. resp.
LYVE1, OPCML, CST6, CDH1, SERPINA7, CTBS, PGA3, IGKV3-20, HPX, IGKV4-1, SIRPA
E: homophilic cell adhesion
SIRPB1, DSC2, CDH11
G: cytoplasmic vesicle
ENPEP, IGHA2, FN1, IGHG2, ANKMY2, ZFYVE20, DNAH8, EPHB4, F11R, IL6ST, LAMP1, USP15, FAAH2, AKAP11, PVRL3, RASGRP1, PRR11, MYO1E, IGKV3-20, AC131180.1, NEU1, LY75, AQP2, HEATR7B2

Figure S 10: Proteins in the overexpression spot modules.

2.7 Spot related pathway signal flows

For functional assignment of the spots we applied pathway flow analysis. Using the protein abundance data at each time point PFA provides pathway flow data for selected proteins in the overexpression spots. Note that in contrast to gene set enrichment analysis PFA uses the topology of selected pathways in combination with the protein data independent of the location of the proteins in the map. Spot assignment was obtained by correlating the pathway flow profiles with the mean meta-feature profiles of each spot and choosing the spot profile of maximum mutual correlation coefficient.

Figure S 11 shows the mean spot profiles (red) of selected spots together with the pathways showing strongest correlation of the PFA values of selected proteins (blue curves). Early and intermediate time range responses are associated with inflammatory processes, cell adhesion, ECM-receptor and antigen processing in qualitative agreement with the results of gene set enrichment analysis. Interestingly, metabolisms of nucleotides (purine and pyrimidine),of fatty acids (butanoate, pyruvate) and of amino acids (cysteine, metheonine and lysine) are also activated in this time range reflecting specific changes of the activity of liver and, partly kidney tissues in agreement with the results of tissue analysis (see below). Increased concentration of these metabolites in blood is characteristic for starvation when nucleotides and fatty acids are converted into glucose as evidenced by substrate balances across organs [5]. Intermediate time responses tentatively reflect regenerative (Wnt-pathway) and recombinant (N-glycan biosynthesis) processes [6]. Observed late time responses (p53- and mTOR-signaling pathway and ubiquinone biosynthesis) are indicators for cellular responses to different types of stress such as hypoxia and DNA damage, for nutrient and/or energy deficiency [7] and for changed energy metabolism.

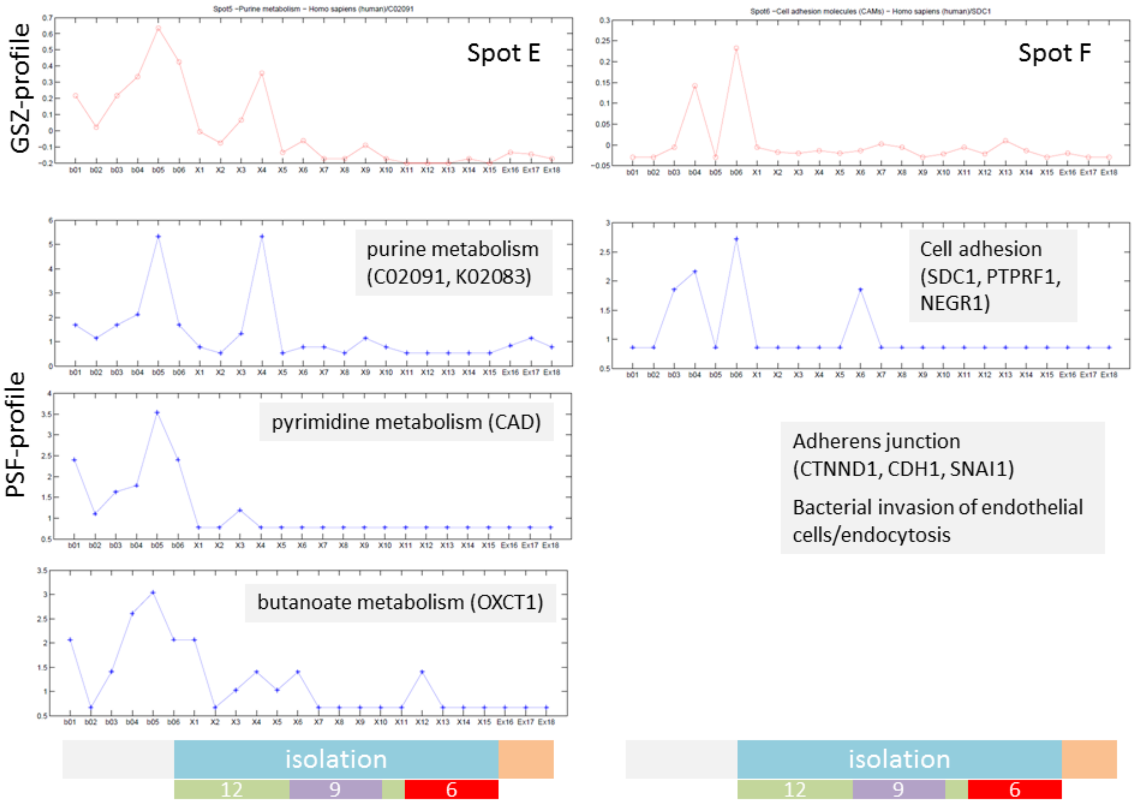
GSZ-profile
PSF-profile
Spot5 –Purine metabolism – Homo sapiens (human)/C02091
Spot E
Spot6 –Cell adhesion molecules (CAMs) – Homo sapiens (human)/SDC1
Spot F
purine metabolism (C02091, K02083)
Cell adhesion (SDC1, PTPRF1, NEGR1)
pyrimidine metabolism (CAD)
Adherens junction (CTNND1, CDH1, SNAI1)
Bacterial invasion of endothelial cells/endocytosis
butanoate metabolism (OXCT1)
b01 b02 b03 b04 b05 b06 X1 X2 X3 X4 X5 X6 X7 X8 X9 X10 X11 X12 X13 X14 X15 Ex16 Ex17 Ex18
isolation
12
9
6
isolation
12
9
6

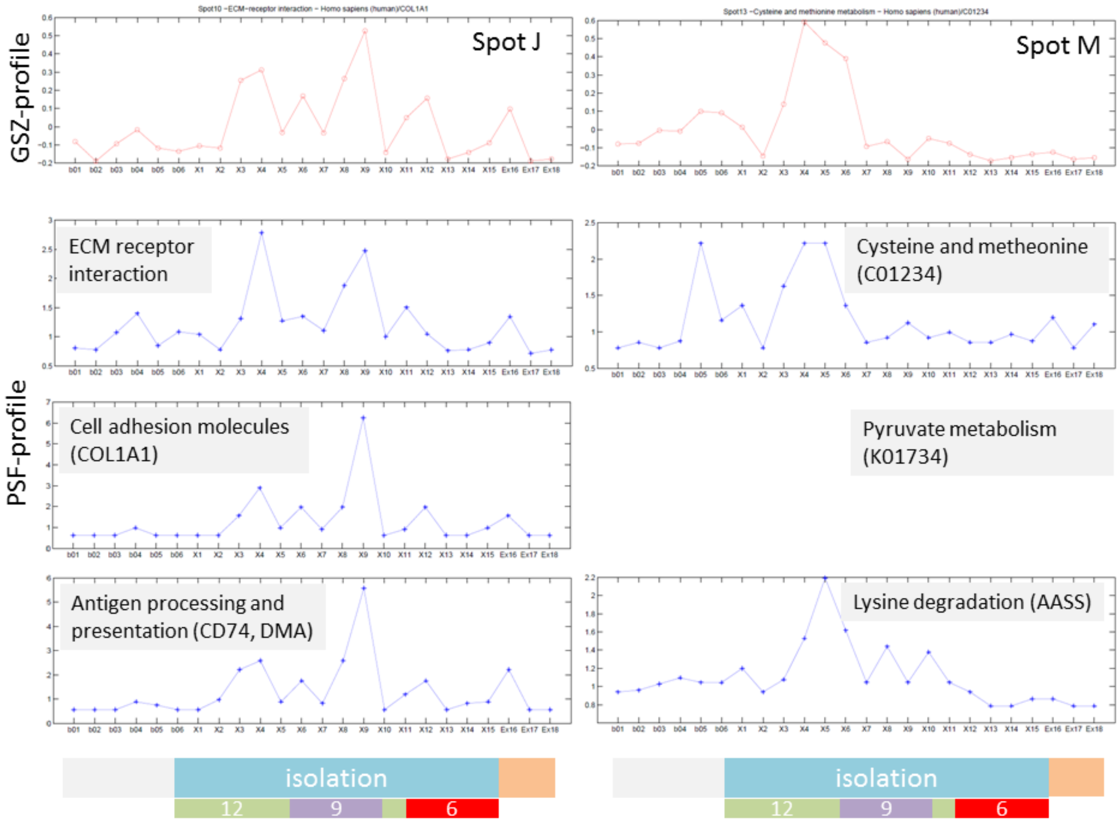
GSZ-profile
PSF-profile
Spot10 –ECM-receptor interaction – Homo sapiens (human)/COL1A1
Spot J
Spot13 –Cysteine and methionine metabolism – Homo sapiens (human)/C01234
Spot M
ECM receptor interaction
Cysteine and metheonine (C01234)
Cell adhesion molecules (COL1A1)
Pyruvate metabolism (K01734)
Antigen processing and presentation (CD74, DMA)
Lysine degradation (AASS)
b01 b02 b03 b04 b05 b06 X1 X2 X3 X4 X5 X6 X7 X8 X9 X10 X11 X12 X13 X14 X15 Ex16 Ex17 Ex18
isolation
12
9
6
isolation
12
9
6

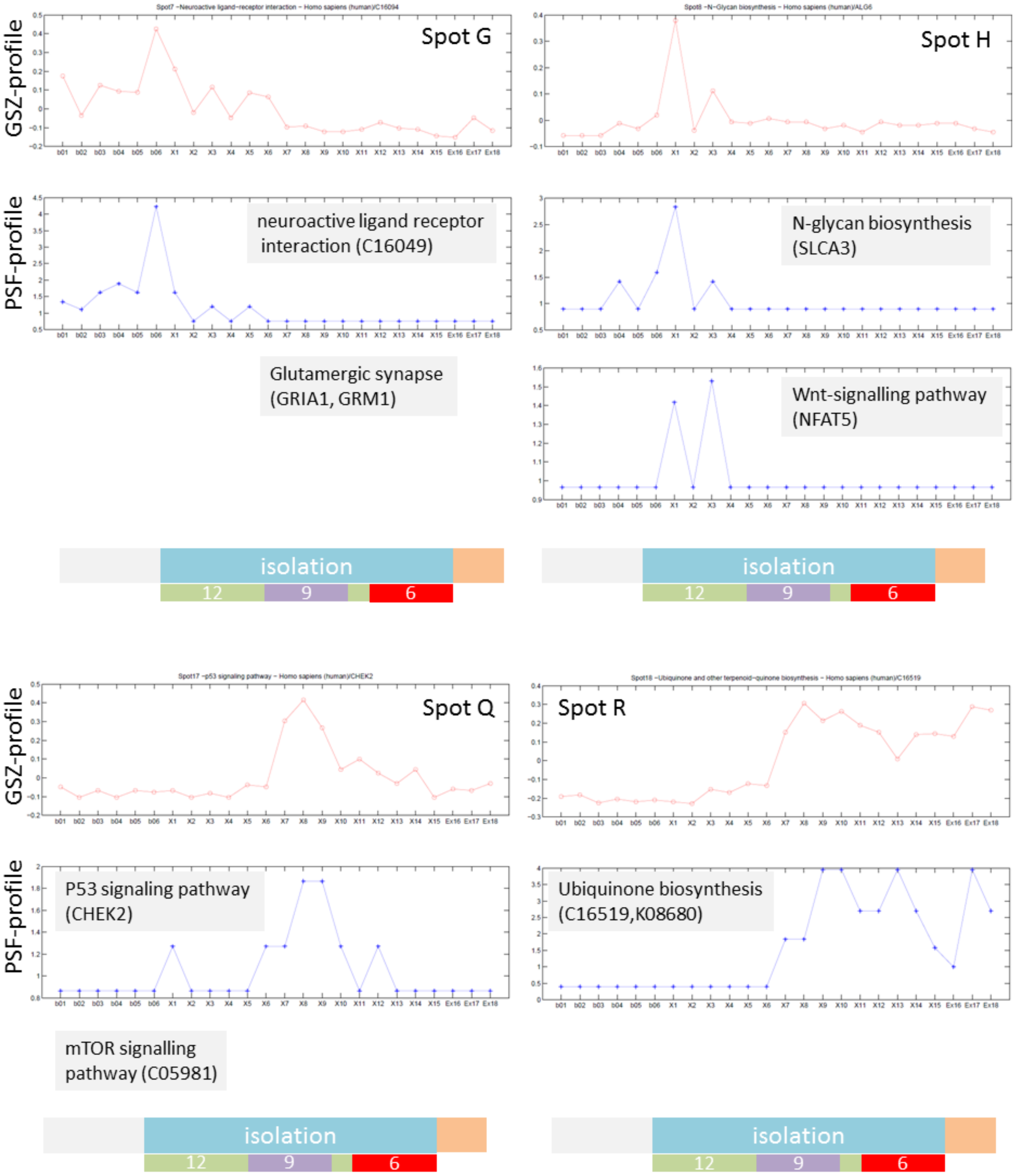

Figure S 11: Pathway flow analysis of selected overexpression spots referring to different time ranges. The mean expression profiles of the spots are shown in red whereas the respective PFA-profiles are shown in blue below together with the respective pathways and outcome-genes in parentheses.

2.8 Mapping of selected protein groups

We mapped groups of genes obtained in previous studies [8, 9] to our SOM space. The proteins collected in clusters 87, 83 and 9 (see [9] for assignments and details) accumulate in different areas in the early time region of the map (Figure S 12). Cluster 87 has been shown to associate with salt effects [9].

Figure S 12 shows the position of proteins commonly detected before and after space flight in urine samples of MIR cosmonauts *and* of the volunteers of the isolation experiment (group 'constant'), detected in either the space flight or the isolation experiment ('variable') or detected only after space flight ('flight specific'). The proteins are found in the regions of early and of late responses as well.

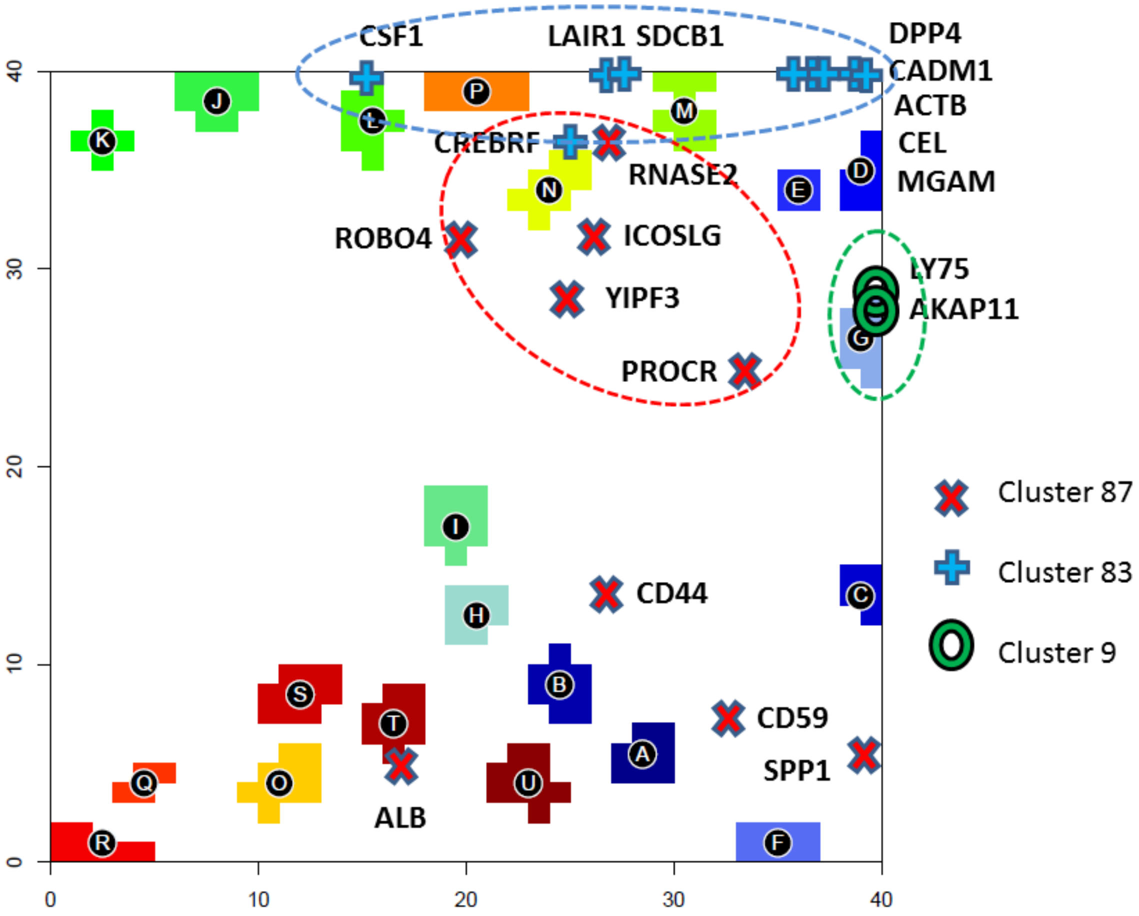

Figure S 12: Mapping of selected protein species from three clusters studied and defined previously [9]. The dashed ellipses indicate regions of increased local densities of the proteins from the three clusters. Cluster 87 is associated with salt effects.

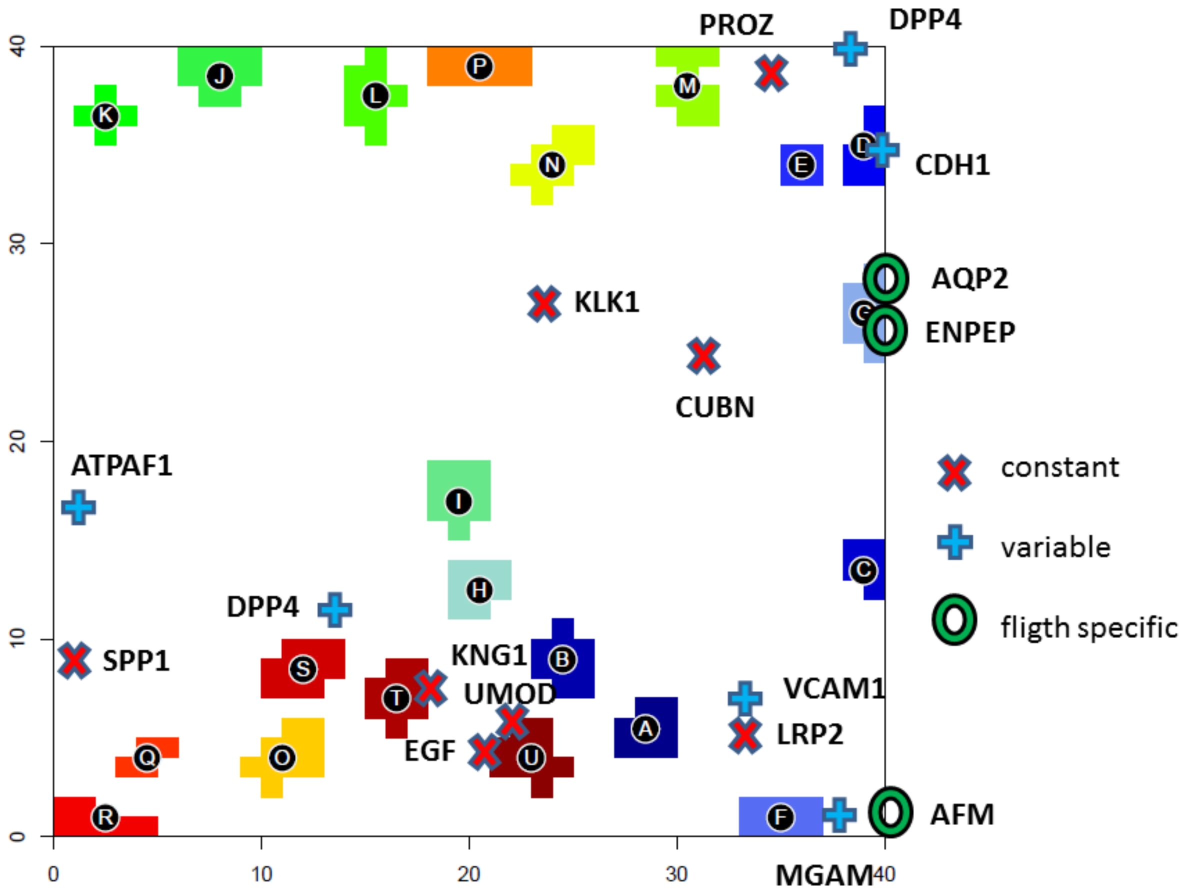

Figure S 13: Mapping of selected proteins to SOM: Constantly present under physiological conditions and after flight (symbol x), variably present (symbol +) and specifically expressed in urine samples of cosmonauts after flight (symbol O). Data are taken form ref. [8]. Most of the ‘constant’ and ‘variable’ proteins belong to the single spiked and rare spot areas whereas the flight specific accumulate in the early_up region, meaning that these species are down regulated before and after isolation experiment.

2.9 Single volunteer analysis

The spot textures of the individual volunteer SOM cannot be directly compared to that of the mean volunteer analysis because both SOM are trained independently. One gets however an analogous number of about 9 – 10 overexpression spot clusters with continuous profiles containing 12 – 61 features per spot. These profiles reflect the essential properties of protein kinetics for each of the probands as observed also in the mean volunteer SOM (Figure S 14). Detailed inspection of these profiles reveals for example, that, the late regime spot characteristics of P5 in the measurements before isolation is due to a slightly reduced overall level of the abundance of the respective proteins compared with the other probands but not to a different time course (see spots H, P and Y in Figure S 14).

In addition, our algorithm detects about 30 spots of the single spiked and rare type (Figure S 15): Each of these profiles shows at minimum one spiked protein expression and contains about 20 single proteins. These spots are insignificant in terms of correlated sets of proteins ($-\log_{10}p(\text{beta})>0.1$). Moreover, each of them was found in less than 5% of the samples and contains usually less than 20 features per spot. They show typically strong positive, spike-like outliers in one or a very few samples only. We attribute these spots tentatively, to technical errors of the measurement and/or to very specific physiological effects of unknown origin. These spots were excluded from further discussion because of their singular character. Importantly, the SOM sorting algorithm reliably separates such features from the features responding continuously to the experimental conditions. The identification of such spiked profiles would allow us to study the origin of this effect more in detail and also to develop and to apply suited correction methods. These issues are however beyond the scope of this publication.

Figure S 16 shows the gene set enrichment heatmap of the single volunteer analysis. Most of the enriched processes ‘switch’ in a coordinated fashion in the different volunteers. One sees however also individual differences, e.g. the volunteers show different degrees of immune response during the experiment.

An alternative approach to extract single volunteer information is illustrated in Figure S 17: It shows the so-called profiling map which is obtained by training of a coarse grained SOM of size 10x10. Each tile of the map compares the profiles of the individual probands referring to the respective meta features. The profiles roughly divide into early_up, intermediate_up and late_up types which show an almost concerted expression among the probands. A fourth group of profiles indcates stronger individual differences in different time ranges of the experiment. Owing to the smaller number of meta features the individual profiles are less resolved as in the larger 40x40 standard map. Single and rare profiles mostly collect in the range of ‘individual’ profiles.

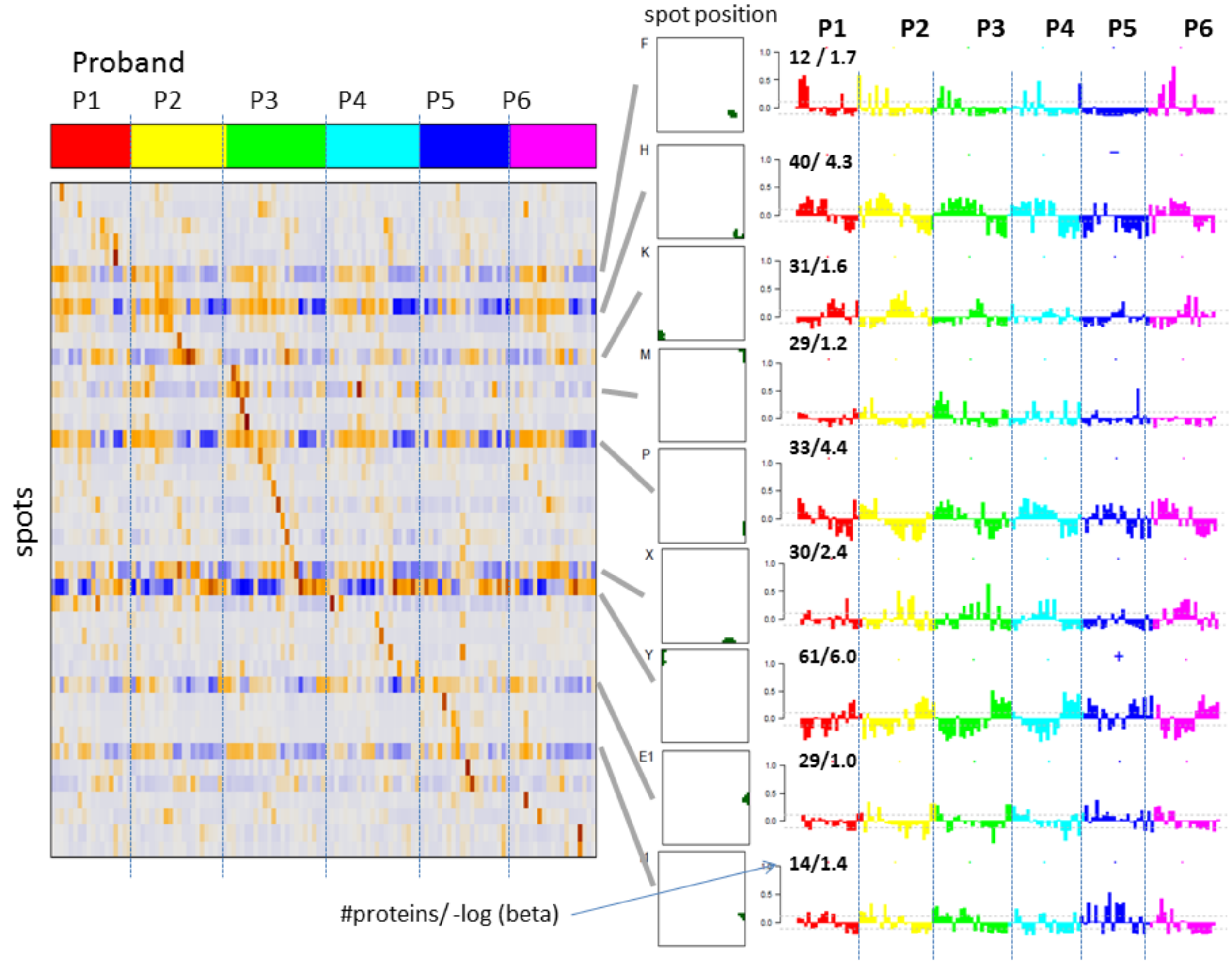

Figure S 14: Protein abundance profiles of overexpression spot clusters. The heat map provides an overview over the abundance profiles (dark brown to blue indicate high to low abundance levels, respectively). The right part selects profiles showing continuous responses, i.e. not referring to so-called single-spiked or rare profiles (these data are shown in the supplementary text). The spiked profiles can be identified in the heat map: They are characterized by single-brown colored bars due to high abundance levels of single or only a few protein species at single time points only (see also the supplementary text for full profiles). Note that the profiles of proband no. 5 (P5) reveal either low (spots H and P) or high (spot Y) abundance levels in the early time range compared with the respective spot profiles of the other probands which causes the deviating abundance portraits (see the main paper) and course of the sample trajectory of P5. On the other hand, the shapes of the profiles of P5 in general agree with that of the other probands showing that the specifics of P5 refer rather to absolute protein abundance levels and not to relative changes during the experiment.

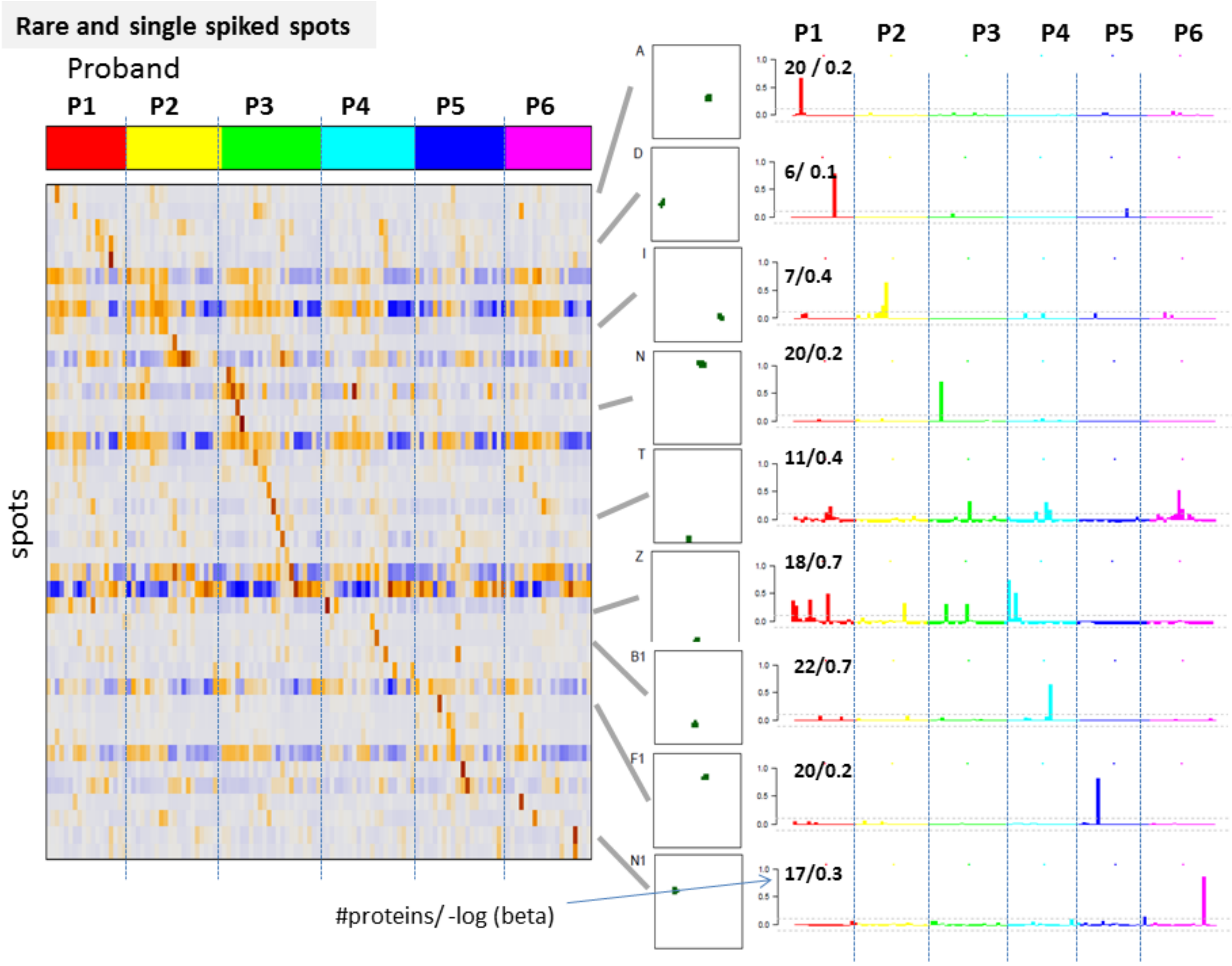

Figure S 15: Protein expression profiles of overexpression spot clusters. The heat map provides an overview over the expression profiles (dark brown to blue indicate high to low expression levels, respectively). The right part selects profiles referring to so-called single-spiked or rare profiles.

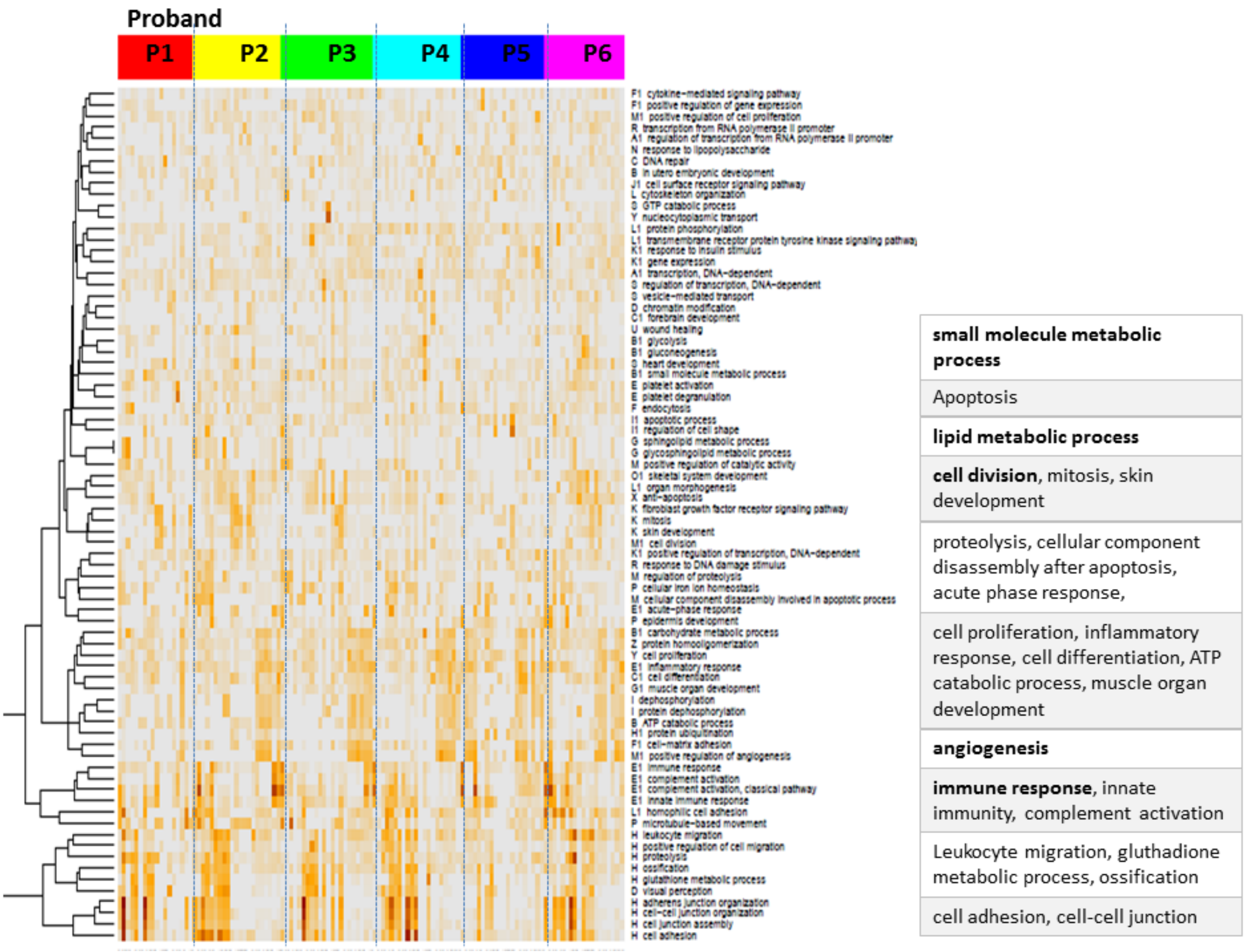

Figure S 16: Global enrichment analysis heat map of the single volunteer analysis: The map clusters top GO-sets of the category 'biological process' enriched in overexpression spots of the time series. Key processes are listed in the right part of the figure. Brown to grey indicates high-to-low enrichment estimated using the GSZ-score.

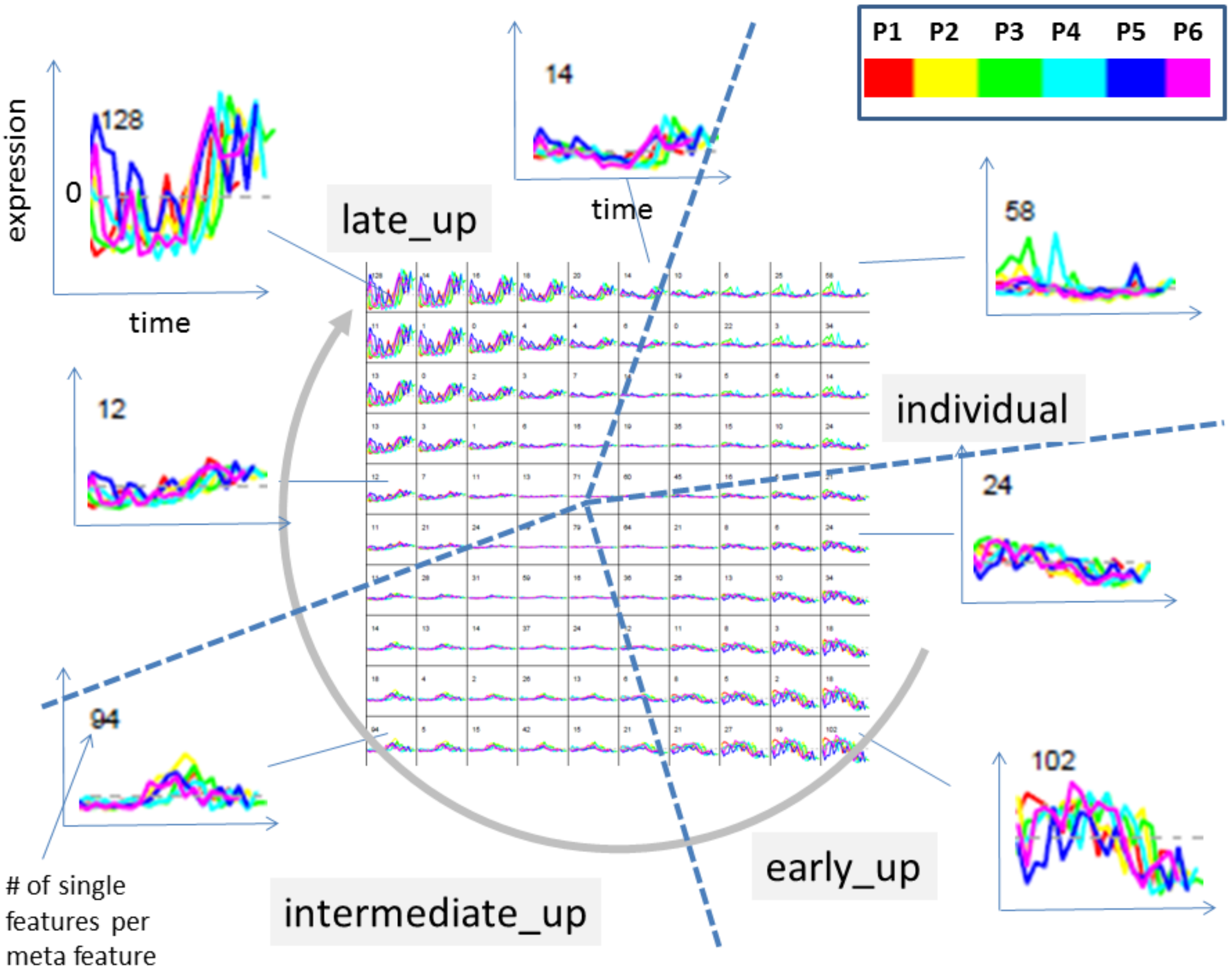

Figure S 17: Meta-feature profile map of single volunteer analysis: A coarsely resolved 10x10 SOM was trained with single volunteer data. The profile map compares the time profiles of the probands P1 – P6 (see legend for assignment) in each of the meta feature tiles. Profiles divide into early_up, intermediate_up, late_up and 'individual' profiles. Profiles of selected tiles are enlarged.

2.10 Organ related protein expression

We analyzed selected tissue-related sets of proteins as described in the main paper. Figure S 18 shows the results for a series of tissues which can be roughly divided into early responders (pancreas, liver, kidney), intermediate (muscle) and late (testis, stomach) responders and into tissues weakly or not responding to the experiment (skin, lymph node, blood, prostate, brain, colon). The type of response is clearly documented in the respective GSZ-profiles which plot the gene set enrichment score of the set as a function of time. Here all protein expression values of the set are considered, compared with the mean expression of all proteins considered and normalized using the variance of the expression values of the set:

$$GSZ_{set,t} = \frac{\left\langle E_{p,t} \right\rangle_{p\in set} - \left\langle E_{p,t} \right\rangle_{all\ p}}{\sqrt{\mathrm{var}\left(E_{p,t}\right)_{p\in set} / n_{set}}} \quad . \tag{12}$$

The GSZ-value thus estimates the consistency of differential expression of the set members compared with the mean expression of all genes in a given state. The GSZ consequently characterizes the expression of the whole protein set.

In addition we show so-called protein set population maps which mark the positions of the protein species of each set in the average volunteer SOM. Accumulation of the proteins in regions assigned to a certain time range (see red rectangles) indicates that the set is affected by the experiment.

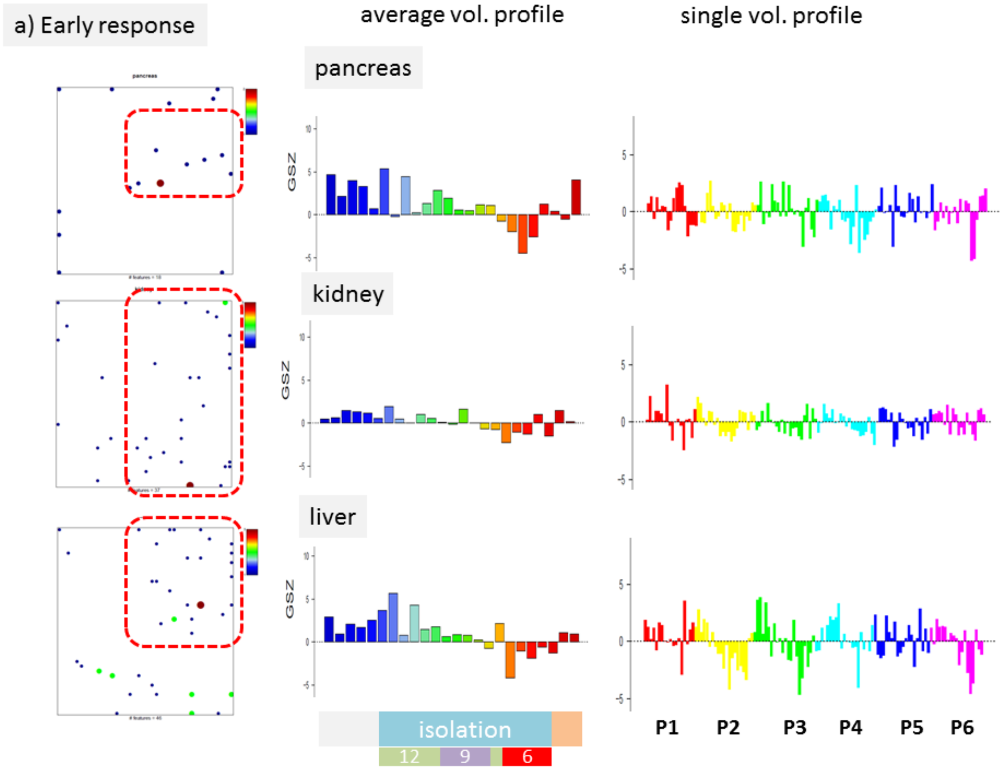

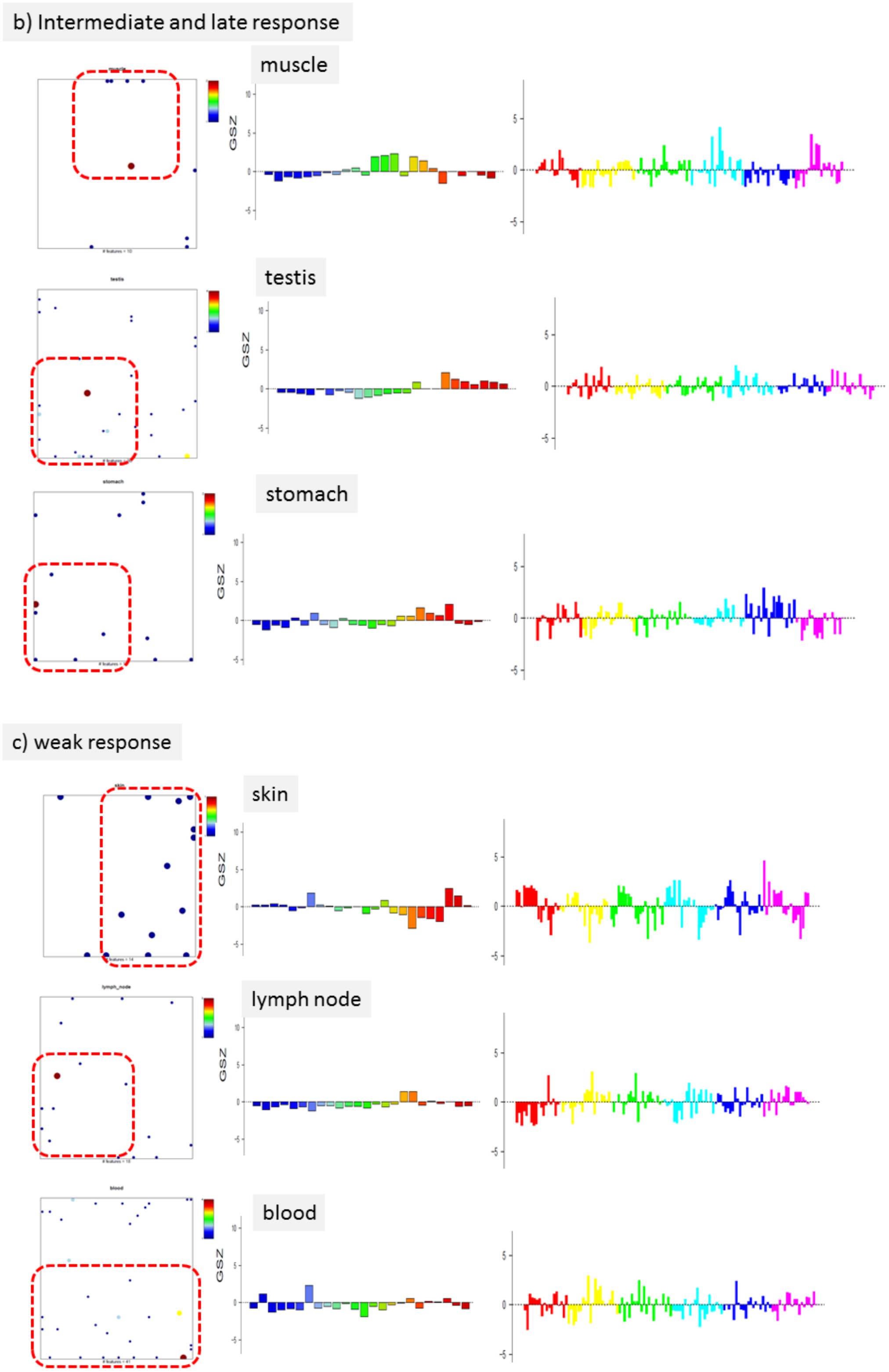

b) Intermediate and late response
muscle
GSZ
10
5
0
-5
testis
stomach
c) weak response
skin
lymph node
blood

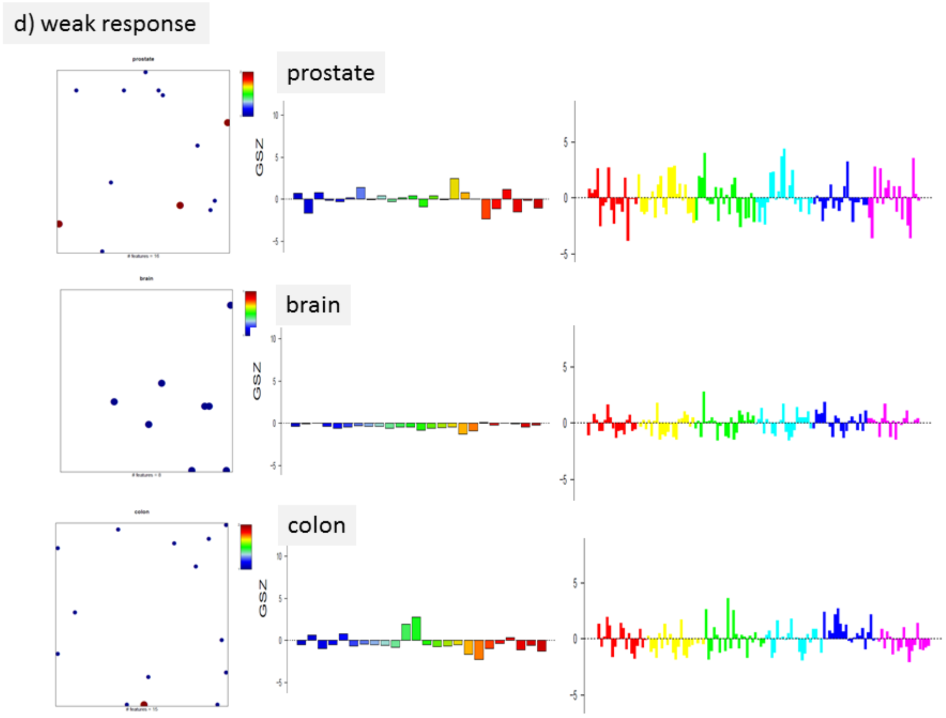

Figure S 18: Tissue specific protein expression: Tissue specific protein sets are taken from TiGR[10] and mapped into the single volunteer map (left part). The red rectangles illustrate regions of increased local density of the respective proteins. These regions refer to different time ranges. The set-profiles shown in the middle part clearly reveal the different time profiles in the average volunteer analysis. The respective single volunteer analysis reflects similarities and proband-specific differences between their tissue expressions.

2.11 Mapping and profiling of selected GO protein sets

Below in Figure S 19 selected protein sets are mapped into the SOM map of average volunteer analysis using the same presentation as for the organ related protein expression in Figure S 18. The bar plots show their average and volunteer specific profiles. The plots support the results obtained using spot analysis and gene set enrichment heat maps shown above.

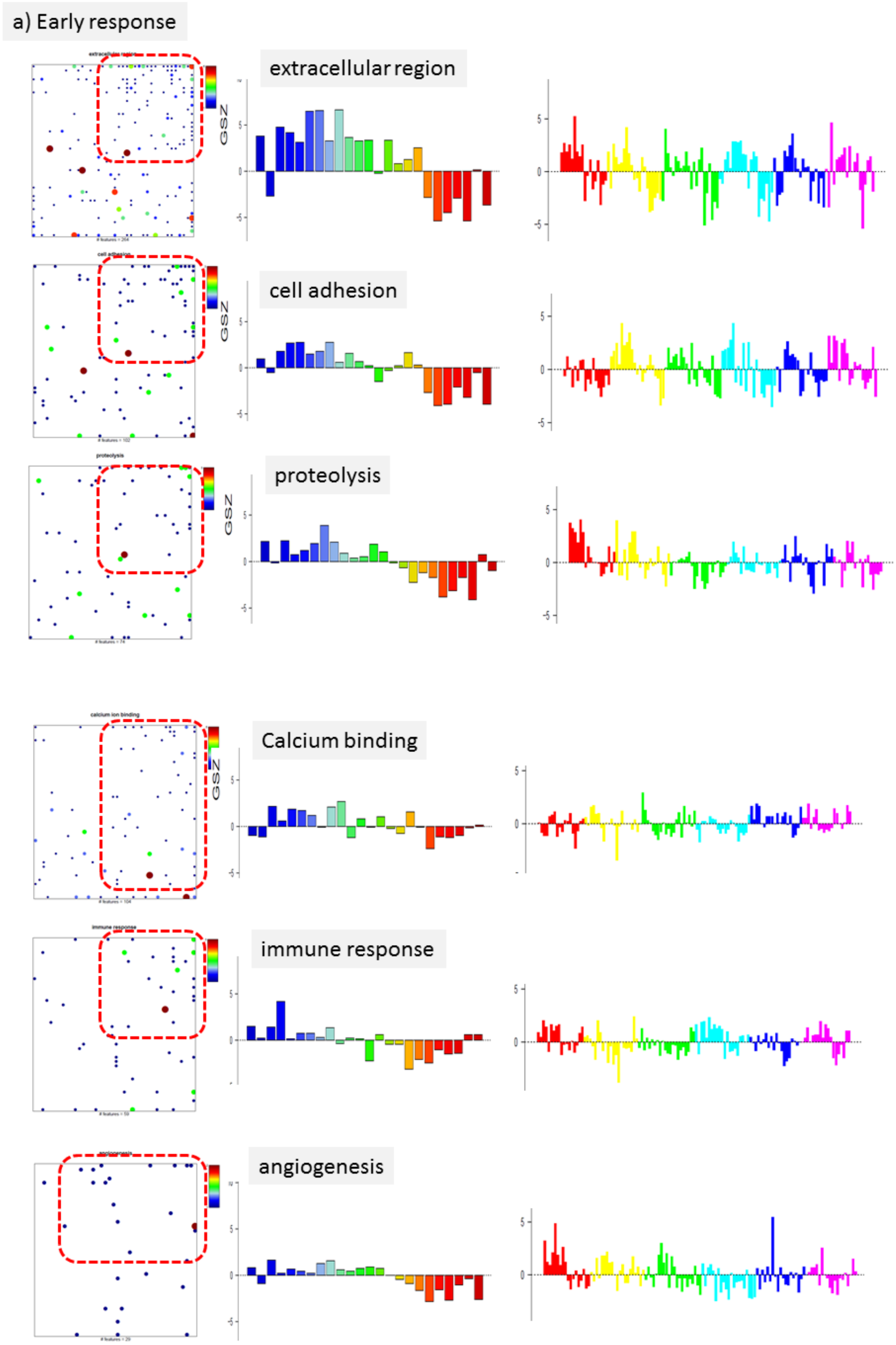

b) Intermediate response

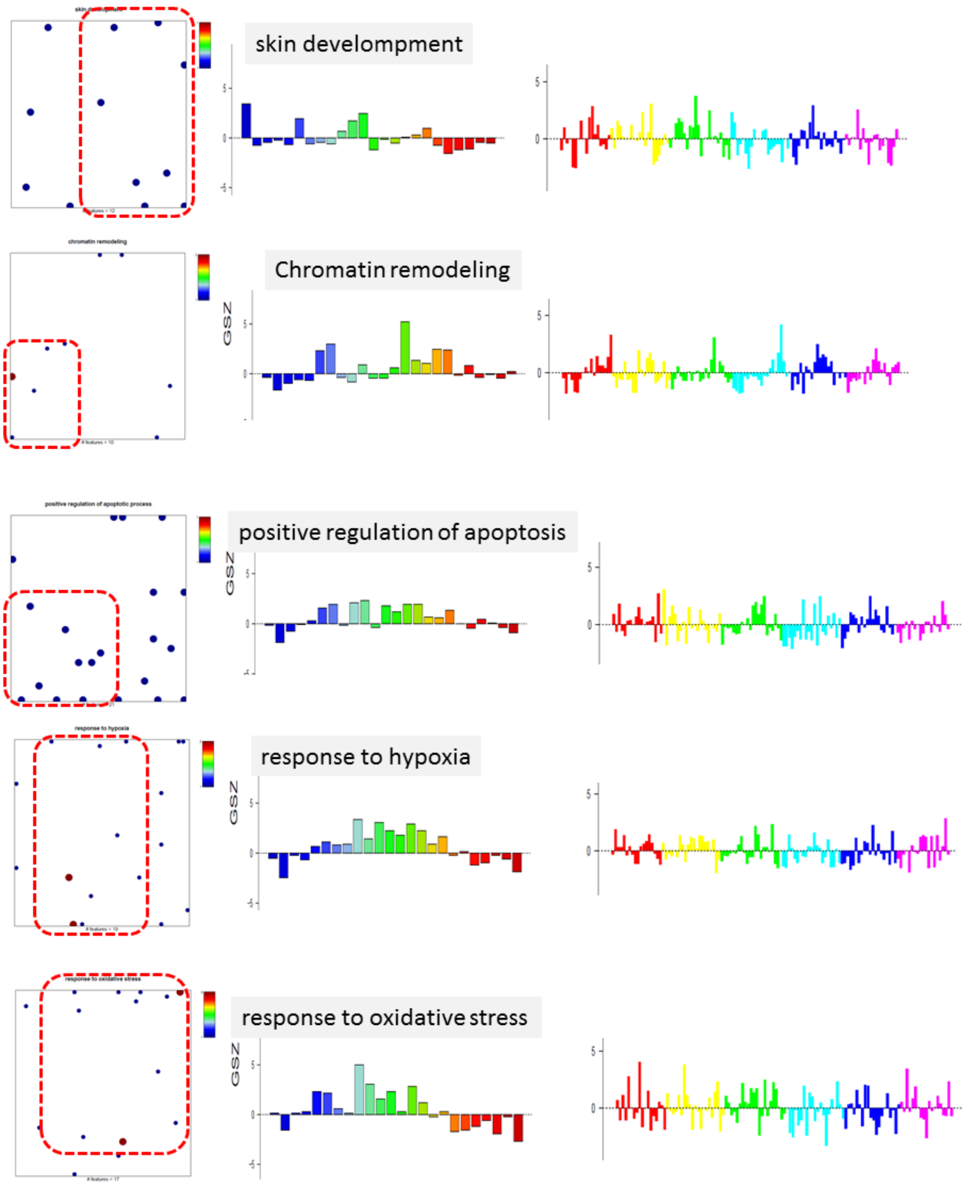

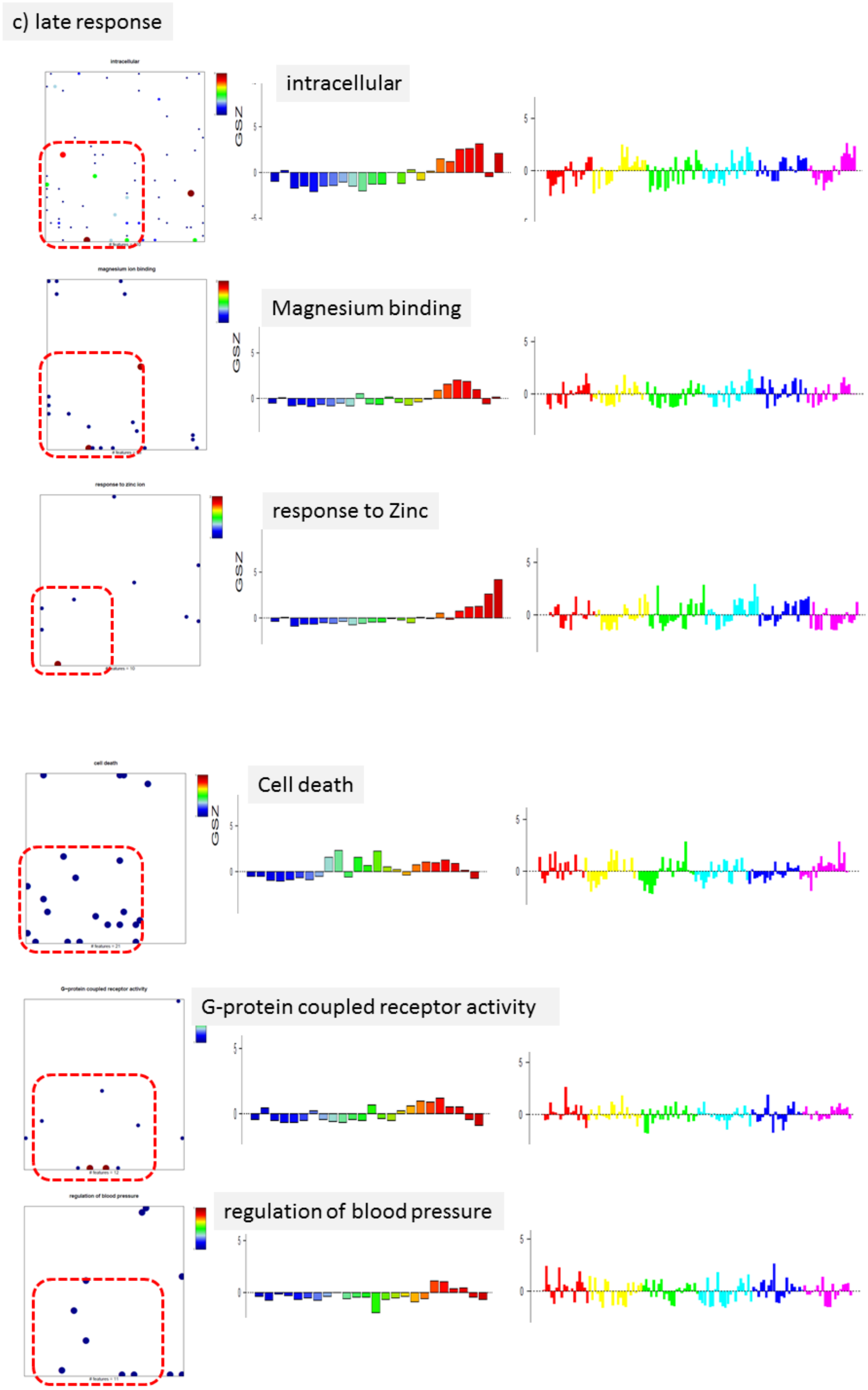

Figure S 19: Mapping and profiling of selected GO gene sets into the single volunteer map (left part). The red rectangles illustrate regions of increased local density of the respective proteins. These regions refer to different time ranges. The set-profiles shown in the middle part clearly reveal the different time profiles in the average volunteer analysis. The respective single volunteer analysis reflects similarities and proband-specific differences between the mean expression of the sets selected.

2.12 SOM analysis of absolute protein expression levels

We trained a SOM with total expression values E_{pt} instead of ΔE_{pt} (see Eq. (1)). This way, absolute levels of protein expression were taken into account. Recall that the expression is defined as the mean detection call of the respective proteins in all six probands. It adopts a value between 0 and 1 defining the fraction of present calls obtained. It means for example that for a value of unity all proteins are detected in all probands. The obtained SOM portraits reveal less structured expression landscapes compared with the SOM of centralized values showing essentially only one global expression maximum and one expression minimum spot in red and blue, respectively. Their position only weakly shifts in the course of the experiment (see the portraits in Figure S 20). These spots obviously collect permanently high and low expressed proteins, respectively. The question arises whether these landscapes contain similar information about the differential expression of groups of proteins detected at early, intermediate and late times of the experiment by means of the SOM analyses performed so far. With this aim we generated the 2nd level SOM of absolute expression landscapes. It closely resembles the respective plot of the centralized data (Figure S 18a). The sample trajectory clearly divides into the three time ranges revealing this way that the individual portraits contain the full information in this respect. The spot trajectory (Figure S 20b) can be assigned to the time ranges discussed so far. In addition to the permanently up and down profiles a 'late down' one is identified (see the detailed profiles shown in Figure S 20 below).

In the next step we used the supporting variance and entropy maps in combination with K-means spot clustering to segment the map into different modules of co-expressed proteins (Figure S 21):

a) The area of low variance and low entropy can be attributed to permanently low expressed proteins. About 63% of all proteins show this kind of behavior.

b) The area of high variance and high entropy collects proteins permanently highly expressed (7%).

c) The area of high variance and high entropy refers to proteins highly expressed in the early and intermediate time ranges only (late down, 13%).

d) Profiles of proteins up-regulated in the intermediate time range only possess medium variance and entropy values (7%). These medium values indicate that the high expression states are observed only at a few time points giving rise to relatively sharp peaks in the profiles.

e) Late_up-regulated proteins collect in a second area of high variance and high entropy (7%) which is however well separated from area b).

Each of these areas splits into several K-means cluster modules of slightly different profiles (see Figure S 21 and Figure S 22). Their inspection reveals a continuum of different shapes which partly cannot be clearly assigned to one of the groups defined above. Instead, they occupy a sort of intermediate position between them. We therefore used the K-means cluster spots for functional analysis using protein set enrichment. We used 'area-filling' K-means clustering because we aim at taking into account all proteins.

Detailed inspection of the spot modules in Figure S 20 shows that a group of about 65 proteins with an inflammatory signature are permanently expressed over the whole period of the experiment. The profiles of the remaining spots of module b) and especially of module c) decrease more or less sharply in the late time range. These modules thus contain the proteins which deplete at low NaCl consumption in the late phase of isolation. Interestingly, part of the spot profiles express onerelative sharp peak in the early time range (spot F and D) or a second one in the intermediate one (e.g. spots M, L, B and F). This second peak becomes more pronounced in intermediate-time mode d). The third peak protrudes already in a few spots of this mode but it becomes much more intense in the late mode e) together with the fourth peak near the end of the experiment. Hence, the more or less constant or decreasing profiles in modes b) and c) overlay with peaked profiles with maxima at distinct positions (as indicated by the asterisks in the figure). Functional analysis essentially supports the results of the previous analysis using centralized expression profiles.

In summary, absolute expression analysis shows that a series of processes become activated in relatively narrow time windows at four fixed times during the experiment, namely at or immediately before isolation (angionesis, complement activation and others), at or immediately after reducing salt consumption to 9 g/day (focal adhesion and cytoskeleton) and to 6 g/day (cell differentiation and organ development) and near the end of the experiment after isolation. The latter trend suggests recovery of the initial state before starting isolation. Double peaked profiles combine peaks at late and intermediate times (e.g. metabolic process and apoptosis).Importantly, immune response processes are permanently active during the experiment with a slight decay in the late time range.

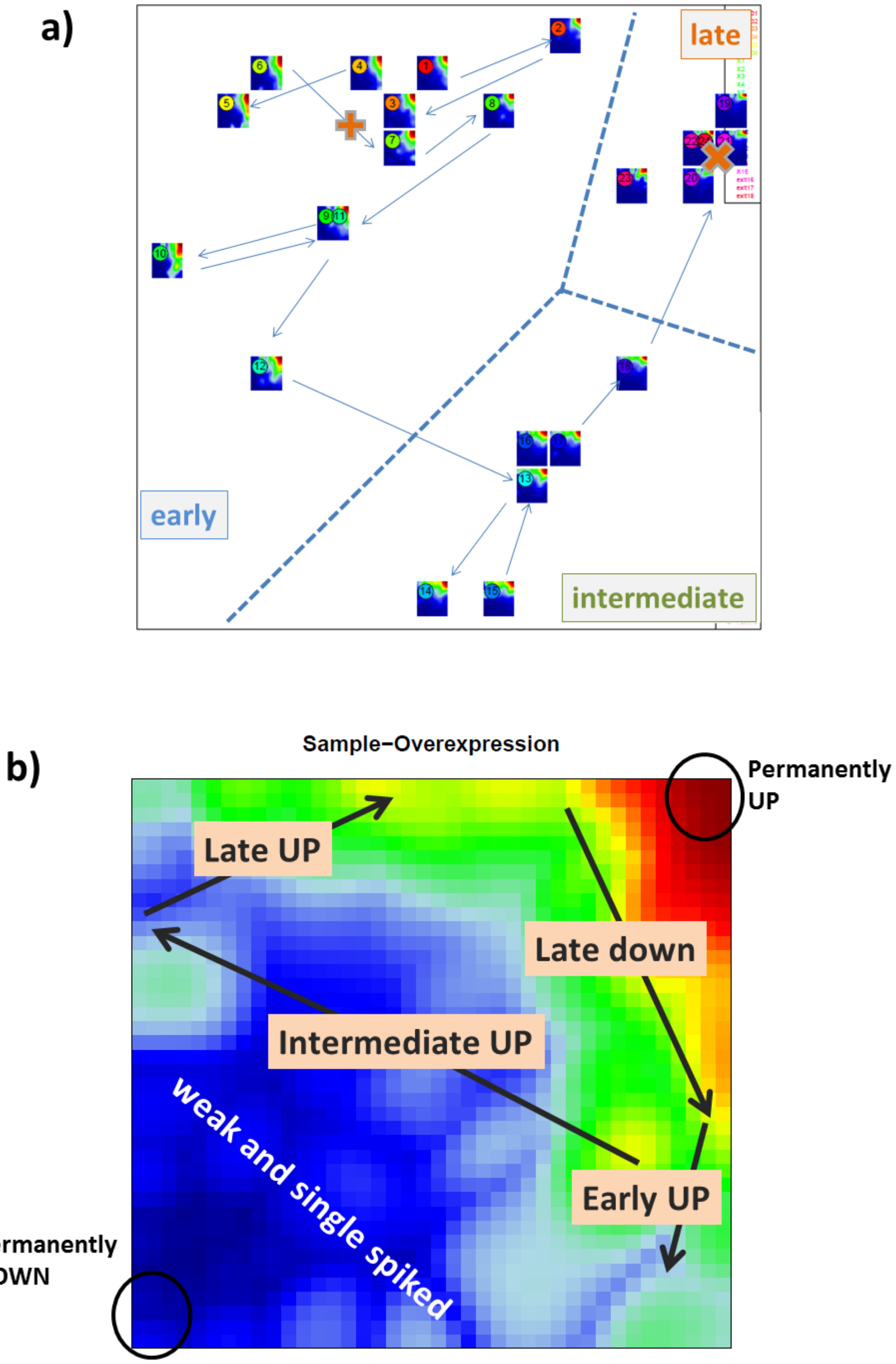

Figure S 20: Sample and spot trajectories of absolute expression SOM analysis: a) 2nd level SOM mapping of the total expression data of the ‘averaged volunteer’. The trajectory divides into an early, intermediate and late regime in agreement with the respective results obtained from centralized data. Note that the portrays (see the small images) are much less structured showing only one red spot compared with the portraits obtained using centralized data. b) Overexpression summary map of the SOM images: The red and blue spots refer to permanently present and almost absent proteins, respectively.

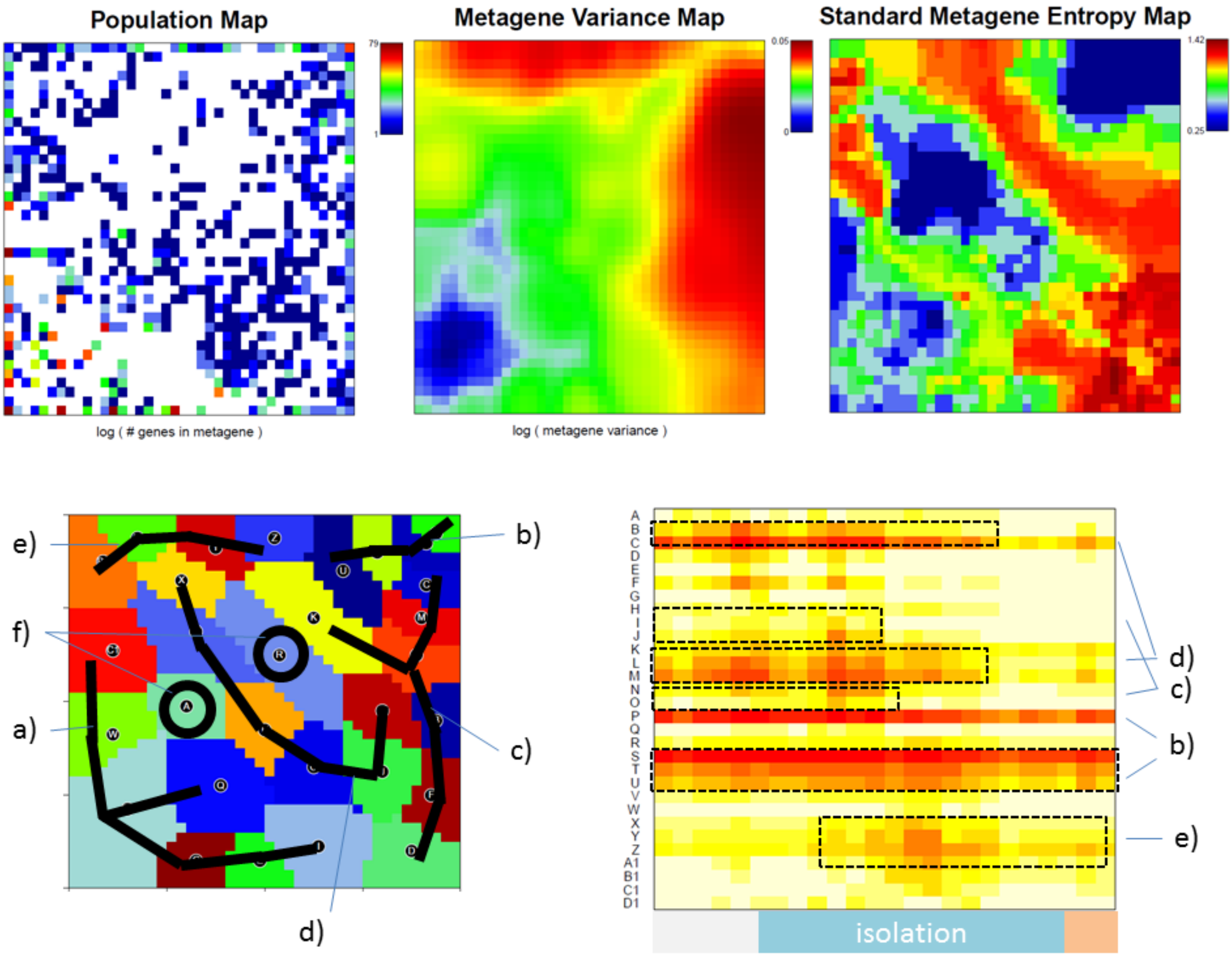

profiles	variance	entropy	#proteins	%proteins
a) low and single spiked	L	L	1302	64%
b) high	H	L	145	7%
c) early_up	H	H	267	13%
d) inter_up	M	M	147	7%
e) late_up	H	H	137	7%
f) diverse	M	L	40	2%

H, M, L .... high, medium and low levels, respectively

Figure S 21: Supporting maps (first row of figures) used to segment the K-means spot map (second row) into six absolute expression modes as indicated by the black curves connecting the spots of each mode. The heat map shows the expression level of each spot (red refers to high, white to low expression). The table assigns the characteristic variance and entropy levels to the modes and provides the number and fraction of proteins per mode.

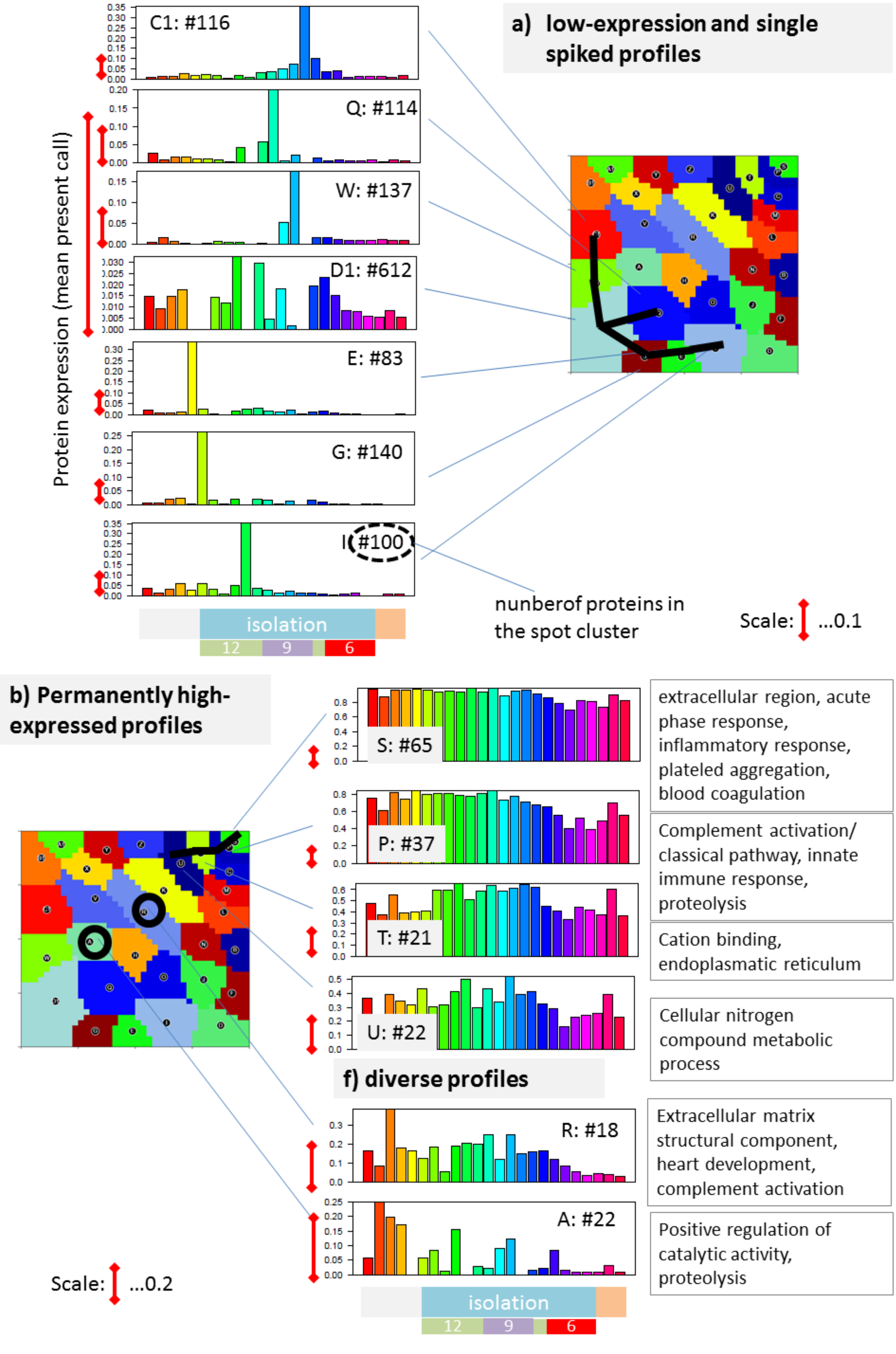
a) low-expression and single spiked profiles

b) Permanently high-expressed profiles

f) diverse profiles

nunberof proteins in the spot cluster

Scale: ...0.1

Scale: ...0.2

extracellular region, acute phase response, inflammatory response, plateled aggregation, blood coagulation

Complement activation/ classical pathway, innate immune response, proteolysis

Cation binding, endoplasmatic reticulum

Cellular nitrogen compound metabolic process

Extracellular matrix structural component, heart development, complement activation

Positive regulation of catalytic activity, proteolysis

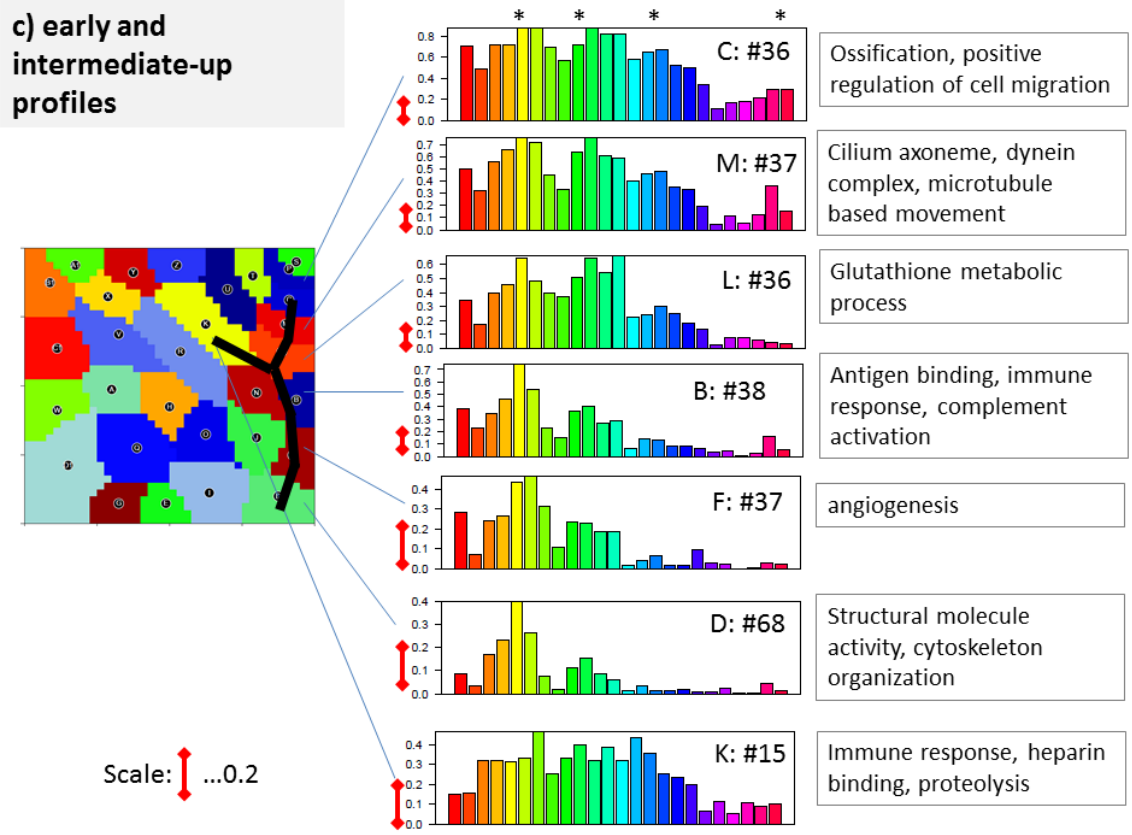

c) early and intermediate-up profiles
C: #36
Ossification, positive regulation of cell migration
M: #37
Cilium axoneme, dynein complex, microtubule based movement
L: #36
Glutathione metabolic process
B: #38
Antigen binding, immune response, complement activation
F: #37
angiogenesis
D: #68
Structural molecule activity, cytoskeleton organization
K: #15
Immune response, heparin binding, proteolysis
Scale: ...0.2
*
*
*
*
0.0
0.1
0.2
0.3
0.4
0.5
0.6
0.7
0.8

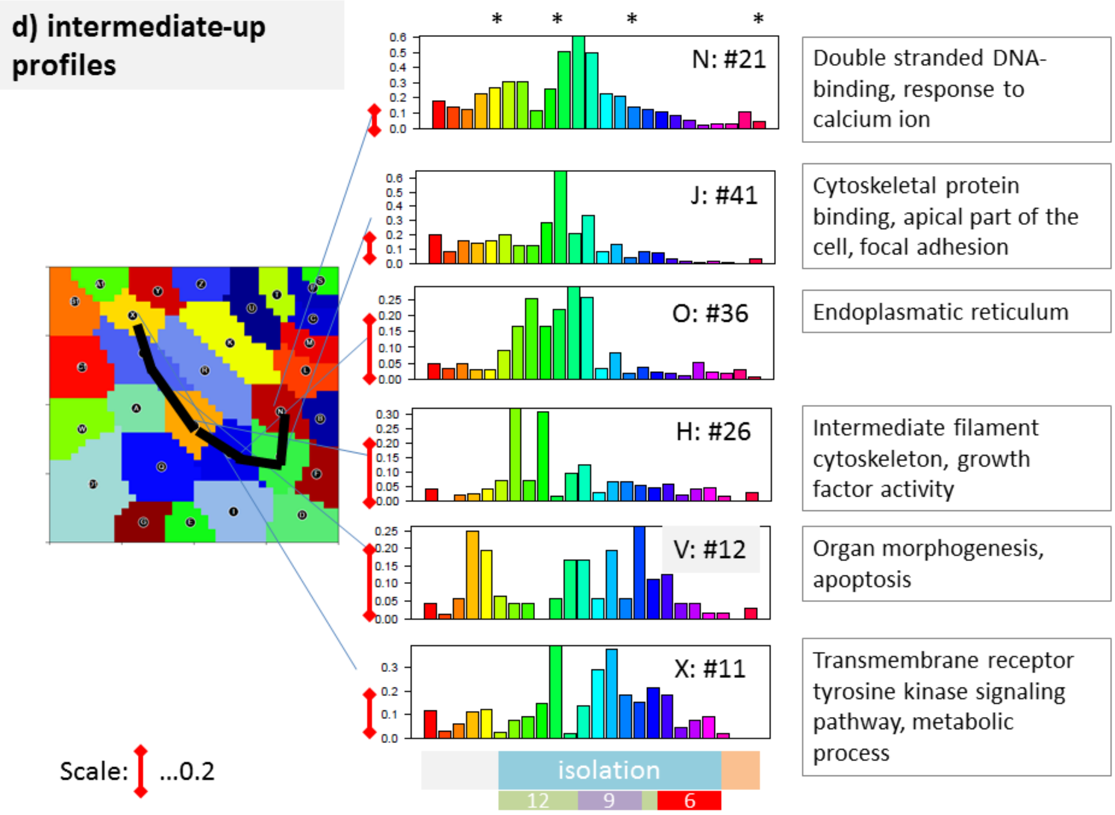

d) intermediate-up profiles
N: #21
Double stranded DNA-binding, response to calcium ion
J: #41
Cytoskeletal protein binding, apical part of the cell, focal adhesion
O: #36
Endoplasmatic reticulum
H: #26
Intermediate filament cytoskeleton, growth factor activity
V: #12
Organ morphogenesis, apoptosis
X: #11
Transmembrane receptor tyrosine kinase signaling pathway, metabolic process
Scale: ...0.2
isolation
12
9
6
*
*
*
*
0.00
0.05
0.10
0.15
0.20
0.25
0.30

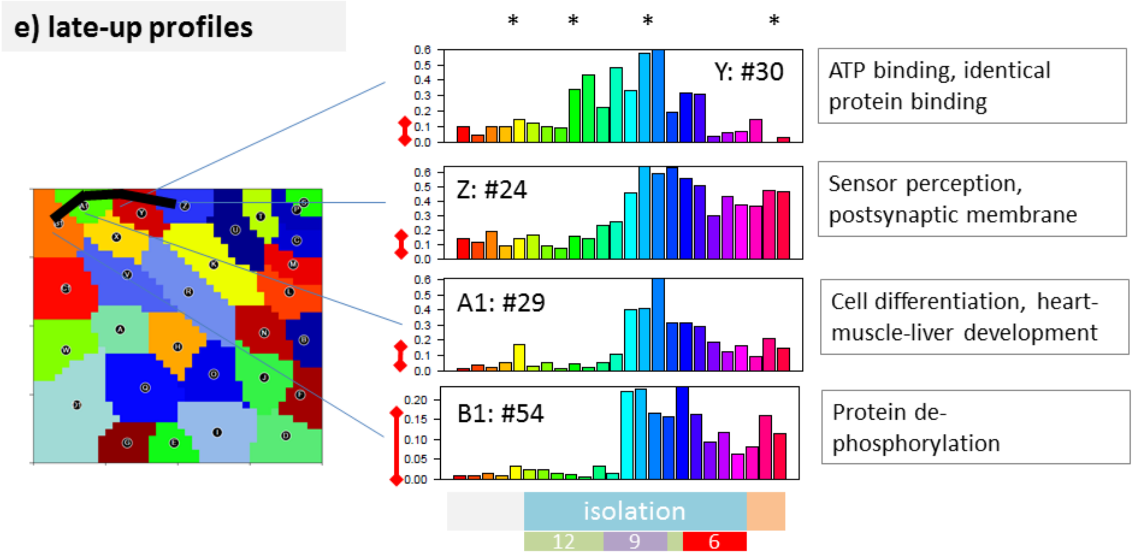

ATP binding, identical protein binding

Sensor perception, postsynaptic membrane

Cell differentiation, heart-muscle-liver development

Protein de-phosphorylation

Figure S 22: Expression profiles of the K-means spot clusters of each of the modes a)-f). Enriched protein sets from the GO-terms biological functions, cellular component and molecular function in each of the spots are listed in the boxes in the right part. The number of proteins per spot is given as #protein_number. The asterisks indicate the peak positions observed also in the overall profiles (see main paper). Note that the scale of vertical expression axis changes from plot to plot. The vertical red dumbbell scales an expression value of 0.1 (module a only) or 0.2. Full protein lists of each of the spot modules are provided in additional file 3.

3 References

1. Läuter J, Glimm E, Eszlinger M: **Search for relevant sets of variables in a high-dimensional setup keeping the familywise error rate**. *Statistica Neerlandica* 2005, **59**:298-312.

2. Läuter J, Horn F, Rosolowski M, Glimm E: **High-dimensional data analysis: Selection of variables, data compression and graphics - Application to gene expression**. *Biometrical Journal* 2009, **51**(2):235-251.

3. Arakelyan A, Nersisyan L: **KEGGParser: parsing and editing KEGG pathway maps in Matlab**. *Bioinformatics* 2013, **29**(4):518-519.

4. Wirth H, Loeffler M, von Bergen M, Binder H: **Expression cartography of human tissues using self organizing maps**. *BMC Bioinformatics* 2011, **12**:306.

5. Owen OE, Felig P, Morgan AP, Wahren J, Cahill GF, Jr.: **Liver and kidney metabolism during prolonged starvation**. *The Journal of Clinical Investigation* 1969, **48**(3):574-583.

6. Pfeiffer G, Strube K-H, Geyer R: **Biosynthesis of sulfated glycoprotein-N-glycans present in recombinant human tissue plasminogen activator**. *Biochemical and Biophysical Research Communications* 1992, **189**(3):1681-1685.

7. Wang X, Proud CG: **The mTOR Pathway in the Control of Protein Synthesis**. *Physiology* 2006, **21**(5):362-369.

8. Pastushkova LK, Kireev KS, Kononikhin AS, Tiys ES, Popov IA, Starodubtseva NL, Dobrokhotov IV, Ivanisenko VA, Larina IM, Kolchanov NA, Nikolaev EN: **Detection of Renal Tissue and Urinary Tract Proteins in the Human Urine after Space Flight**. *PLOS one* 2013, **8**(8):e71652.

9. Larina IM, Kolchanov NA, Dobrokhotov IV, Ivanisenko VA, Demenkov PS, Tiys ES, Valeeva OA, Pastushkova LK, Nikolaev EN: **Reconstruction of associative protein networks connected with processes of sodium exchange regulation and sodium deposition in healthy volunteers based on urine proteome analysis**. *Hum Physiol* 2012, **38**(3):316-323.

10. Liu X, Yu X, Zack D, Zhu H, Qian J: **TiGER: A database for tissue-specific gene expression and regulation**. *BMC Bioinformatics* 2008, **9**(1):271.